UC Davis
Research reports

Title

First-Level Analysis of Phase 1 Heavy Vehicle Simulator and Laboratory Testing on Four RHMA-G Mixes to Investigate Nominal Maximum Aggregate Size, Layer Thickness, and Performance with Aggregate Replacement from Reclaimed Asphalt Pavement

Permalink

Authors

Jones, David
Louw, Stephanus
Hammack, Joseph
et al.

Publication Date

DOI

First-Level Analysis of Phase 1 Heavy Vehicle Simulator and Laboratory Testing on Four RHMA-G Mixes to Investigate Nominal Maximum Aggregate Size, Layer Thickness, and Performance with Aggregate Replacement from Reclaimed Asphalt Pavement

Authors:

David Jones, Stephanus Louw, Joseph Hammack, and Robel Ayalew

PREPARED FOR:

California Department of Transportation
Division of Research, Innovation and System Information
Office of Materials and Infrastructure Roadway Research

PREPARED BY:

University of California
Pavement Research Center
UC Davis and UC Berkeley

TECHNICAL REPORT DOCUMENTATION PAGE

1. REPORT NUMBER UCPRC-RR-2022-05	2. GOVERNMENT ASSOCIATION NUMBER	3. RECIPIENT'S CATALOG NUMBER
4. TITLE AND SUBTITLE First-Level Analysis of Phase 1 Heavy Vehicle Simulator and Laboratory Testing on Four RHMA-G Mixes to Investigate Nominal Maximum Aggregate Size, Layer Thickness, and Performance with Aggregate Replacement from Reclaimed Asphalt Pavement		5. REPORT PUBLICATION DATE February 2023
		6. PERFORMING ORGANIZATION CODE
7. AUTHOR(S) David Jones (ORCID 0000-0002-2938-076X) Stephanus Louw (ORCID 0000-0002-1021-7110) Joseph Hammack (ORCID: 0000-0002-2410-0896) Robel Ayalew (ORCID: 0000-0002-5467-0021)		8. PERFORMING ORGANIZATION REPORT NO. UCPRC-RR-2022-05 UCD-ITS-RR-22-124
9. PERFORMING ORGANIZATION NAME AND ADDRESS University of California Pavement Research Center Department of Civil and Environmental Engineering, UC Davis 1 Shields Avenue Davis, CA 95616		10. WORK UNIT NUMBER
		11. CONTRACT OR GRANT NUMBER 65A0788
12. SPONSORING AGENCY AND ADDRESS California Department of Transportation Division of Research, Innovation, and System Information P.O. Box 942873 Sacramento, CA 94273-0001		13. TYPE OF REPORT AND PERIOD COVERED Research Report
		14. SPONSORING AGENCY CODE

15. SUPPLEMENTAL NOTES
doi:10.7922/G2HT2MNZ

16. ABSTRACT

This research report summarizes a literature review update, construction of a test track to assess various aspects of gap-graded rubberized asphalt concrete (RHMA-G) mixes with and without the addition of reclaimed asphalt pavement (RAP) as aggregate replacement, a first-level analysis of the results from five Heavy Vehicle Simulator (HVS) tests, and a first-level analysis of laboratory test results on the four mixes.

Four different RHMA-G mixes were placed on seven cells on the test track at the UCPRC. Mixes differed by nominal maximum aggregate size (NMAS, 1/2 and 3/4 in.) and the addition of 10% RAP by weight of the aggregate as an aggregate replacement. Single and double lifts of each mix were placed. Apart from the addition of RAP, the mix designs all met current Caltrans specifications. Although Caltrans currently does not permit more than one lift of RHMA-G on projects, the placement of each lift of each mix on the test track met current Caltrans specifications for RHMA-G layers.

The five HVS tests discussed in this report covered the control section (0.2 ft. [60 mm], 1/2 in. NMAS with no RAP), a section with two lifts (0.4 ft. [120 mm]) of the 1/2 in. mix with no RAP, a section with one lift of 1/2 in. mix with RAP, a section with one lift of 3/4 in. mix with no RAP, and a section with two lifts (0.5 ft. [150 mm]) of 3/4 in. mix with RAP. The untested sections included a section with two lifts of 1/2 in. mix with RAP, and a section with two lifts of 3/4 in. mix with no RAP. Findings include the following:

- Performance of all four mixes was satisfactory in terms of the level of trafficking required to reach a terminal average maximum rut of 0.5 in. (12.5 mm).
- Differences in nominal maximum aggregate size and/or the addition of RAP as a coarse aggregate replacement did not appear to have any significant influence on the HVS and laboratory test results. The time that the mix was stored in the silo and the interval between construction and start of HVS testing (i.e., degree of aging of the RHMA-G) appeared to have a larger influence on results.
- The backcalculated stiffnesses of the RHMA-G layer on each section before and after HVS testing indicate that trafficking generally caused some damage on the sections, as expected. An exception to this observation was noted on the first test, which was attributed in part to stiffening of the mix through diffusion of small amounts of RAP binder, which possibly countered the effect of damage by trafficking, and potentially in part to the method used for backcalculation.
- A hydraulic oil spill on one of the sections had a notable negative effect on rutting performance.
- No cracks or other distresses were observed on any of the sections after trafficking.

Recommendations, if justified, for changes to limits for nominal maximum aggregate size in relation to RHMA-G lift thickness, RHMA-G lift thickness, whether more than one RHMA-G lift can be considered in pavement designs, and the use of RAP as aggregate replacement in RHMA-G mixes will be made in a separate report that documents, second-level analysis, and mechanistic simulations.

17. KEYWORDS RHMA-G nominal maximum aggregate size, RHMA-G thickness limits, RAP in RHMA, Heavy Vehicle Simulator testing	18. DISTRIBUTION STATEMENT No restrictions. This document is available to the public through the National Technical Information Service, Springfield, VA 22161
19. SECURITY CLASSIFICATION (of this report) Unclassified	20. NUMBER OF PAGES 162 21. PRICE None

Reproduction of completed page authorized

UCPRC ADDITIONAL INFORMATION

1.	DRAFT STAGE Final	2.	VERSION NUMBER 1
3.	UCPRC STRATEGIC PLAN ELEMENT NUMBER 4.75	4.	CALTRANS TASK NUMBER 3760
5.	CALTRANS TECHNICAL LEAD AND REVIEWER(S) Raghu Shrestha and Kee Foo	6.	FHWA NUMBER CA233760A

7. PROPOSALS FOR IMPLEMENTATION
Proposals for implementation will be included in the second-level analysis report (UCPRC-RR-2022-06).

8. RELATED DOCUMENTS
UCPRC-RR-2022-06

9. LABORATORY ACCREDITATION
The UCPRC laboratory is accredited by AASHTO re:source for the tests listed in this report

10. SIGNATURES

D. Jones **FIRST AUTHOR**	J.T. Harvey **TECHNICAL REVIEW**	C. Fink **EDITOR**	J.T. Harvey **PRINCIPAL INVESTIGATOR**	R. Shrestha & K. Foo **CALTRANS TECH. LEADS**	T.J. Holland **CALTRANS CONTRACT MANAGER**

Reproduction of completed page authorized

DISCLAIMER STATEMENT

This document is disseminated in the interest of information exchange. The contents of this report reflect the views of the authors who are responsible for the facts and accuracy of the data presented herein. The contents do not necessarily reflect the official views or policies of the State of California or the Federal Highway Administration. This publication does not constitute a standard, specification, or regulation. This report does not constitute an endorsement by the Department of any product described herein.

PROJECT OBJECTIVES

This study is a continuation of PPRC Project 4.63. The objective of this project is to develop updated criteria for determining optimal thickness limits of gap-graded rubberized hot mix asphalt (RHMA-G) layers, whether RHMA-G layers can be used in layers other than surface layers, and whether reclaimed asphalt pavement (RAP) can be effectively used in RHMA mixes. This objective will be achieved through the following tasks:

Task 1: Complete Heavy Vehicle Simulator (HVS) and associated laboratory testing of RHMA-G mixes that focus on nominal maximum aggregate size in 0.2 ft. thick layers, layer thickness (one or two lifts), and the use of coarse RAP as aggregate replacement.

Task 2: Complete *CalME* simulations using HVS and laboratory test results collected during Task 1.

Task 3: Revise life cycle cost analysis and environmental life cycle analysis criteria for RHMA-G applications using the results from Task 2.

Task 4: Prepare first- and second-level analysis research reports documenting the study findings and, if justified, recommendations for updated *Highway Design Manual* language for RHMA-G design and use criteria.

This report covers the work completed in the first phase (assessing rutting resistance) of Task 1.

ACKNOWLEDGMENTS

EXECUTIVE SUMMARY

Introduction

This research report summarizes a literature review update, the construction of a test track to assess various aspects of gap-graded rubberized asphalt concrete (RHMA-G) mixes with and without the use of reclaimed asphalt pavement (RAP) as aggregate replacement, a first-level analysis of the results from five of the planned seven Phase 1 Heavy Vehicle Simulator (HVS) tests, which focused on rutting resistance, and a first-level analysis of the laboratory test results on specimens prepared from the four different mixes sampled during production.

Literature Review

Apart from the research previously undertaken by the University of California Pavement Research Center (UCPRC) for the California Department of Resources Recycling and Recovery (CalRecycle), only limited published research on the use of RAP in new RHMA mixes was located. The few documents available focused on laboratory testing of dense-graded mixes produced with terminal-blended binders containing completely digested rubber particles smaller than 0.4 mm (passing the #40 sieve). No documented research involving accelerated pavement testing of RHMA mixes containing RAP was located.

Test Track Construction

The inside north track at the UCPRC was reconstructed for this project between January and May 2019. Construction included ripping and recompacting the subgrade, placement of an aggregate subbase and an aggregate base, and placement of a cold central plant recycled layer (100% RAP with foamed asphalt recycling agent). Four different RHMA-G mixes were placed on seven cells on the test track at the UCPRC. Mixes differed by nominal maximum aggregate size (NMAS; 1/2 and 3/4 in.) and the addition of 10% RAP by weight of the aggregate as a coarse aggregate replacement. Single and double lifts of each mix were placed. Apart from the addition of RAP, the mix designs all met current Caltrans specifications. Although Caltrans currently does not permit more than one lift of RHMA-G on projects, the placement of each lift of each mix on the test track met current Caltrans construction specifications for RHMA-G layers. Based on observed construction practice and quality control test results, the test track was considered to be representative of a highway project and was approved for HVS testing.

Heavy Vehicle Simulator Testing

The five HVS tests discussed in this report covered the control section (0.2 ft. [60 mm], 1/2 in. NMAS with no RAP), a section with two lifts (0.4 ft. [120 mm]) of the 1/2 in. mix with no RAP, a section with one lift of 1/2 in. mix with RAP, a section with one lift of 3/4 in. mix with no RAP, and a section with two lifts (0.5 ft. [150 mm]) of 3/4 in. mix with RAP. The untested sections included a section with two lifts of 1/2 in. mix with RAP and a section with two lifts of 3/4 in. mix with no RAP. Results from these five HVS tests and associated laboratory testing indicated the following:

- Performance of all four mixes was satisfactory in terms of the level of trafficking required to reach a terminal average maximum rut of 0.5 in. (12.5 mm).
- Differences in nominal maximum aggregate size and/or the addition of RAP as a coarse aggregate replacement did not appear to have any significant influence on the test results. The time that the mix was stored in the silo prior to placement and the interval between test track construction and the start of HVS testing on a specific section (i.e., aging of the RHMA-G layer) both appeared to have a larger influence.
- Deflection measurements and backcalculated stiffnesses of the RHMA-G layer on each section before and after HVS testing indicate that HVS trafficking generally caused some damage on the sections, as expected. An exception to this observation was noted on the first test, which was attributed in part to stiffening of the mix through diffusion of small amounts of RAP binder, which possibly countered the effect of damage by trafficking, and potentially in part to the method followed to distinguish stiffness contributions of the RHMA-G and CCPR layers. Note that the first lift of RHMA-G placed on this cell had very little silo time, while the mix placed in the second lift had spent approximately eight hours in the silo.
- A hydraulic oil spill on one of the sections had a notable negative effect on rutting performance.
- Variation in rutting performance between sections and in the rut depth along the length of individual sections may be attributed to shear failures in the aggregate base layer. Although the layer met all Caltrans specifications for Class 2 Aggregate Base, the uncrushed, rounded particles had poor interlock and the layer appeared to be susceptible to shearing, as observed during construction with it and later placement of the CCPR layer. This will be checked during the forensic investigation.
- No cracks or other distresses were observed on any of the sections after trafficking.

Second-Level Analysis

A separate report will document the second-level analysis of the results in terms of mechanistic simulations to understand long-term performance in typical pavement structures under different traffic volumes and climatic conditions in California. Recommendations will be made in the report, if justified, for changes to limits for NMAS in relation to RHMA-G lift thickness, RHMA-G lift thickness, whether more than one RHMA-G lift can be considered in pavement designs, the use of RAP as aggregate replacement in RHMA-G mixes, and whether crushed aggregate faces for aggregate base and subbase materials should be a specification requirement.

Blank page

TABLE OF CONTENTS

LIST OF TABLES

LIST OF FIGURES

Blank page

LIST OF ABBREVIATIONS

AASHTO	American Association of State Highway and Transportation Officials
AMPT	Asphalt mix performance tester
ASTM	American Society for Testing and Materials
Caltrans	California Department of Transportation
CalRecycle	California Department of Resources Recycling and Recovery
CCP	Cold central plant
CCPR	Cold central plant recycling
CCPR-EA	Cold central plant recycling with emulsified asphalt
CCPR-FA	Cold central plant recycling with foamed asphalt
ESAL	Equivalent single axle load
FDR	Full-depth recycling
FI	Flexibility index
FWD	Falling weight deflectometer
G_f	Fracture energy
HMA	Hot mix asphalt
HVS	Heavy Vehicle Simulator
HWT	Hamburg wheel track
HWTT	Hamburg wheel track test
LMP	Laboratory-determined modified Proctor density
LVDT	Linear variable differential transformer
MDD	Multi-depth deflectometer
MaxDD	Maximum dry density
MTD	Maximum theoretical density
NMAS	Nominal maximum aggregate size
OMC	Optimum moisture content
PDR	Partial-depth recycling
PPRC	Partnered Pavement Research Center
RAP	Reclaimed asphalt pavement
R-RAP	Rubberized reclaimed asphalt pavement
RHMA	Rubberized hot mix asphalt
RHMA-G	Gap-graded rubberized hot mix asphalt
RHMA-O	Open-graded rubberized hot mix asphalt
RSD	Road surface deflectometer
SCB	Semicircular bend test
UCPRC	University of California Pavement Research Center

TEST METHODS CITED IN THE TEXT

AASHTO

T 11 Standard Method of Test for Materials Finer Than 75-μm (No. 200) Sieve in Mineral Aggregates by Washing

T 27 Standard Method of Test for Sieve Analysis of Fine and Coarse Aggregates

T 89 Standard Method of Test for Determining the Liquid Limit of Soils

T 90 Standard Method of Test for Determining the Plastic Limit and Plasticity Index of Soils

T 166 Standard Method of Test for Bulk Specific Gravity (Gmb) of Compacted Hot Mix Asphalt (HMA) Using Saturated Surface-Dry Specimens

T 180 Standard Method of Test for Moisture-Density Relations of Soils Using a 4.54-kg (10-lb) Rammer and a 457-mm (18-in.) Drop

T 209 Standard Method of Test for Theoretical Maximum Specific Gravity (Gmm) and Density of Hot-Mix Asphalt (HMA)

T 269 Standard Method of Test for Percent Air Voids in Compacted Dense and Open Asphalt Mixtures

T 321 Standard Method of Test for Determining the Fatigue Life of Compacted Asphalt Mixtures Subjected to Repeated Flexural Bending

T 331 Bulk Specific Gravity (Gmb) and Density of Compacted Hot Mix Asphalt (HMA) Using Automatic Vacuum Sealing Method

T 378 Standard Method of Test for Determining the Dynamic Modulus and Flow Number for Asphalt Mixtures Using the Asphalt Mixture Performance Tester (AMPT)

T 393 Standard Method of Test for Determining the Fracture Potential of Asphalt Mixtures Using Illinois Flexibility Index Test (I-FIT)

ASTM

D2487 Standard Practice for Classification of Soils for Engineering Purposes (Unified Soil Classification System)

D8225 Standard Test Method for Determination of Cracking Tolerance Index of Asphalt Mixture Using the Indirect Tensile Cracking Test at Intermediate Temperature

Caltrans Test

CT 216 Method of Test for Relative Compaction of Untreated and Treated Soils and Aggregates

CT 231 Method of Test for Relative Compaction of Untreated and Treated Soils and Aggregates Using Nuclear Gage

CT 375 Determining the In-Place Density and Relative Compaction of Hot Mix Asphalt Pavement Using Nuclear Gages

CONVERSION FACTORS

APPROXIMATE CONVERSIONS TO SI UNITS				
Symbol	**When You Know**	**Multiply By**	**To Find**	**Symbol**
LENGTH				
in.	inches	25.40	millimeters	mm
ft.	feet	0.3048	meters	m
yd.	yards	0.9144	meters	m
mi.	miles	1.609	kilometers	km
AREA				
in^2	square inches	645.2	square millimeters	mm^2
ft^2	square feet	0.09290	square meters	m^2
yd^2	square yards	0.8361	square meters	m^2
ac.	acres	0.4047	hectares	ha
mi^2	square miles	2.590	square kilometers	km^2
VOLUME				
fl. oz.	fluid ounces	29.57	milliliters	mL
gal.	gallons	3.785	liters	L
ft^3	cubic feet	0.02832	cubic meters	m^3
yd^3	cubic yards	0.7646	cubic meters	m^3
MASS				
oz.	ounces	28.35	grams	g
lb.	pounds	0.4536	kilograms	kg
T	short tons (2000 pounds)	0.9072	metric tons	t
TEMPERATURE (exact degrees)				
°F	Fahrenheit	(F-32)/1.8	Celsius	°C
FORCE and PRESSURE or STRESS				
lbf	pound-force	4.448	newtons	N
lbf/in^2	pound-force per square inch	6.895	kilopascals	kPa
APPROXIMATE CONVERSIONS FROM SI UNITS				
Symbol	**When You Know**	**Multiply By**	**To Find**	**Symbol**
LENGTH				
mm	millimeters	0.03937	inches	in.
m	meters	3.281	feet	ft.
m	meters	1.094	yards	yd.
km	kilometers	0.6214	miles	mi.
AREA				
mm^2	square millimeters	0.001550	square inches	in^2
m^2	square meters	10.76	square feet	ft^2
m^2	square meters	1.196	square yards	yd^2
ha	hectares	2.471	acres	ac.
km^2	square kilometers	0.3861	square miles	mi^2
VOLUME				
mL	milliliters	0.03381	fluid ounces	fl. oz.
L	liters	0.2642	gallons	gal.
m^3	cubic meters	35.31	cubic feet	ft^3
m^3	cubic meters	1.308	cubic yards	yd^3
MASS				
g	grams	0.03527	ounces	oz.
kg	kilograms	2.205	pounds	lb.
t	metric tons	1.102	short tons (2000 pounds)	T
TEMPERATURE (exact degrees)				
°C	Celsius	1.8C + 32	Fahrenheit	°F
FORCE and PRESSURE or STRESS				
N	newtons	0.2248	pound-force	lbf
kPa	kilopascals	0.1450	pound-force per square inch	lbf/in^2

*SI is the abbreviation for the International System of Units. Appropriate rounding should be made to comply with Section 4 of ASTM E380.
 (Revised April 2021)

Blank page

1.   INTRODUCTION

1.1   Background to the Study

The California Department of Transportation (Caltrans) design procedures and specifications currently limit the thickness of gap-graded rubberized hot mix asphalt (RHMA-G) layers to 0.2 ft. (60 mm) and only allow RHMA-G to be used in surface layers. These requirements are historically based on the higher costs of RHMA-G mixes compared to conventional hot mix asphalt (HMA) when first used by Caltrans and concerns with regard to rutting potential. Over the years with increasing use, the difference in cost between HMA and RHMA-G has reduced and rutting performance has been improved by changes to mix design procedures, the requirement for Hamburg Wheel Track testing during mix design and quality control, and tighter compaction specifications. Consequently, thicker and/or multiple layers of RHMA-G might offer cost-effective comparable performance to conventional HMA layers and will increase the use of recycled tire rubber by Caltrans.

As asphalt concrete surface layers on highways and airfields reach the end of their design lives, they are being milled off and replaced with new HMA or new RHMA. The millings are being added to reclaimed asphalt pavement (RAP) stockpiles, which in turn are reused in new conventional HMA. The amount of RAP used in new conventional HMA in California currently varies between 15% and 25% by weight of total mix, but this could increase to 40% or higher in the future. Caltrans currently does not permit the use of any RAP in RHMA-G mixes or in rubberized open-graded mixes (RHMA-O). However, there is increasing interest in allowing some RAP either as binder or aggregate replacement in RHMA in order to reduce the amount of virgin materials required in new mixes.

1.2   Completed Research in California

The University of California Pavement Research Center (UCPRC) completed a preliminary study *(1)* for the California Department of Resources Recycling and Recovery (CalRecycle) in 2017 that investigated the potential implications of using reclaimed rubberized asphalt pavement (R-RAP) materials as partial binder and aggregate replacement in new conventional dense-graded

HMA mixes and using reclaimed conventional asphalt pavement (RAP) materials as partial binder and aggregate replacement in new RHMA-G mixes.

Limited laboratory test results *(1)* indicated that adding R-RAP to dense-graded HMA could potentially yield some improvement in overall rutting performance, but it could also have a potentially overall negative effect on fatigue and low-temperature cracking performance. These findings were consistent with those from tests where conventional RAP was used. The degree of change in rutting and cracking resistance in the HMA mixes was dependent on the R-RAP source, with mixes containing millings only from RHMA layers performing slightly better than mixes containing both R-RAP and RAP. These findings did not indicate a reason or justification for separating R-RAP and RAP millings or maintaining separate stockpiles at asphalt plants.

Test results *(1)* from the RHMA-G mixes containing RAP indicated that rutting performance is likely to improve but that adding RAP could have a potentially overall negative effect on fatigue and low-temperature cracking performance, which would negate the benefits of selecting RHMA-G as an overlay to retard the rate of reflection cracking.

Since only limited testing on asphalt rubber mixes containing RAP was undertaken in the preliminary study, further laboratory testing followed by full-scale field testing in pilot projects or accelerated wheel load testing was recommended on a wider range of virgin binder, virgin aggregate, and RAP material sources to confirm the findings before any changes to current practice are considered.

1.3 Problem Statements

The decision criteria for thickness limits of RHMA-G layers, whether 1/2 in. nominal maximum aggregate size (NMAS) mixes can be used in 0.2 ft. (60 mm) thick layers, and whether RHMA-G layers can be used in layers other than surface layers are dated. These criteria need to be updated based on life cycle cost analyses, environmental life cycle analyses, and expected performance based on mechanistic-empirical design simulations.

There is growing interest in adding some RAP to RHMA mixes. However, if binder replacement is the goal, then the amount of recycled tire rubber used by Caltrans will be reduced. Binder replacement in HMA mixes is typically achieved by using finer fractions of RAP (i.e., finer than

3/8 in. [9.5 mm]). Research is needed to assess using coarser RAP, left over after removing the finer fractions, in RHMA mixes, focusing on aggregate replacement with minimal binder replacement. This will allow some RAP addition to RHMA-G and potentially RHMA-O mixes, thereby using all processed RAP without reducing the amount of recycled tires that are used.

1.4   Project Objectives

This study is a continuation of PPRC Project 4.63. The objective of this project is to develop updated criteria for determining optimal thickness limits of RHMA-G layers, whether RHMA-G layers can be used in layers other than surface layers, and whether RAP can be effectively used in RHMA mixes. This objective will be achieved through the following tasks:

Task 1:   Complete Heavy Vehicle Simulator (HVS) and associated laboratory testing of RHMA-G mixes that focus on nominal maximum aggregate size in 0.2 ft. thick layers, layer thickness (one or two lifts), and the use of coarse RAP as aggregate replacement.

Task 2:   Complete *CalME* simulations using HVS and laboratory test results collected during Task 1.

Task 3:   Revise life cycle cost analysis and environmental life cycle assessment criteria for RHMA-G applications using the results from Task 2.

Task 4:   Prepare first- and second-level analysis research reports documenting the study findings and, if justified, recommendations for updated Highway Design Manual language for RHMA-G design and use criteria.

This report covers the work completed in the first phase (assessing rutting resistance) of Task 1.

1.5   Report Layout

This research report details test track construction and a first-level analysis of the HVS and laboratory test results, and it is organized as follows:

- Chapter 2 summarizes the updated literature review findings on the use of RAP in RHMA-G mixes.
- Chapter 3 details the location and design of the test track.
- Chapter 4 summarizes the construction of the test track.
- Chapter 5 explains the track layout, instrumentation, and testing criteria.
- Chapter 6 summarizes test durations, loading programs, and rainfall measurements over the testing period.
- Chapters 7 through 11 cover the first-level analysis of the test results on each section. Results include temperatures, permanent deformation on the surface and in the underlying

layers, vertical pressure at the midpoint of the aggregate base layer, deflection on the surface, deflection in the underlying layers, deflection and backcalculated stiffness in the pavement structure, and the visual assessment and preliminary forensic coring on completion of testing.

- Chapter 12 compares selected results from the five test sections.
- Chapter 13 summarizes the results from laboratory testing of specimens produced with the four mixes sampled during test track construction.
- Chapter 14 provides a project summary and conclusions.

The findings from the second-level analysis of the HVS and laboratory test results, including *CalME* simulations and model calibration will be documented in a separate report *(2)*.

1.6   Measurement Units

Although Caltrans recently returned to the use of US standard measurement units, metric units have always been used by the UCPRC in the design and layout of HVS test tracks, and for laboratory, HVS, and field measurements and data storage. In this report, both US and metric units (provided in parentheses after the US units) are provided in general discussion. In keeping with convention, metric units are used in HVS and laboratory data analyses and reporting, with some US units, where appropriate, to assist the reader. A conversion table is provided on page xvii.

2. LITERATURE REVIEW

A literature review of research undertaken on incorporating reclaimed asphalt pavement (RAP) materials in rubberized hot mix asphalt (RHMA), with special focus on accelerated pavement testing, was completed. Research on both RAP binder replacement and RAP aggregate replacement was considered.

Apart from the research previously undertaken by the UCPRC for CalRecycle *(1)*, only limited published research on the use of RAP in new RHMA mixes was located, with most of it focused on laboratory testing of dense-graded mixes produced with terminal-blended binders containing completely digested rubber particles smaller than 0.4 mm (passing the #40 sieve) in size *(3–10)*.

One Canadian study investigated adding 20% RAP (by weight of the mix) into RHMA-G mixes produced with asphalt rubber binder containing 20% rubber by weight of the binder *(11)*. Stiffness, rutting performance, and thermal cracking performance were evaluated. Test results showed that the mixes containing both rubber and RAP performed better than the mixes containing only RAP. The gap-graded mixes were stiffer and performed better in low-temperature cracking tests, while the dense-graded control mix performed better in rutting tests. Mixes containing RAP had lower fracture stress and fracture temperature than the control mixes with conventional binder and the same quantity of RAP, suggesting that rubberized asphalt mixes in general would have better resistance to thermal cracking.

No documented research involving accelerated pavement testing of RHMA mixes containing RAP was located.

Blank page

3. TEST TRACK LOCATION AND DESIGN

3.1 Test Track Location

The RHMA-G experiment is located on the North Test Track at the University of California Pavement Research Center (UCPRC) facility in Davis, California. An aerial view of the site is shown in Figure 3.1. The track was reconstructed for this project between 01/03/2019 and 05/08/2019. The study described in this report is the fourth research project involving Heavy Vehicle Simulator (HVS) testing undertaken on this test track.

Figure 3.1: Aerial view of the UCPRC research facility.

3.2 Test Track Layout

The North Test Track is 361 ft. (110 m) long and 52.5 ft. (16 m) wide. It has a 2% crossfall in the north-south direction. Four standard-width lanes can be constructed in this space.

The test track layout is shown in Figure 3.2. The gray-shaded area (Cells D though J) in the figure covers the seven RHMA-G cells tested in this study. The unshaded area (Cells A, B and C) covers the three cold central plant recycled (CCPR) materials tested in another parallel study not discussed in this report. All test track measurements and locations discussed in this report are based on this layout.
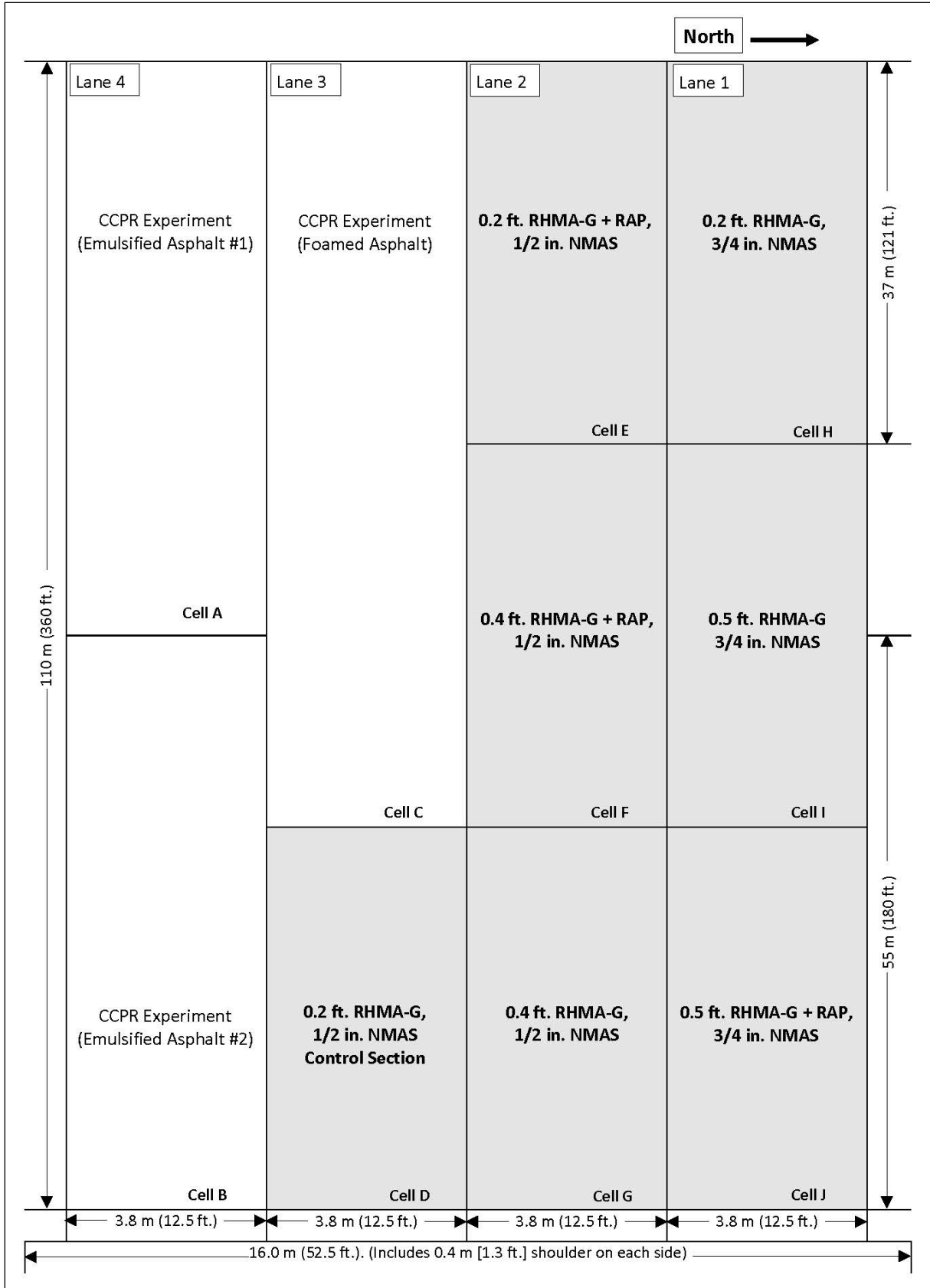
Figure 3.2: Test track layout (shaded area [Cells D through J] is the RHMA-G experiment).

3.3 Test Track Pavement Design

The pavement design for the test track focused on assessment of both the CCPR layers and the different RHMA-G layers. Given that CCPR layers had not been constructed on the Caltrans road network at the time of starting this study, the test track was designed to be consistent with a typical Caltrans partial-depth recycling (PDR) capital maintenance project to understand the behavior and performance of similar pavement materials recycled using cold central plant technology. A relatively thin (0.2 ft. [60 mm]) RHMA-G surfacing was used in the CCPR material study design and as the control in the RHMA-G part of the study. A total of four different RHMA-G mixes and three different thicknesses were evaluated in the RHMA-G part of the study. The pavement design for the test track is shown in Figure 3.3 (cells with one RHMA-G layer) and Figure 3.4 (cells with two RHMA-G layers).
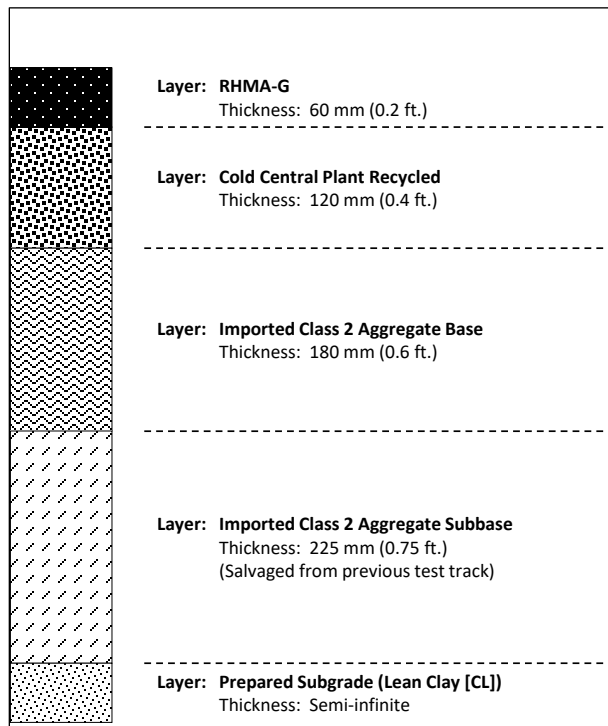
Figure 3.3: Test track design: One RHMA-G layer.
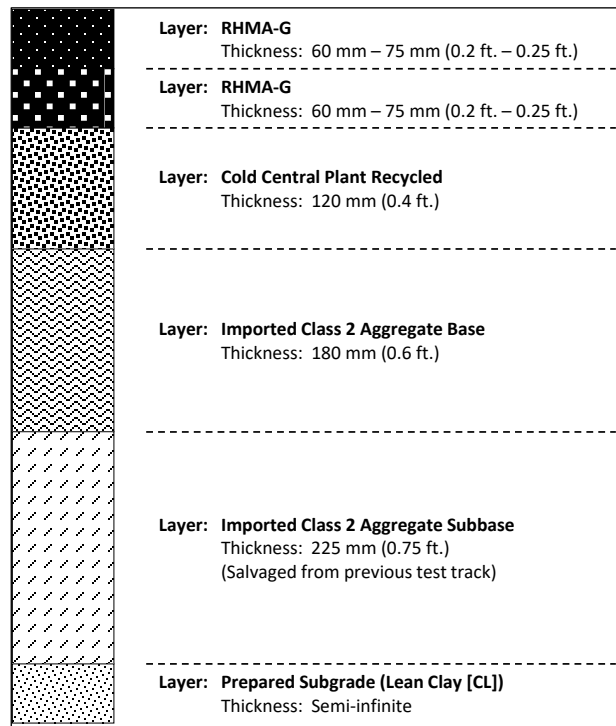
Figure 3.4: Test track design: Two RHMA-G layers.

The different mixes, layer thicknesses, and reasons for inclusion in the study are summarized in Table 3.1.

Table 3.1: Summary of Test Track Cells in the RHMA-G Study

Cell	RHMA-G Mix	Thickness (ft.)	(mm)	Purpose in the Experiment
D	1/2 in. nominal maximum aggregate size (NMAS), no RAP	0.2	60	Control for all 1/2 in. RHMA-G mixes
E	1/2 in. NMAS with 10% RAP, no binder replacement	0.2	60	Compare mix with RAP to control mix for same layer thickness
F	1/2 in. NMAS with 10% RAP, no binder replacement	0.4	120	Compare two layers, both with RAP, to two layers with no RAP
G	1/2 in. NMAS, no RAP	0.4	120	Compare two layers with single layer
H	3/4 in. NMAS, no RAP	0.2	60	Control for all 3/4 in. RHMA-G mixes. Compare 3/4 in. mix with 1/2 in. mix
I	3/4 in. NMAS, no RAP	0.5	150	Compare two layers with single layer
J	3/4 in. NMAS with 10% RAP, no binder replacement	0.5	150	Compare two layers, both with RAP, to two layers with no RAP

3.4 RHMA-G Mix Design

The RHMA-G mixes placed on the test track were designed and produced by George Reed Inc. Key material design parameters from the job mix formulas for the four mixes are summarized in Table 3.2 (no RAP) and Table 3.3 (with RAP).

Table 3.2: Mix Design Parameters for RHMA-G with No RAP

Parameter		1/2 in. NMAS Actual	Compliance	3/4 in. NMAS Actual	Compliance
Grading (% passing sieve)	1	100	100	100	100
	3/4	100	100	98	95 − 98
	1/2	97	90 − 98	84	83 − 87
	3/8	84	83 − 87	72	65 − 70
	#4	39	28 − 42	36	28 − 42
	#8	19	14 − 22	19	14 − 22
	#200	3.6	0.0 − 6.0	2.7	0.0 − 6.0
RAP content by total weight of aggregate (%)		0	N/A	0	N/A
Base asphalt binder performance grade		64-16	N/A	64-16	N/A
Rubber content (% by weight of binder)		18	18 − 22	18	18 − 22
AR binder cone penetration (mm)		3.6	2.5 − 7.0	3.6	2.5 − 7.0
AR binder resilience (% rebound)		48	>18	48	>18
AR binder softening point (°C)		62	52 − 74	62	52 − 74
AR binder viscosity (centipoise)		1,600	1,500 − 4,000	1,600	1,500 − 4,000
Binder content by total weight of mix (%)		7.8	7.4 − 8.3	7.6	7.1 − 8.0
Number of gyrations		150	50 − 150	135	50 − 150
Air-void content (%)		3.8	4.0	4.0	4.0
Voids in mineral aggregate (%)		19.8	18 − 23	19.5	18 − 23
Dust proportion		0.52	N/A	0.44	N/A
Hamburg (rut depth [mm] at 20,000 passes)		2.2	<12.5	2.5	<12.5
Moisture susceptibility, dry strength (psi)		169	>100	155	>100
Moisture susceptibility, wet strength (psi)		120	>70	124	>70

Table 3.3: Mix Design Parameters for RHMA-G with RAP

Parameter		1/2 in. NMAS		3/4 in. NMAS	
		Actual	Compliance	Actual	Compliance
Grading (% passing sieve)	1	100	100	100	100
	3/4	100	100	97	95 − 98
	1/2	97	90 − 98	83	83 − 87
	3/8	84	83 − 87	72	65 − 70
	#4	41	28 − 42	36	28 − 42
	#8	21	14 − 22	19	14 − 22
	#200	3.4	0.0 − 6.0	2.7	0.0 − 6.0
RAP content by total weight of aggregate (%)		10	N/A	10	N/A
Base asphalt binder performance grade		64-16	N/A	64-16	N/A
Rubber content (% by weight of binder)		18	18 − 22	18	18 − 22
AR binder cone penetration (mm)		3.6	2.5 − 7.0	3.6	2.5 − 7.0
AR binder resilience (% rebound)		48	>18	48	>18
AR binder softening point (°C)		62	52 − 74	62	52 − 74
AR binder viscosity (centipoise)		1,600	1,500 − 4,000	1,600	1,500 − 4,000
Binder content by total weight of mix (%)		7.8	7.4 − 8.3	7.75	7.1 − 8.0
Number of gyrations		150	50 − 150	135	50 − 150
Air-void content (%)		4.0	4.0	4.0	4.0
Voids in mineral aggregate (%)		20	18 − 23	19.5	18 − 23
Dust proportion		0.5	N/A	0.43	N/A
Hamburg (rut depth [mm] at 20,000 passes)		Not tested	<12.5	Not tested	<12.5
Moisture susceptibility, dry strength (psi)		Not tested	>100	Not tested	>100
Moisture susceptibility, wet strength (psi)		Not tested	>70	Not tested	>70

Although Caltrans currently does not allow the use of any RAP materials in RHMA-G mixes, all of the mixes did meet all other Caltrans standard specification requirements for 1/2 in. and 3/4 in. nominal maximum aggregate size (NMAS) RHMA-G mixes.

3.5 Cold Central Plant Recycled Material Mix Designs

The mix design for the cold central plant recycled material with foamed asphalt recycling agent (CCPR-FA) was completed by the UCPRC, while the mix designs for the two CCPR material mixes with emulsified asphalt (CCPR-EA) mixes were completed by Pavement Recycling Systems, the contractor who constructed the test track. Designs followed the Caltrans LP-8 procedures that were current at the time. Key design parameters are summarized in Table 3.4. The recycling agent (2.5% residual asphalt) and active filler (1% cement) contents were the same for all three mixes.

Table 3.4: Mix Design Parameters for Cold Central Plant Recycled Materials

Parameter		CCPR-FA	CCPR-EA #1	CCPR-EA #2	Compliance
Grading (% passing sieve)	1	100	100	100	—
	3/4	95	95	95	—
	#4	50	50	50	—
	#30	10	10	10	—
	#200	2	2	2	—
Residual recycling agent content (% of dry aggregate weight)		2.5	2.5	2.5	—
Cement content (% of dry aggregate weight)		1.0	1.0	1.0	—
Water for mixing (% of dry aggregate weight)		5.2	2.0	2.0	—
Maximum theoretical specific gravity		Not tested	2.465	2.499	—
Bulk specific gravity		Not tested	2.131	2.117	—
Density (lb./ft^3)		129	133.1	132.0	—
Air-void content (%)		Not tested	13.5	15.4	10.0–16.0
Indirect tensile strength, dry (psi)		60	Not tested	Not tested	—
Indirect tensile strength, wet (psi)		51	Not tested	Not tested	>35
Tensile strength retained (%)		85	Not tested	Not tested	>70
Marshall stability, dry (lb.)		Not tested	3,525	3,260	>1,250
Marshall stability, wet (lb.)		Not tested	2,720	2,320	—
Marshall retained stability (%)		Not tested	77.2	71.2	>70
Ratio of recycling agent residue to cement		2.5:1	2.5:1	2.5:1	2.5:1
Raveling resistance (% loss)		Not tested	Not tested	Not tested	>95

3.6   Subgrade, Aggregate Subbase, and Aggregate Base Properties

Samples were taken during construction of the subgrade, aggregate subbase, and aggregate base layers for indicator tests. Three samples were taken from the same coordinates on each layer, with sampling locations shown on Figure 3.5. Material properties for each layer are summarized in Table 3.5 through Table 3.7.
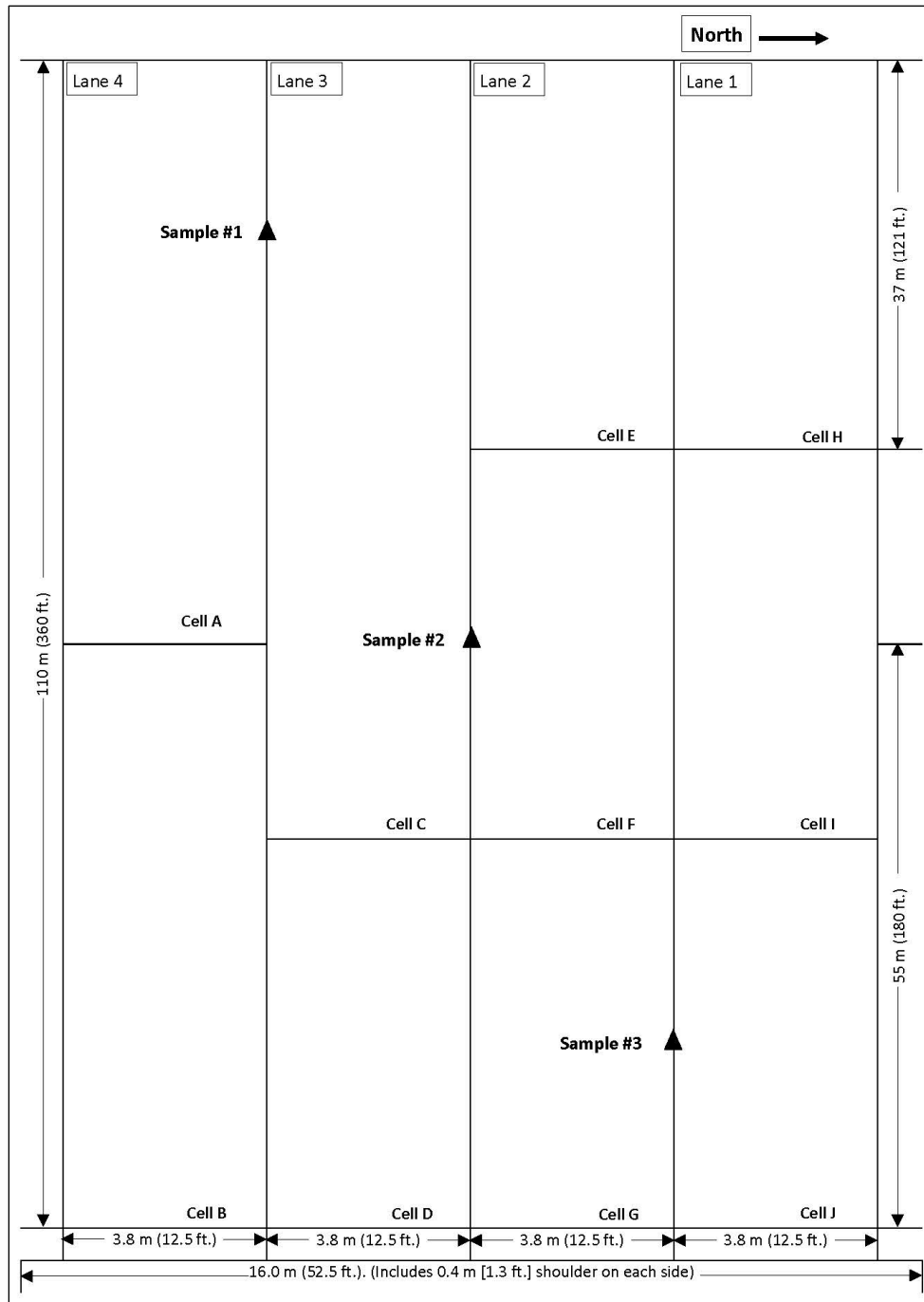
Figure 3.5: Sampling locations.

Table 3.5: Subgrade Material Properties

Property		Result				Operating Range	Contract Compliance
		Sample 1	Sample 2	Sample 3	Average		
Grading:[a] 1" (25 mm)		100	100	100	100	–	–
3/4" (19 mm)		88	100	98	95	–	–
1/2" (12.5 mm)		86	98	97	94	–	–
3/8" (9.5 mm)		84	97	96	92	–	–
#4 (4.75 mm)		78	95	94	89	–	–
#8 (2.36 mm)		74	93	91	86	–	–
#16 (1.18 mm)		71	91	89	84	–	–
#30 (600 µm)		69	90	88	82	–	–
#50 (300 µm)		67	87	86	80	–	–
#100 (150 µm)		63	82	81	75	–	–
#200 (75 µm)		57	71	73	67	–	–
Atterberg Limits:[b] Liquid Limit		34	35	37	35	–	–
Plastic Limit		17	19	16	17	–	–
Plasticity Index		17	16	21	18	–	–
Max. Dry Density (lb./ft^3)(kg/m^3)[c]		122.5 (1,963)	121.5 (1,946)	122.1 (1,954)	122.0 (1,954)	–	–
Optimum Moisture Content (%)[c]		10.7	11.2	11.0	11.0	–	–
Resilient modulus from DCP (ksi [MPa])[d]		9.6 (66)	9.1 (63)	9.6 (66)	9.4 (65)	–	–
Unified Soil Classification[e]		Lean clay (CL)	Lean clay (CL)	Lean clay (CL)	–	–	–

[a]   Determined according to AASHTO T 11 and AASHTO T 27
[b]   Determined according to AASHTO T 89 and AASHTO T 90
[c]   Modified Proctor determined according to AASHTO T 180
[d]   Resilient modulus estimated from dynamic cone penetrometer measurements according to Caltrans Site Investigation Guide *(12)*
[e]   Unified Soil Classification System according to ASTM D2487

Table 3.6: Aggregate Subbase Material Properties

Property		Result				Operating Range	Contract Compliance
		Sample 1	Sample 2	Sample 3	Average		
Grading:[a] 3"	(75 mm)	100	100	100	100	100	100
2 1/2	(63 mm)					90–100	87–100
1"	(25 mm)	100	100	100	100	–	–
3/4"	(19 mm)	98	99	98	98	–	–
1/2"	(12.5 mm)	86	87	84	86	–	–
3/8"	(9.5 mm)	76	77	72	75	–	–
#4	(4.75 mm)	56	57	52	55	40–90	35–95
#8	(2.36 mm)	43	44	41	43	–	–
#16	(1.18 mm)	35	36	33	35	–	–
#30	(600 μm)	28	29	27	28	–	–
#50	(300 μm)	20	21	20	20	–	–
#100	(150 μm)	15	16	15	15	–	–
#200	(75 μm)	12	12	12	12	0–25	0–29
Atterberg Limits:[b] Liquid Limit						–	–
Plastic Limit		Non-plastic	Non-plastic	Non-plastic	Non-plastic	–	–
Plasticity Index						–	–
Max. Dry Density (lb./ft^3)(kg/m^3)[c]		142.6 (2,285)	142.0 (2,274)	142.3 (2,280)	142.3 (2279.7)	–	–
Optimum Moisture Content (%)[c]		4.8	5.1	4.9	5	–	–
R-Value		–	79	–	79	–	>50
Sand equivalent		–	30	–	30	>21	>18

[a] Determined according to AASHTO T 11 and AASHTO T 27
[b] Determined according to AASHTO T 89 and AASHTO T 90
[c] Modified Proctor determined according to AASHTO T 180

Table 3.7: Aggregate Base Material Properties

Property	Result				Operating Range	Contract Compliance
	Sample 1	Sample 2	Sample 3	Average		
Grading:[a] 1" (25 mm)	100	100			100	100–100
3/4" (19 mm)	94	93			93	90–100
1/2" (12.5 mm)	83	78			78	–
3/8" (9.5 mm)	76	68			68	–
#4 (4.75 mm)	56	44			44	35–60
#8 (2.36 mm)	35	28			28	–
#16 (1.18 mm)	23	20			20	–
#30 (600 μm)	16	14			14	10–30
#50 (300 μm)	10	9			9	–
#100 (150 μm)	7	6			6	–
#200 (75 μm)	5	5			5	2–9
Atterberg Limits:[b] Liquid Limit					–	–
Plastic Limit	Non-plastic	Non-plastic	Non-plastic	Non-plastic	–	–
Plasticity Index					–	–
Max. Dry Density (lb./ft^3)(kg/m^3)[c]		140.6 (2,252)			–	–
Optimum Moisture Content (%)[c]		6.0			–	–
R-Value[d]	–	79	–	79	–	>78
Sand equivalent[d]	–	31	–	31	>25	>22
Durability index[d]	–	78	–	78	–	>35

[a] Determined according to AASHTO T 11 and AASHTO T 27
[b] Determined according to AASHTO T 89 and AASHTO T 90
[c] Modified Proctor determined according to AASHTO T 180
[d] Test results provided by aggregate supplier

4.   TEST TRACK CONSTRUCTION

4.1   Introduction

Test track reconstruction included the following steps:

1. Remove the old surfacing layers from the previous experiment.
2. Remove the old full-depth recycled layers.
3. Remove and temporarily stockpile the remaining aggregate base layer.
4. Rip and recompact the upper 1 ft. (300 mm) of the subgrade following Caltrans standard specifications. This work was completed on 01/03/2019.
5. Spread the stockpiled old aggregate base materials and shape and compact them to form an aggregate subbase, 0.75 ft. (225 mm) thick, following Caltrans standard specifications. This work was completed on 01/04/2019.
6. Place a new Class 2 aggregate base, 0.6 ft. (180 mm) thick, following Caltrans standard specifications. This work was completed on 01/23/2019.
7. Apply an emulsified asphalt prime coat to the completed base. This work was completed on 03/14/2019.
8. Produce and place a layer of cold central plant recycled (CCPR) material 0.4 ft. (120 mm) thick. The recycling agents included two different emulsified asphalts (CCPR-EA) and one foamed asphalt (CCPR-FA). Residual asphalt contents of 2.5% by weight of the dry aggregate were used for all tests, with 1% portland cement active filler. The provisional Caltrans mix design method and nonstandard specification for partial-depth recycling (PDR) were followed for the mix design and placement of the materials. The CCPR-EA cells were built on 04/23/2019 and the CCPR-FA cells on 04/24/2019.
9. Apply a fog seal to the CCPR layer. This work was completed on 04/25/2019.
10. Apply a tack coat and place the first lift of RHMA-G mix following Caltrans standard specifications. This work was completed on 05/08/2019.
11. On the applicable RHMA-G study cells, apply a tack coat and the second lift of RHMA-G mix following Caltrans standard specifications. This work was also completed on 05/08/2019.

4.2   Existing Track Removal

The cement concrete, asphalt concrete, and full-depth recycled layers from the existing test track were removed and discarded on a waste pile at a nearby asphalt plant. The remaining existing base was ripped, windrowed, and removed with a scraper. Material was stockpiled on site for later use as the subbase on the new track.

4.3   Subgrade Preparation

The track subgrade was prepared on January 3, 2019. This involved ripping the material with a grader to a depth of approximately 1 ft. (300 mm), mixing and preliminary leveling of the material with the grader, primary compaction with a padfoot roller, finish leveling, and final compaction with a smooth drum roller. The process met the requirements of Section 19 in the Caltrans Specifications. Photographs of the subgrade preparation are shown in Figure 4.1 through Figure 4.5. Levels were determined with a base station. Compaction density was measured with a nuclear density gauge. Moisture gauges were installed in predetermined locations (discussed in Section 5.4).

Figure 4.1: Subgrade: Ripping with a grader.

Figure 4.2: Subgrade: Mixing and shaping.

Figure 4.3: Subgrade: Padfoot roller compaction.

Figure 4.4: Subgrade: Final shaping and compaction.

Figure 4.5: Subgrade: Completed preparation.

4.3.1 Subgrade Quality Control Testing

Compaction Density

Compaction density was measured using a nuclear gauge (CT 231) at two randomly selected locations in each cell on the day of construction. Compaction moisture content was determined by oven drying samples taken in the vicinity of the nuclear gauge measurements. Relative compaction was determined using the moisture-corrected dry nuclear gauge densities and the laboratory-determined modified Proctor density (AASHTO T 180) on materials sampled during material spreading. Although reference wet densities were also determined following CT 216, the modified Proctor results were considered to be a more representative measure of the density and only these results are reported (i.e., the CT 216 results were generally lower than the modified Proctor results, leading to unrealistically high relative compaction numbers). A summary of the results is provided in Table 4.1. The relative compaction achieved exceeded the specification requirements on all lanes.

Table 4.1: Summary of Subgrade Dry Density Measurements

Cell	MaxDD[a] (kg/cm³)	Nuclear Gauge Density					Moisture Content (%)	
		Average (kg/cm³)	Std. Dev.[b] (kg/cm³)	Relative (% of LMP)	Average (pcf)	Std. Dev. (pcf)	OMC[a]	Actual
D	1,954	1,899	104	97	118.6	6.4	17.0	15.8
E	1,954	1,908	18	97	119.1	1.1	17.0	16.0
F	1,954	1,887	26	96	117.8	1.6	17.0	16.0
G	1,954	1,885	25	96	117.7	1.5	17.0	16.0
H	1,954	1,931	6	98	120.5	0.4	17.0	14.8
I	1,954	1,929	11	98	120.4	0.7	17.0	14.8
J	1,954	1,906	36	97	119.0	2.2	17.0	14.8

[a] MaxDD/OMC = Laboratory-determined modified Proctor (LMP) dry density and optimum moisture content (AASHTO T 180)
[b] Std. Dev. = Standard deviation

4.4 Subbase Construction

Subbase construction was completed on January 4, 2019. Stockpiled base material from the previous full-depth recycling (FDR) study test track was distributed onto the prepared subgrade with a scraper, spread with a grader, and compacted with a smooth drum roller at optimum moisture content (additional water was applied with a water tanker when required). The process met the requirements of Section 25 in the Caltrans Specifications. Photographs of the subbase construction are shown in Figure 4.6 through Figure 4.10. Levels and layer thickness were

determined with a base station. Compaction density was measured with a nuclear density gauge. Moisture gauges were installed in predetermined locations (discussed in Section 5.4).

Figure 4.6: Subbase: Importing and spreading material with a scraper.

Figure 4.7: Subbase: Spreading and compacting.

Figure 4.8: Subbase: Water spraying.

Figure 4.9: Subbase: Final shaping and compaction.

Figure 4.10: Subbase: Completed preparation.

4.4.1   Subbase Quality Control Testing

<u>Compaction Density</u>

Compaction density measurements on the subbase followed the same procedure as that followed for testing on the subgrade. A summary of the results is provided in Table 4.2. The

relative compaction achieved met the specification requirements (95% of laboratory-determined dry density [i.e., modified Proctor, not CT 216]) on all lanes.

Table 4.2: Summary of Subbase Dry Density Measurements

Cell	MaxDD[a] (kg/cm³)	Nuclear Gauge Density					Moisture Content (%)	
		Average (kg/cm³)	Std. Dev.[b] (kg/cm³)	Relative (% of LMP)	Average (pcf)	Std. Dev. (pcf)	OMC[a]	Actual
D	2,281	2206	5.0	97	137.7	0.3	5.3	4.9
E	2,281	2170	17.9	95	135.5	1.1	5.3	4.9
F	2,281	2205	32.8	97	137.7	2.0	5.3	4.7
G	2,281	2164	21.8	95	135.1	1.4	5.3	4.5
H	2,281	2169	25.2	95	135.4	1.6	5.3	4.5
I	2,281	2205	7.9	97	137.7	0.5	5.3	4.9
J	2,281	2194	3.5	96	137.0	0.2	5.3	4.5

[a] MaxDD/OMC = Laboratory-determined modified Proctor (LMP) dry density and optimum moisture content (AASHTO T 180)
[b] Std. Dev. = Standard deviation

4.5 Base Construction

The aggregate base was constructed on January 23, 2019. Base material meeting Caltrans specifications for Class 2 aggregate base was trucked from a nearby alluvial quarry in bottom dump trucks. The aggregates were not crushed and most were rounded in shape. The material was spread with a grader and compacted with a smooth drum roller. The material was at or close to optimum moisture content at delivery, but additional water was applied with a water tanker when required. The process met the requirements of Section 26 in the Caltrans Specifications. Photographs of the base construction are shown in Figure 4.11 through Figure 4.15.

Levels and layer thickness were determined with a base station. Compaction density was measured with a nuclear density gauge. Moisture gauges and pressure cells were installed in predetermined locations at mid-depth in the layer. Strain gauges were installed on top of the layer (instrumentation is discussed in Section 5.4).
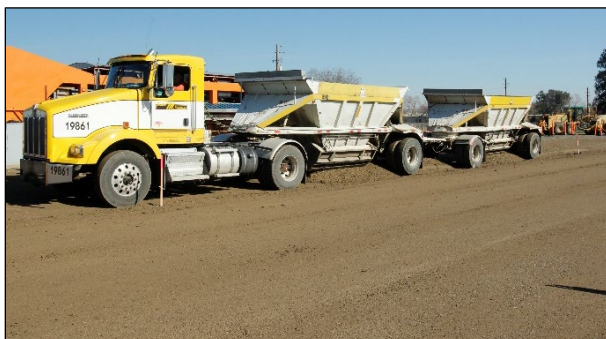
Figure 4.11: Base: Dumping imported material.
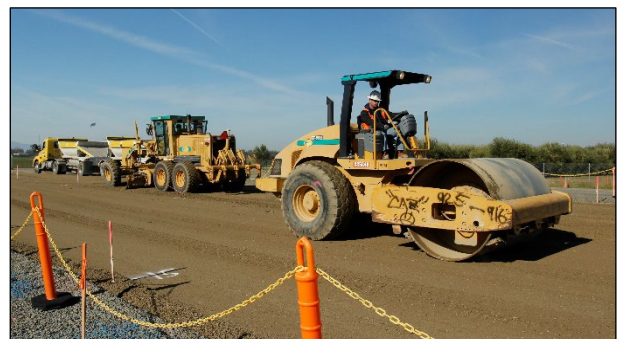
Figure 4.12: Base: Spreading and compacting.

Figure 4.13: Base: Water spraying.

Figure 4.14: Base: Final compaction.

Figure 4.15: Base: Completed preparation.

4.5.1 Base Quality Control Testing

Compaction Density

Compaction density measurements on the base followed the same procedure as that followed for testing on the subgrade and subbase. A summary of the results is provided in Table 4.3.

Table 4.3: Summary of Base Dry Density Measurements

Cell	MaxDD[a] (kg/cm³)	Nuclear Gauge Density					Moisture Content (%)	
		Average (kg/cm³)	Std. Dev.[b] (kg/cm³)	Relative (% of LMP)	Average (pcf)	Std. Dev. (pcf)	OMC[a]	Actual
D	2,252	2,187	17.7	97	136.5	1.1	6.2	5.4
E	2,252	2,210	9.8	98	138.0	0.6	6.2	5.9
F	2,252	2,223	11.0	99	138.8	0.7	6.2	6.1
G	2,252	2,209	25.3	98	137.9	1.6	6.2	5.0
H	2,252	2,238	45.8	99	139.7	2.9	6.2	6.5
I	2,252	2,192	32.5	97	136.8	2.0	6.2	6.1
J	2,252	2,219	19.3	99	138.5	1.2	6.2	5.6

[a] MaxDD/OMC = Laboratory-determined modified Proctor (LMP) density and optimum moisture content (AASHTO T 180)
[b] Std. Dev. = Standard deviation

The relative compaction achieved exceeded the specification requirements (95% of laboratory-determined dry density [i.e., modified Proctor, not CT 216]) on both lanes. Although compaction requirements were met, the surface material could be easily dislodged, which was attributed to the rounded nature of the aggregates and consequent poor aggregate interlock. This could result in the material being more susceptible to shearing under traffic loading.

4.5.2 Prime Coat Application on Base

An SS1h prime coat was applied at a rate of 0.25 gal./yd^2 (1.13 L/m^2) on March 14, 2019, approximately six weeks prior to placement of the CCPR layer (delay between construction of the base and CCPR layers was due to different contractors with different availability). The surface was sprayed with water prior to application of the prime coat (Figure 4.16 through Figure 4.18). No vehicle traffic was permitted on the prime-coated track prior to placement of the CCPR layer.

Figure 4.16: Base: Water spray prior to prime coat application.

Figure 4.17: Base: Prime coat application.

Figure 4.18: Base: Completed prime coat application.

4.6 Cold Central Plant Recycled Layer Construction

Materials for the cold central plant recycled layer were crushed on 04/18/2019 and 04/19/2019. The CCPR-EA layer on Lane 4 was constructed on 04/23/2019. The CCPR-FA layers on Lanes 1, 2,

and 3 were constructed on 04/24/2019. Material was placed as it was produced, and no treated materials were stockpiled.

4.6.1 Recycled Asphalt Pavement Processing

Recycled asphalt millings were sourced from the CCPR contractor's stockpile in Sacramento. The material was trucked to the site and stockpiled close to the screen and crushing plant. Material was taken from the stockpile and dumped onto a 4 in. (100 mm) static screen. Material that passed this screen was belt fed onto a 1 in. (25 mm) vibrating screen. Oversize material was fed from the screen into an impact crusher and then passed back over the 1 in. screen. All screened material was then belt fed onto a stockpile ready for processing through the cold central plant. The screening and crushing setup, RAP millings stockpile, and crushed materials are shown in Figure 4.19 through Figure 4.21, respectively.

Figure 4.19: CCPR: Screening and crushing setup.

Figure 4.20: CCPR: RAP millings stockpile.

Figure 4.21: CCPR: Crushed materials.

4.6.2 Cold Central Plant Material Processing

The cold central plant (CCP) was set up next to the crushing plant (Figure 4.22). Recycling agent was fed from a tanker. Active filler (cement) was fed from a super sack directly into the CCP hopper. Compaction and foaming water was sourced from the onboard tank and replenished as required from a water tanker. Samples for quality control and other testing were sampled from the belt. Issues with foaming water content for the CCPR-FA mix were noted in the early stages of production of this mix (mix placed on Lane 3 on Cell D and then Cell C). This was corrected for the mix placed on Lane 2 and Lane 1.

Figure 4.22: CCPR: Central plant setup.

4.6.3 Cold Central Plant Material Placement

Processed material was fed from the plant belt into waiting trucks (Figure 4.23) and then end-dumped from the truck directly into the paver hopper (Figure 4.24). Paving and compaction followed conventional procedures consistent with Caltrans partial-depth recycling (PDR) requirements (Figure 4.25 and Figure 4.26). A rolling pattern was established on each CCPR-EA cell and each CCPR-FA lane. A 10-ton vibrating steel drum roller was used for breakdown compaction, followed by a 20-ton (12 tons with ballast) pneumatic tired roller, and then a 10-ton steel drum roller without vibration for finish rolling.

Placement of the CCPR layers was completed with no major issues that might have influenced later performance of the structure. Some shearing of the recycled layer was observed during compaction with the pneumatic tired roller (Figure 4.27), which was attributed to deflection of the underlying aggregate base under the weight of the roller. Shear cracks were not observed after completion of final compaction with the finish roller (Figure 4.28).

Figure 4.23: CCPR: Belt-feed of processed material to truck.
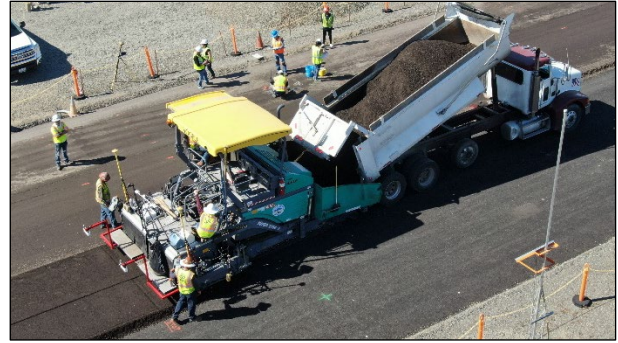
Figure 4.24: CCPR: Material transfer to paver.

Figure 4.25: CCPR: Paving and breakdown compaction.

Figure 4.26: CCPR: Intermediate compaction with pneumatic tired roller.
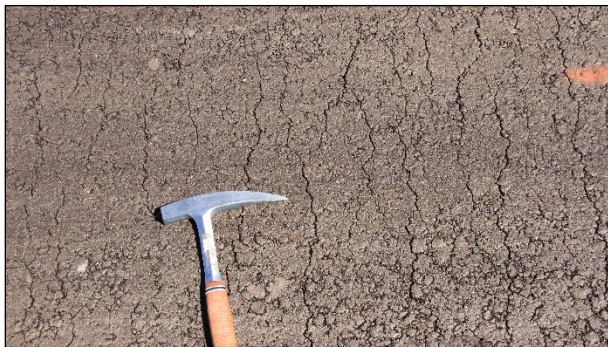
Figure 4.27: CCPR: Shear cracks after pneumatic tired roller passes.

Figure 4.28: CCPR: Crack-free surface after final compaction.

4.6.4 Cold Central Plant Layer Quality Control

<u>Compaction Density</u>

Compaction density on the CCPR layers was measured using a nuclear gauge in backscatter mode (CT 375) on the day of construction. Measurements were taken at three randomly selected locations on each cell. Relative compaction was determined using the CT 216 method on one sample from each cell. A summary of the density results is provided in Table 4.4. Relative

compaction ranged between 97% and 98%. However, these results may be questionable given that the CT 216 method is not always an accurate measure of compaction given the coarse gradation of the material and small specimen size. Relative compaction around 98% was expected.

Table 4.4: Summary of CCPR Layer Density Measurements

Cell	CT 216 (kg/cm^3)	Nuclear Gauge Density					Moisture Content (%)	
		Average (kg/cm^3)	Std. Dev.[a] (kg/cm^3)	Relative (% of 216)	Average (pcf)	Std. Dev.[a] (pcf)	Gauge	Gravimetric
D	2,121	2,082	32	98	130.0	2	13.2	6.0
E	2,121	2,073	6	98	129.4	0.4	13.1	6.0
F	2,121	2,070	28	98	129.2	1.7	13.0	6.0
G	2,121	2,055	15	97	128.3	0.9	14.0	6.0
H	2,121	2,065	7	97	128.9	0.4	12.7	6.2
I	2,121	2,072	5	98	129.4	0.3	14.3	6.2
J	2,121	2,041	22	98	127.4	1.4	14.6	6.2

[a] Std. Dev. = Standard deviation

Layer Thickness

Recycled layer thicknesses were determined from a precise leveling survey with measurements taken every 9.8 ft. (3 m) along the centerline of each lane. Measurements were also recorded from cores cut from the centerline 16.4 ft. (5 m) from the start and end of each cell. No cores were taken between these points to ensure that future HVS test sections would not be affected. Measurements were also taken from the density cores and from cores removed to install the multi-depth deflectometers at Station 13 on each HVS section. The results are summarized in Table 4.5 and indicate that the as-built thicknesses were close to the design thicknesses.

Table 4.5: Summary of CCPR Layer Thickness Measurements

Cell	Design Thickness		Average Thickness		Standard Deviation	
	(ft.)	(mm)	(ft.)	(mm)	(ft.)	(mm)
D			0.41	123	0.03	8.4
E			0.40	121	0.03	7.9
F			0.41	123	0.03	8.1
G	0.4	120	0.41	122	0.03	8.0
H			0.41	122	0.03	8.3
I			0.40	123	0.03	8.3
J			0.41	122	0.03	8.2

4.6.5 Curing Seal Application

A curing seal using the same emulsified asphalt used in the CCPR-EA layer was applied at a rate of 0.03 gal./yd^2 (0.14 L/m^2) after completion of all quality control testing (Figure 4.29 and

Figure 4.30). Given that the test track would not be trafficked until placement of the asphalt concrete surfacing, no sand cover was applied with the curing seal.

Figure 4.29: CCPR: Curing seal application.

Figure 4.30: CCPR: Completed recycled layer after construction.

4.7   RHMA-G Mix Placement

The RHMA-G mixes were placed on the four lanes of the test track on 05/08/2019, well within the Caltrans specification allowable 15-day period between construction of PDR and CCPR layers and placement of the asphalt surfacing. All mixes were produced at the George Reed asphalt plant in Clements, California. Mix was transported in end-dumps, and travel time between the plant and the test track was between 75 and 90 minutes depending on traffic. Production at the plant started at 04:00 hours with the control mix, followed by the other three mixes. The control mix was stored in a silo prior to transport for between 3.0 and 5.5 hours, depending on where it was placed. The first loads (3/4 in. with 10% RAP) departed from the plant at 06:30. The last load was placed at approximately 20:30. Compaction on the last cell was completed at approximately 22:00.

Ambient air temperature at 06:30, when activities on the test track started, was 50°F (10°C). Temperatures increased to a high of 85°F (29°C) at 16:00, falling to 65°F (18°C) at 22:00 when compaction on the last cell was completed. No clouds were observed during the day. Winds were light, with speeds ranging between 0.3 and 3.0 mph (0.5 and 4.8 km/h) for most of the day, increasing to 6.0 mph (9.6 km/h) in the late afternoon. Relative humidity ranged between a high of 91% at 06:30 and a low of 40% at 16:00, increasing again to 69% at 22:00.

Cells were paved in the following sequence:

1. Cell J (3/4 in. with 10% RAP), lift #1

2. Cells I and H (3/4 in. no RAP), lift #1
3. Cells F and E (1/2 in. with 10% RAP), lift #1
4. Cells G, D, C, B, and A (1/2 in. no RAP), lift #1 (mix was in silo for 3 to 4 hours)
5. Cell G, lift #2 (mix was in silo for up to 5.5 hours)
6. Cell J, lift #2 (mix was in silo for up to 8 hours)
7. Cell I, lift #2
8. Cell F, lift #2

4.7.1 Tack Coat Application

An SS1h tack coat was applied at a rate of 0.03 gal./yd^2 (0.14 L/m^2) approximately 60 minutes prior to placement of the first lift of RHMA-G on each cell (Figure 4.31 and Figure 4.32). The tack coat application was repeated prior to placing the second lift of RHMA-G on Cells F, G, I, and J (Figure 4.33).

Figure 4.31: RHMA-G: Tack coat application before first lift of RHMA-G (Cells H and I).

Figure 4.32: RHMA-G: Close-up view of tack coat application.

Figure 4.33: RHMA-G: Tack coat application between lifts of RHMA-G (Cell J).

4.7.2 Mix Temperatures

The temperature of the mix in each truckload was measured on arrival when the delivery documentation was checked. Average temperatures for the mixes placed on each cell are summarized in Table 4.6.

Table 4.6: Average RHMA-G Temperatures Measured in the Trucks

Cell (In Order of Paving)	Mix	Lift	Trucks	Time	Temperature	
					°F	°C
J	3/4 in. + 10% RAP	1	2	08:15	333.0	167.2
I and H	3/4 in. no RAP	1	4	09:00 – 09:20	323.9	162.2
F and E	1/2 in. + 10% RAP	1	4	09:30 – 09:50	366.1	185.6
G, D, C, B, and A	1/2 in. no RAP	1	10	12:00 – 15:45	330.5	165.8
G	1/2 in. no RAP	2	2	16:10	373.1	189.5
J	3/4 in. + 10% RAP	2	2	18:00	322.2	161.2
I	3/4 in. no RAP	2	2	18:10	349.4	176.4
F	1/2 in. + 10% RAP	2	2	19:50	342.6	172.6

4.7.3 Paving

Paving followed the sequence listed above. Given the confined working space on the test track, the short length of the cells, and small quantities of material required, mix was end-dumped directly into the paver (Figure 4.34) rather than dumping into a windrow and then using a material transfer vehicle to load the paver, as specified in the Caltrans specifications. Thereafter, paving and compaction followed conventional procedures consistent with the Caltrans Section 39 RHMA-G specification requirements (Figure 4.35 through Figure 4.38).

Figure 4.34: RHMA-G: Dumping mix into the paver (Cell J).

Figure 4.35: RHMA-G: Paving first lift of RHMA-G (Cell J).

Figure 4.36: RHMA-G: Breakdown compaction (Cell J).

Figure 4.37: RHMA-G: Breakdown (Cell G, front) and intermediate compaction (Cell J).

Figure 4.38: RHMA-G: Final compaction (Cells H and I).

4.7.4 RHMA-G Layer Quality Control

<u>Temperature</u>

Temperatures were systematically recorded throughout the placement of the RHMA-G using thermocouples (Figure 4.39) and an infrared camera attached to the paver (Figure 4.40). Approximate average mix temperatures behind the paver screed and at the start and completion of rolling for each cell are summarized in Table 4.7. These temperatures are consistent with typical temperatures on RHMA-G construction projects.

Figure 4.39: Temperature measurement with thermocouple.
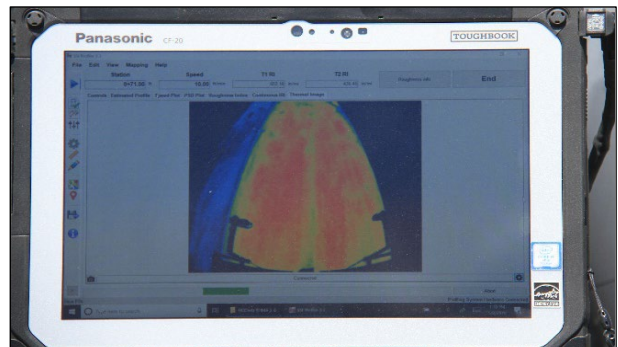
Figure 4.40: Temperature measurement with paver-mounted infrared camera.

Table 4.7: Approximate Average Mix Temperatures During Construction

Cell	Mix (In Order of Paving)	Lift	Average Temperature					
			Behind Paver		Start of Compaction		End of Compaction	
			(°F)	(°C)	(°F)	(°C)	(°F)	(°C)
D	1/2 in. no RAP	1	313	156	304	151	189	87
E	1/2 in. + 10% RAP	1	315	157	295	146	187	86
F	1/2 in. + 10% RAP	1	300	149	280	138	187	86
G	1/2 in. no RAP	1	Not tested					
H	3/4 in. no RAP	1	275	135	309	154	226	108
I	3/4 in. no RAP	1	318	159	288	142	180	82
J	3/4 in. + 10% RAP	1	327	164	259	126	214	101
F	1/2 in. + 10% RAP	2	Not tested					
G	1/2 in. no RAP	2	Not tested					
I	3/4 in. no RAP	2	322	161	255	124	271	133
J	3/4 in. + 10% RAP	2	286	141	277	136	192	89

Compaction Density

Compaction density was measured using a nuclear gauge (CT 375) on the day of construction and on cores removed from each cell on the days following construction. Relative compaction was determined using the theoretical specific gravity values (AASHTO T 209) of samples collected from the paver on each cell. Nuclear gauge measurements were taken at three randomly selected locations on each cell. A summary of the core density and nuclear gauge density results is provided in Table 4.8. The relative compaction (i.e., percent of maximum theoretical density) achieved on each lift on each cell is plotted in Figure 4.41.

Table 4.8: Summary of RHMA-G Layer Density Measurements

Cell	Lift	MTD[a] (g/cm³)	Core Density			Nuclear Gauge Density		
			Average (g/cm³)	Std. Dev.[b] (g/cm³)	Relative (% of MTD)	Average (g/cm³)	Std. Dev. (g/cm³)	Relative (% of MTD)
D	1	2.522	2.378	0.014	94.3	2.299	0.012	91.2
E	1	2.533	2.377	0.029	93.8	2.324	0.020	91.7
F	1	2.533	2.404	0.033	94.9	2.307	0.011	91.1
G	1	2.522	2.373	0.014	94.1	2.324	0.034	92.1
H	1	2.558	2.412	0.044	94.3	2.362	0.056	92.3
I	1	2.558	2.436	0.009	95.2	2.330	0.009	91.1
J	1	2.530	2.390	0.035	94.5	2.382	0.015	94.2
F	2	2.533	2.393	0.016	94.5	2.350	0.027	92.8
G	2	2.522	2.419	0.014	95.9	2.320	0.006	92.0
I	2	2.558	2.436	0.005	95.2	2.357	0.011	92.1
J	2	2.530	2.412	0.035	95.3	2.358	0.019	93.2

[a] MTD = Maximum theoretical density (determined according to AASHTO T 209)
[b] Std. Dev. = Standard deviation
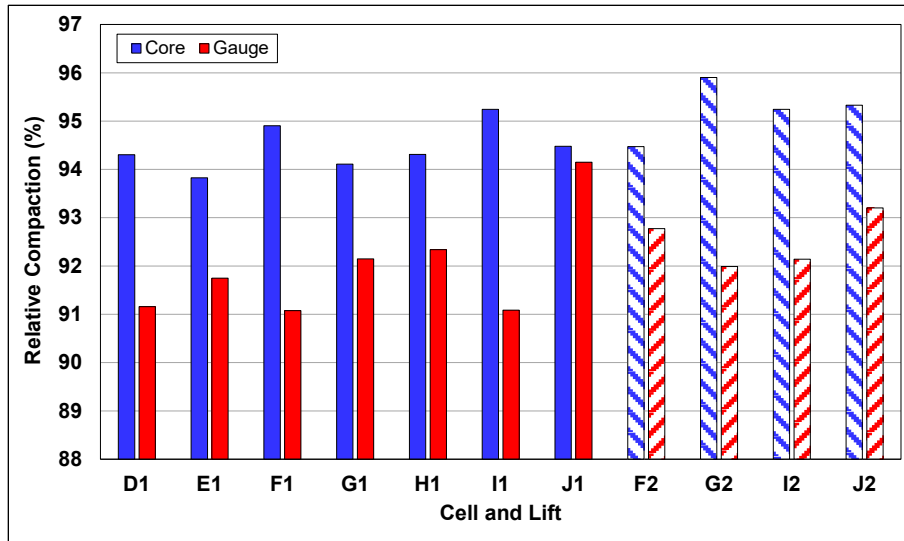
Figure 4.41: Summary of relative density measurements.

The results from cores were used for analysis purposes and indicate that all of the cells had satisfactory compaction and met Caltrans specifications (i.e., 91% to 97% of maximum theoretical density). There was some variability in the measurements across the seven cells, with relative compaction varying between 93.8% and 95.9%, an average of 94.7%, and a standard deviation of 2.1%. There were no clear reasons to explain the compaction differences across the seven cells (e.g., mix type, presence of RAP, mix temperature, number of roller passes, etc.), and it was therefore attributed to normal construction variability.

<u>As-Built RHMA-G Layer Thicknesses</u>

RHMA-G layer thicknesses were determined from a precise leveling survey with measurements taken every 9.8 ft. (3 m) along the centerline of each lane. Measurements were also recorded from cores cut from the centerline 16.4 ft. (5 m) from the start and end of each cell. No cores were taken between these points to ensure that future HVS test sections would not be affected. However, measurements were also taken from the density cores and later from cores removed to install the multi-depth deflectometers at Station 13 on each HVS section. The results are summarized in Table 4.9 and indicate that the as-built thicknesses were close to the design thicknesses.

Table 4.9: Layer Thickness Measurements

Cell	Mix Type	Design Thickness		Average Thickness		Standard Deviation	
		(ft.)	(mm)	(ft.)	(mm)	(ft.)	(mm)
D	1/2 in. NMAS, no RAP	0.2	60	0.2	65	0.01	3.1
E	1/2 in. NMAS + 10% RAP	0.2	60	0.2	62	0.01	1.6
F	1/2 in. NMAS + 10% RAP	0.4	120	0.4	117	0.01	1.7
G	1/2 in. NMAS + 10% RAP	0.4	120	0.4	119	0.01	2.5
H	3/4 in. NMAS, no RAP	0.2	60	0.2	64	0.01	2.5
I	3/4 in. NMAS, no RAP	0.5	150	0.5	149	0.01	3.2
J	3/4 in. NMAS + 10% RAP	0.5	150	0.5	149	0.01	3.7

4.8   Test Track Approval

The test track was considered to be representative of a highway project and was approved for HVS testing.

5.   TRACK LAYOUT, INSTRUMENTATION, AND TEST CRITERIA

5.1   Testing Protocols

The Heavy Vehicle Simulator (HVS) test section layout, test setup, trafficking, and measurements followed standard University of California Pavement Research Center (UCPRC) protocols *(13)*. Details specific to this project are discussed in the following sections.

5.2   Test Track Layout

The test track layout for this project is shown in Figure 5.1. Falling weight deflectometer (FWD) test results were used to identify two uniform HVS test sections in each mix cell, the first for assessing rutting performance under high pavement temperature conditions (Phase 1) and the second for potential repeat or additional testing (e.g., fatigue cracking performance). Additional testing, if justified, will be identified and motivated based on the results of the first round of testing and associated laboratory testing.
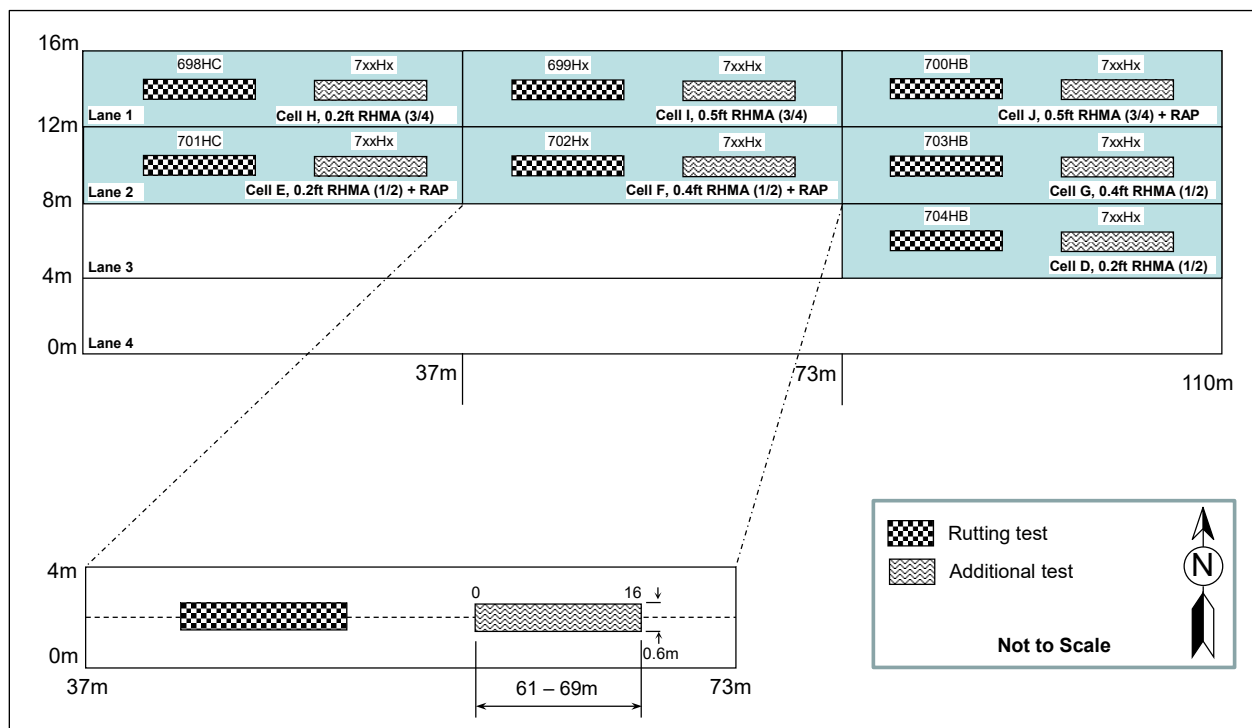
Figure 5.1: Test track layout.

The test section numbers were allocated in order of location on the test track, as follows, and do not represent testing sequence. The letters HB and HC refer to the specific HVS equipment used

for testing (x implies that a section number and/or equipment has not been assigned). Section 704HB was considered to be the control section:

- Section 698HC: 0.2 ft. (60 mm) RHMA-G, with 3/4 in. nominal maximum aggregate size (NMAS) and no RAP
- Section 699Hx: 0.5 ft. (150 mm) RHMA-G, with 3/4 in. NMAS and no RAP
- Section 700HB: 0.5 ft. (150 mm) RHMA-G, with 3/4 in. NMAS with 10% RAP aggregate replacement
- Section 701HC: 0.2 ft. (60 mm) RHMA-G, with 1/2 in. NMAS with 10% RAP aggregate replacement
- Section 702Hx: 0.4 ft. (120 mm) RHMA-G, with 1/2 in. NMAS with 10% RAP aggregate replacement
- Section 703HB: 0.4 ft. (120 mm) RHMA-G, with 1/2 in. NMAS and no RAP
- Section 704HB: 0.2 ft. (60 mm) RHMA-G, with 1/2 in. NMAS and no RAP (Control Section)

This report covers the testing on Sections 698HC, 700HB, 701HC, 703HB, and 704HB. Testing on Sections 699Hx and 702Hx was put on hold due to resource availability.

5.3   HVS Test Section Layout

An HVS test section for assessing rutting performance is 8.0 m (≈26.2 ft.) long and 0.6 m (≈2 ft.) wide. The schematic in Figure 5.2 shows a typical HVS test section along with the stationing and coordinate system. Station numbers (0 to 16) refer to fixed points on the test section and are used for measurements and as a reference for discussing performance in later chapters. Stations are placed at 0.5 m (≈1.6 ft.) increments. A sensor installed 50 mm (≈2 in.) below the center of the test section would have an x-coordinate of 4,000 mm, a y-coordinate of 300 mm (≈1.0 ft.), and z-coordinate of 50 mm (≈2 in.).

5.4   Test Section Instrumentation

Measurements were taken with the equipment and instruments listed as follows. Instrument positions are shown in Figure 5.2.

- A laser profilometer was used to measure surface profile; measurements were taken at each station.
- A road surface deflectometer (RSD) was used to measure elastic surface deflection during the test. RSD measurements were taken under a creep-speed 40 kN (9,000 lb.) half-axle load at regular intervals. Note that RSD measurements under a creep-speed load (2 km/h

[1.2 mph] would not be the same as those recorded under the trafficking speed loads. After load changes, deflections were measured under the new load, as well as under the 40 kN load, which serves as a baseline for assessing damage under the heavier loads. Note that a 40 kN half-axle load on the HVS equates to an 80 kN (18,000 lb.) full axle load on a truck, or one equivalent single axle load (ESAL).
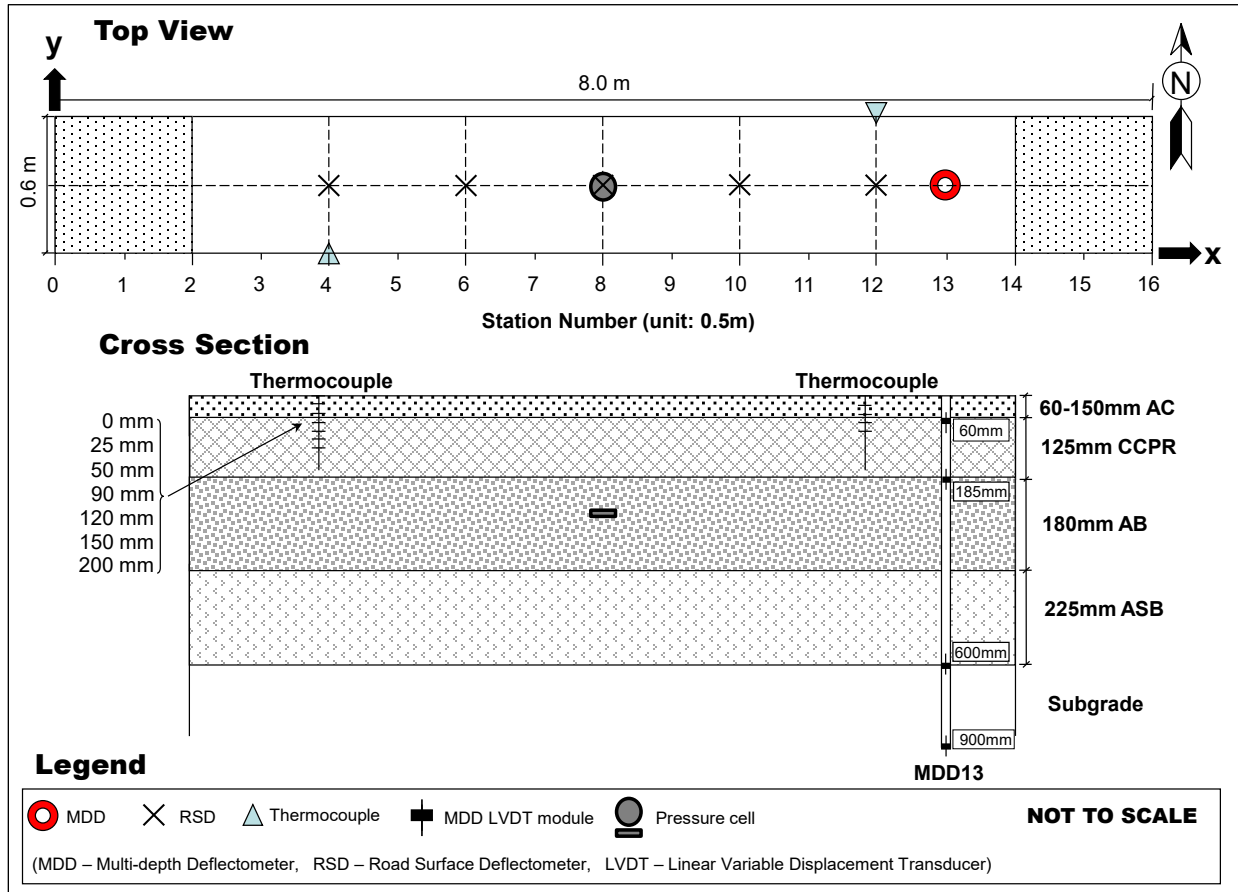
Figure 5.2: Schematic of an HVS test section layout.

- An FWD was used to measure surface deflection on the section before and after HVS testing to evaluate the change in stiffness caused by trafficking. Testing was undertaken on both the trafficked and adjacent untrafficked areas (i.e., 4 m on either end of the 8 m test section) at 500 mm (≈19.7 in.) intervals. Two sets of tests were undertaken on each day to obtain a temperature range for backcalculation of layer stiffnesses.

- Type-T thermocouples were used to measure pavement and air temperatures (both inside and outside the HVS environmental chamber). Seven thermocouples were bundled together to form a "thermocouple tree" for measuring air, pavement surface, and pavement layer temperatures inside the environmental chamber. Pavement layer temperatures were measured at the pavement surface, and at depths of 25, 50, 90, 120, 150, and 200 mm (≈1, 2, 3.5, 4.7, 6, and 8 in.). Air temperatures were measured with

thermocouples attached to the outside walls of the environmental chamber, with at least one thermocouple in direct sunlight during any part of the day. Additional air temperatures were recorded at a weather station at the northwest end of the test track.

- One multi-depth deflectometer (MDD) was installed on each Phase 1 test section. An MDD is essentially a stack of linear variable differential transformer (LVDT) modules fixed at different depths in a single borehole. The LVDT modules have non-spring-loaded core slugs that are linked together into one long rod that is anchored at the bottom of a 3.3 m (≈10.8 ft.) borehole. The LVDT modules are fixed to the pavement layer, which allows permanent vertical deformations at various depths to be recorded, in addition to measurement of the elastic deformation caused by the passage of the HVS wheels. The borehole is 38 mm (≈1.5 in.) in diameter. A model MDD with five modules is shown in Figure 5.3. In this project, the MDD was installed at Station 13 between the two wheelpaths of the dual-wheel configuration, with modules 10 mm below the top of the CCPR layer, 10 mm below the top of the aggregate subbase layer, and 10 and 300 mm below the top of the subgrade layer. On one section, a second MDD was installed in the wheelpath at Station 3 to assess differences in results between data collected between the wheelpaths of the dual wheel and data collected in one of the wheepaths, as well to assess upgrades to the device and changes to the installation procedure.

Figure 5.3: A model multi-depth deflectometer (MDD), showing five modules.

- One RST LPTPC09-S pressure cell was installed at mid-depth in the aggregate base layer (Figure 5.4) on each Phase 1 test section to measure vertical pressure (stress) under the moving wheel.

Figure 5.4: Pressure cell installation.

- Multiple moisture sensors (Decogon GS1) were installed in the subgrade, subbase, and base layers (Figure 5.5), positioned next to and between select sections, as shown in Figure 5.6 and Figure 5.7.

Figure 5.5: Moisture sensor installation on top of subbase.

Figure 5.6: Moisture sensor locations on top of subbase.
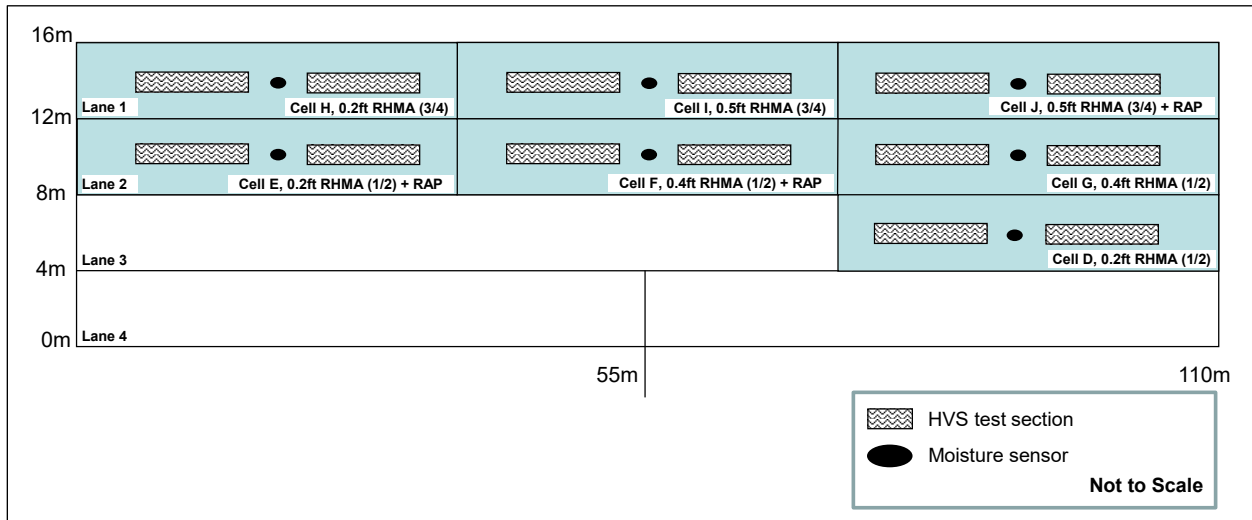
Figure 5.7: Moisture sensor locations.

5.5 Test Section Measurements

5.5.1 Temperature

Pavement temperatures were controlled using an environmental chamber. Both pavement and air (inside and outside the environmental chamber) temperatures were monitored and recorded hourly during the entire trafficking period. In assessing rutting performance, the temperature at the bottom of the asphalt concrete and the temperature gradient from top to bottom of the asphalt concrete layers are two important controlling temperature parameters that influence the stiffness of the asphalt concrete and are used to compute plastic strain.

5.5.2 Surface Profile

The following rut parameters were determined from laser profilometer measurements:

- Maximum total rut depth at each station
- Average maximum total rut depth for all stations
- Average deformation for all stations
- Location and magnitude of the maximum rut depth for the section
- Rate of rut development over the duration of the test

The difference between the surface profile after HVS trafficking and the initial surface profile before HVS trafficking is the permanent change in surface profile. Based on the change in surface profile, the maximum total rut is determined for each station, as illustrated for a dual wheel configuration in Figure 5.8. The average maximum total rut for the section is the average of all of the maximum total ruts measured between Stations 3 and 13.
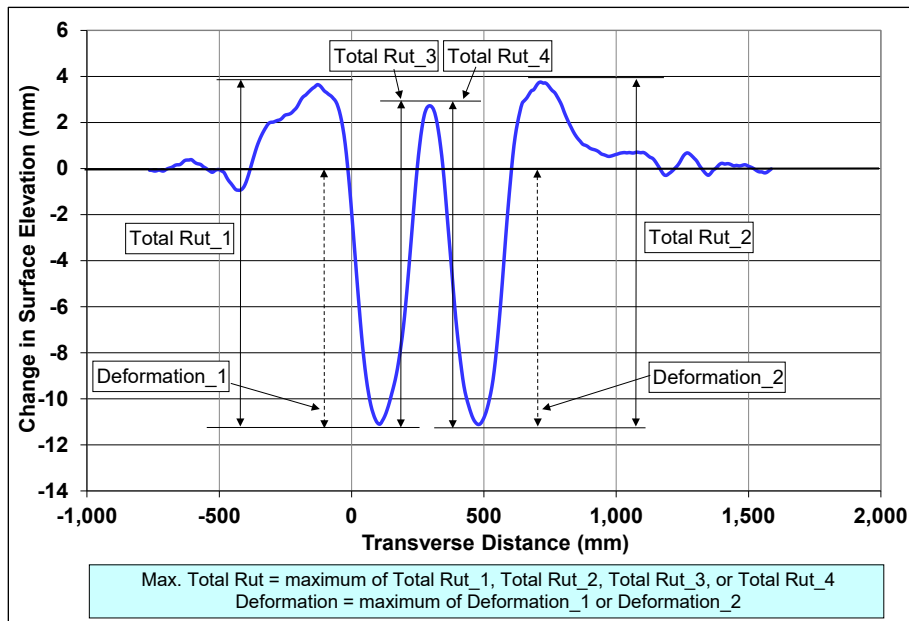
Figure 5.8: Illustration of maximum rut depth and deformation for a leveled profile.

5.5.3 Elastic Vertical Deflection

An example set of MDD data is presented in Figure 5.9, which shows the variation of the elastic vertical deflections measured at different depths versus wheel position as the wheel travels from one end of the test section to the other. The elastic vertical deflection is the difference between the total vertical deflection and the reference value, which is the measurement recorded when

the wheel is at the far end of the test section. The peak values are the maximum elastic vertical deflection for each individual MDD module.
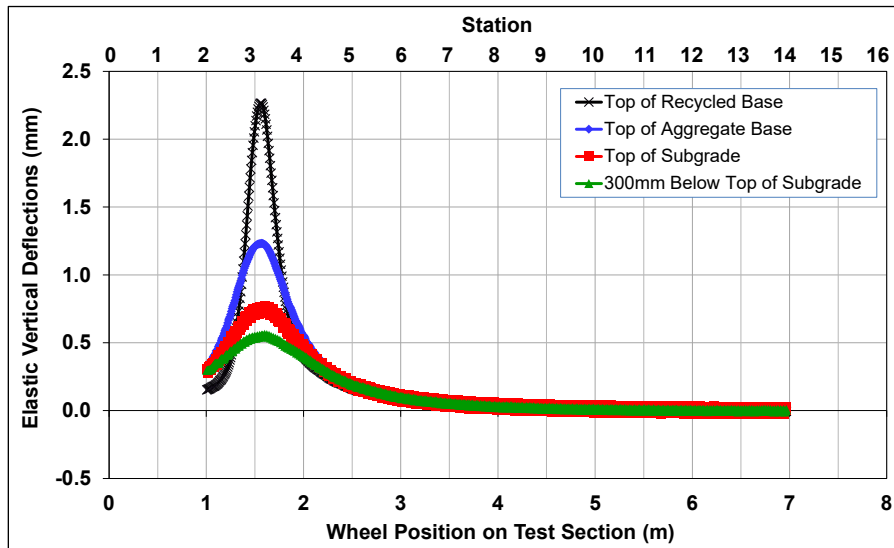
Figure 5.9: Example elastic vertical deflection measured with MDD at Station 3.

5.5.4 Pressure

Example data recorded from a pressure cell is shown in Figure 5.10, which shows the variation of the cell reading versus wheel position as the wheel travels from one end of the test section to the other. Several quantities are summarized based on the raw readings. The peak pressure reported is the difference between the maximum value and the reference value, defined as the value of the first reading recorded at the point furthest away from the instrument (i.e., Station 2).
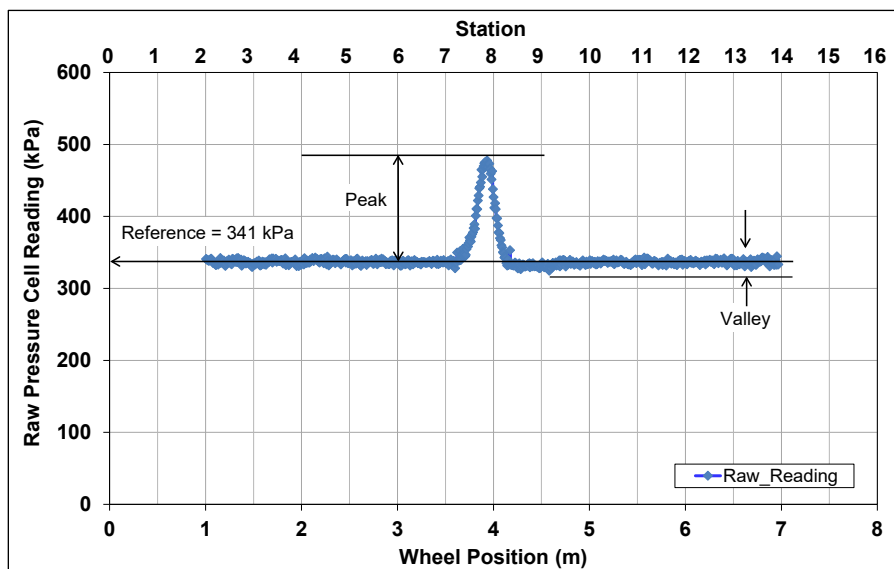
Figure 5.10: Example pressure cell reading and definition of summary quantities.

5.5.5 Backcalculation of Layer Stiffness from Falling Weight Deflectometer

A recursive process of changing the stiffnesses of the pavement structure to match the calculated deflection with the measured deflection at the various FWD geophone locations in a layer elastic software package (*Openpave*) is used to backcalculate layer stiffnesses on each test cell. The FWD geophone locations are provided in Table 5.1. The sensitivity of the layer backcalculated stiffnesses are affected by the relative location of the geophones and the number of measurements taken in the layer when projecting the measurement location at a 45° angle downward (e.g., the second geophone, at 200 mm [≈8 in.] from the center of the plate, measures approximately the deflection 200 mm below the plate). Note that 200 mm is the shortest spacing possible between Sensor 1 and Sensor 2 due to the radius of the drop plate.

Table 5.1: FWD Geophone Locations

Distance from Plate	Geophone Number							
	1	2	3	4	5	6	7	8
Distance from plate (mm)	0	200	300	450	600	900	1,200	1,500
Distance from plate (in.)	0.0	7.9	11.8	17.7	23.6	35.4	47.2	59.1

The pavement structures on the current test track have an RHMA-G overlay between 0.2 and 0.5 ft. thick on top of a 0.4 ft. thick CCPR layer. The interface between the RHMA-G and CCPR layers is therefore at a depth that is less than the distance between the first two geophones on the FWD, which cannot be shortened because of the diameter of the plate. At this geophone spacing, no data is available to separate the deflection in the RHMA-G and CCPR layers. In terms of backcalculation, the result is a structure that has several solutions (stiffness combinations) that fit the deflection bowl measured by the FWD. The most appropriate solution for the test track was considered to be the combination of the top two layers in the backcalculation process to calculate the effective stiffness of each layer.

The pavement structure was modeled as a three-layer structure, resulting in the following three stiffness results:

- Layer 1 (E1) – Composite of RHMA-G ($E1_1$) and CCPR ($E1_2$) layers
- Layer 2 (E2) – Composite of aggregate base and aggregate subbase layers
- Layer 3 (E3) – Subgrade

In *CalME*, Equation 5.1 is used to calculate the bending stiffness of unbound layers as a result of the non-linearity of the material. Equation 5.1 is also applicable to bound layers without slip.

$$S_n = \sum_{i=1}^{n-1} h_i \times \sqrt[3]{E_i}$$ (5.1)

where: S_n is the bending stiffness of layer n
h_i is the layer thickness for layer i
E_i is the layer stiffness for layer i

Equation 5.1 was expanded in Equation 5.2 to include each of the composite layers to provide the bending stiffness of the second layer. Equation 5.2 was further simplified to Equation 5.3 and Equation 5.4 to calculate the stiffnesses of the RHMA-G and CCPR layers, respectively. The laboratory-determined dynamic modulus (results at 10 Hz at 21°C) of each material was used as the value for n in Equation 5.3, and was measured on cores removed from points next to the test section after completion of HVS testing.

$$S_2 = h_{1\_1} \times \sqrt[3]{E_{1\_1}} + h_{1\_2} \times \sqrt[3]{E_{1\_2}}$$ (5.2)

$$E_{1\_1} = \left(\frac{S_2}{h_{1\_1} + h_{1\_2}\sqrt[3]{n}}\right)^3$$ (5.3)

$$E_{1\_2} = n \times E_{1\_1}$$ (5.4)

where: $n = E_{1\_2}/E_{1\_1}$
E_{1_1} is the stiffness of the RHMA-G layer
E_{1_2} is the stiffness of the CCPR layer
H_{1_1} is the thickness of the RHMA-G layer
H_{1_2} is the thickness of the CCPR layer

This approach provided a means of obtaining a realistic estimate of the backcalculated stiffness of the RHMA-G and CCPR layers using the stiffness ratio between the two layers.

5.5.6   Visual Assessments

A thorough visual assessment of the test section is carried out during each data collection exercise and the condition and any distresses are noted. If cracks are observed, they are traced with a yellow lumber crayon and then the section is photographed. The photograph is then digitized and the crack lengths measured.

5.6   HVS Test Criteria

5.6.1   Tire Configuration and Traffic Pattern

All trafficking was carried out with a dual-wheel configuration, using steel-belt radial truck tires (11R22.5) inflated to a pressure of 720 kPa (104 psi), in a channelized, unidirectional loading

mode with no wander (i.e., trafficking in one direction consistent with standard procedures for testing asphalt concrete layer performance). Load was checked with a calibrated portable weigh-in-motion pad at the beginning of each test.

5.6.2 Test Section Failure Criteria

An average maximum rut depth of 12.5 mm (≈0.5 in.) and/or an average crack density of 2.5 m/m^2 (≈0.75 ft./ft^2) over the full monitored section (Station 3 to Station 13) were set as the failure criteria for the experiment. In some instances, HVS trafficking was continued past these points so the rutting and/or cracking behavior of a test section could be fully understood.

5.6.3 Environmental Conditions

Infrared heaters and a chilling unit inside the HVS environmental chamber were used to maintain pavement temperatures. The test sections received no direct rainfall as they were protected by the environmental chamber.

The pavement temperature at 50 mm (≈2.0 in.) pavement depth was maintained at 50±2°C (≈122±4°F) to assess rutting performance in the RHMA-G layers under hot pavement conditions.

6. PHASE 1 HVS TEST DATA SUMMARY

6.1   Introduction

This phase of HVS testing was carried out to compare performance of four different RHMA-G mixes. Pavement temperature at 50 mm (≈2.0 in.) pavement depth was maintained at 50±2°C (≈122±4°F) to assess primarily rutting but also cracking potential in the RHMA-G surfacing layer(s). This temperature is consistent with similar HVS testing in past projects. The following chapters provide a summary of the data collected from the five Phase 1 HVS tests sequenced in terms of nominal maximum aggregate size, thickness, and use of recycled asphalt pavement (i.e., 704HB, 703HB, 701HC, 698HC, and 700HB) and a brief discussion of the first-level result analysis. The following data were collected:

- Rainfall
- Air temperatures outside and inside the environmental chamber
- Pavement temperatures at the surface and 25, 50, 90, 120, 150, and 200 mm below the surface
- Surface permanent deformation (rutting)
- Permanent deformation at the top of the recycled layer, top of the aggregate base layer, top of the original subbase layer, top of the subgrade, and approximately 300 mm below the top of the subgrade
- Pressure (vertical stress) in the middle of the recycled layer
- Elastic vertical deflection on the surface and at the top of the recycled layer, top of the aggregate base layer, top of the original subbase layer, top of the subgrade, and approximately 300 mm below the top of the subgrade
- Pavement deflection and layer stiffnesses

Note that, where possible, x and y axis scales in graphs have been kept the same for the five tests to facilitate visual comparison of the results.

6.2   Test Duration

HVS trafficking on each section was initiated and completed, as shown in Table 6.1. The sequence of testing was adjusted to accommodate positioning of the two HVS machines on the test sections (i.e., the machines cannot test side by side on the test track configuration because of space limitations). Note that significant delays in testing were experienced due to COVID-19

mandated shutdowns, which also led to delays in receiving critical parts for a scheduled overhaul and for equipment maintenance and repairs.

Table 6.1: HVS Test Duration

Section No.	Test Sequence	Layer Properties	Start Date	Finish Date[a]	Load Repetitions
704HB	3	0.2 ft. RHMA-G (1/2 in.)	07/05/2020	09/16/2020	320,000
703HB	4	0.4 ft. RHMA-G (1/2 in.)	09/24/2020	12/06/2020	400,000
701HC	2	0.2 ft. RHMA-G (1/2 in.) + RAP	09/06/2019	07/23/2020	300,000
698HC	5	0.2 ft RHMA-G (3/4 in.)	07/21/2021	11/15/2021	383,579
700HB	1	0.5 ft. RHMA-G (3/4 in.) + RAP	08/09/2019	11/27/2019	600,000
699Hx[b]	Not tested	0.5 ft. RHMA-G (3/4 in.)	Not applicable		
702Hx[b]	Not tested	0.4 ft. RHMA-G (1/2 in.) + RAP	Not applicable		

[a] 701HC was tested in two phases (09/09/2019 to 11/25/2019 and then 06/17/2020 to 07/23/2020) due to an equipment breakdown followed by mandated COVID-19 shutdowns.
[b] 699Hx and 702Hx were not tested due to limited resources available after completion after the first five tests and because the research team agreed that sufficient data had been collected for the 2nd level analysis from the HVS and laboratory tests.

6.3 HVS Loading Program

The HVS loading program for each section in each testing phase is summarized in Table 6.2.

Table 6.2: Summary of HVS Loading Program

Section No.	Layer Properties	Wheel Load[a] (kN)	Load Repetitions	ESALs[b]	Test to Failure?
704HB	0.2 ft. RHMA-G (1/2 in.) Control	40	160,000	160,000	Yes (Rut depth)
		60	100,000	549,014	
		80	60,000	1,102,750	
	Section Total		320,000	1,811,764	
703HB	0.4 ft. RHMA-G (1/2 in.)	40	160,000	160,000	Yes (Rut depth)
		60	100,000	549,014	
		80	140,000	2,573,084	
	Section Total		400,000	3,282,098	
701HC	0.2 ft. RHMA-G (1/2 in.) + RAP	40	160,000	160,000	Yes (Rut depth)
		60	100,000	549,014	
		80	40,000	735,167	
	Section Total		300,000	1,444,181	
698HC	0.2 ft. RHMA-G (3/4 in.)	40	160,000	160,000	Yes (Rut depth)
		60	100,000	549,014	
		80	123,579	2,271,280	
	Section Total		383,579	2,980,294	
700HB	0.5 ft. RHMA-G (3/4 in.) + RAP	40	160,000	160,000	Yes (Rut depth)
		60	100,000	549,014	
		80	340,000	6,248,919	
	Section Total		600,000	6,957,933	
Total for the Five Sections			**2,003,579**	**16,475,270**	

[a] 40 kN = 9,000 lb.; 60 kN = 13,500 lb.; 80 kN = 18,000 half-axle loads
[b] ESAL: Equivalent single axle load using the following Caltrans conversion ESALs = (axle load/18,000)[4.2]

6.4 Rainfall

Figure 6.1 shows the monthly rainfall data from August 1, 2019, through November 31, 2021, as measured at the weather station next to the test track. All sections were tested predominantly during dry conditions, with small amounts of infrequent rainfall recorded during four of the five tests (no rainfall was recorded during testing on 704HB and only trace amounts were recorded during testing on 703HB). Only three significant rainfall events (i.e., more than 25 mm [≈1.0 in.] in 24 hours for this study) occurred, with one event recording 112 mm (≈4.5 in.) in 24 hours (698HC).
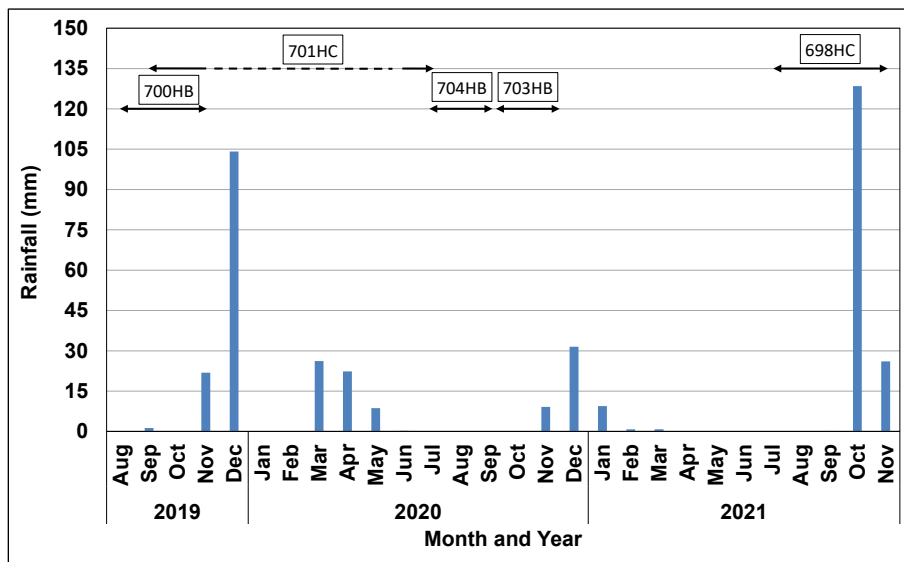
Figure 6.1: Measured rainfall during Phase 1 HVS testing.

Blank page

7.   SECTION 704HB: 0.2 ft. RHMA-G (1/2 in.) CONTROL

7.1   Test Summary

Loading commenced with a 40 kN half-axle load on July 6, 2020, and ended with an 80 kN load on September 18, 2020. A total of 320,000 load repetitions were applied, and 36 datasets were collected. Load was increased from 40 kN to 60 kN after 160,000 load repetitions, and then to 80 kN after 260,000 load repetitions. The HVS loading history for Section 704HB is shown in Figure 7.1. A 21-day breakdown resulting from a hydraulic system failure occurred between August 6 and August 26.
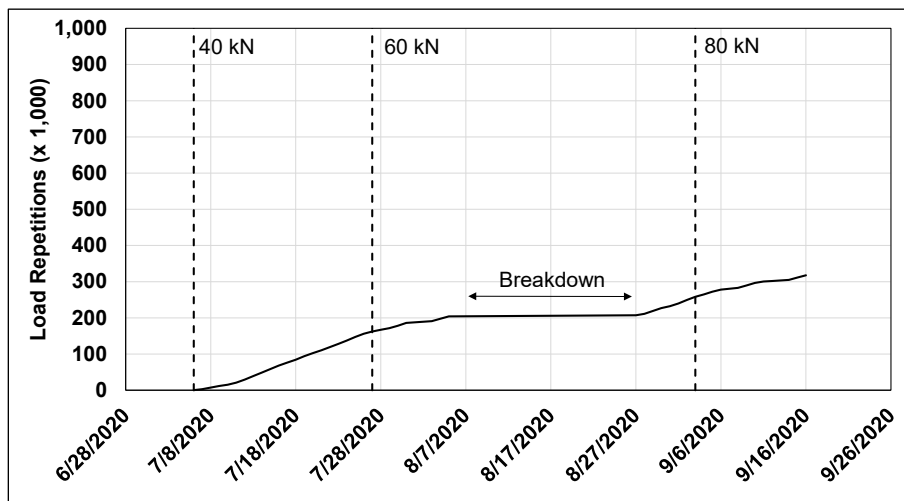
Figure 7.1: 704HB: HVS loading history.

7.2   Air Temperatures

7.2.1   Outside Air Temperatures

Daily 24-hour average outside air temperatures, measured with thermocouples attached to either side of the HVS environmental chamber (i.e., in direct sunlight), are summarized in Figure 7.2. Vertical error bars on each point on the graph show the daily temperature range. Temperatures ranged from 13.4°C to 52.9°C (≈56°F to 127°F) during the course of HVS testing, with a daily 24-hour average of 27.2°C (≈81°F), an average minimum of 19.2°C (≈67°F), and an average maximum of 40.4°C (≈104°F).
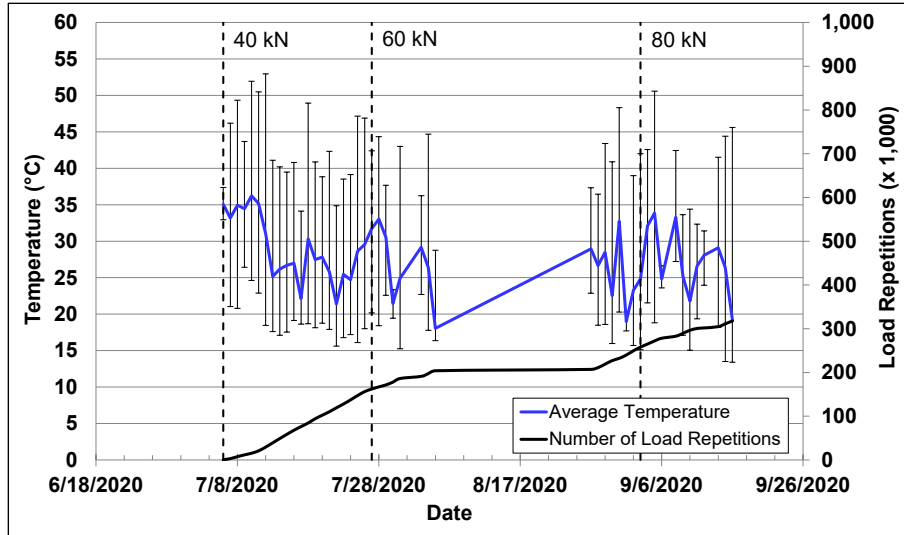
Figure 7.2: 704HB: Daily average air temperatures outside the environmental chamber.

7.2.2 Air Temperatures Inside the Environmental Chamber

The daily 24-hour average air temperatures, measured with thermocouples attached to either side of the HVS environmental chamber above the heaters, were calculated from the hourly temperatures recorded during HVS operations, and are shown in Figure 7.3. Vertical error bars on each point on the graph show the daily temperature range. During the test, air temperatures inside the environmental chamber ranged from 21.9°C to 51.2°C (≈71°F to 124°F) with an average of 42.8°C (≈109°F) and a standard deviation of 2.9°C (≈5.1°F). Heaters were automatically adjusted to maintain a pavement temperature of 50±2°C at a pavement depth of 50 mm. The recorded pavement temperatures discussed in Section 7.3 indicate that the inside air temperatures were adjusted appropriately to maintain the required pavement temperature.

7.3 Pavement Temperatures

Daily 24-hour averages of the air, surface, and in-depth temperatures of the RHMA-G and recycled layers are shown in Figure 7.4 and listed in Table 7.1. Pavement temperatures were constant and in the target range (50±2°C at a pavement depth of 50 mm) in the RHMA-G layer. Temperatures decreased with increasing depth in the underlying layers, as expected.
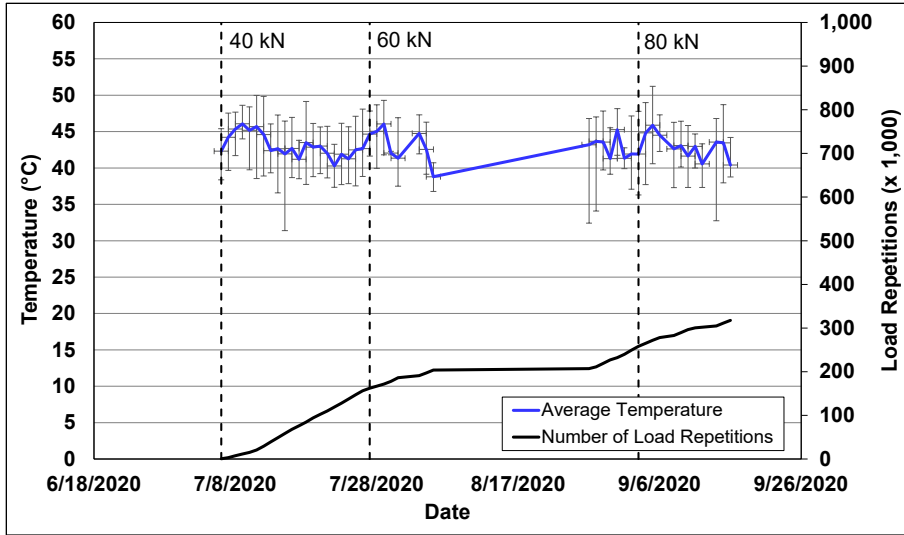
Figure 7.3: 704HB: Daily average air temperatures inside the environmental chamber.
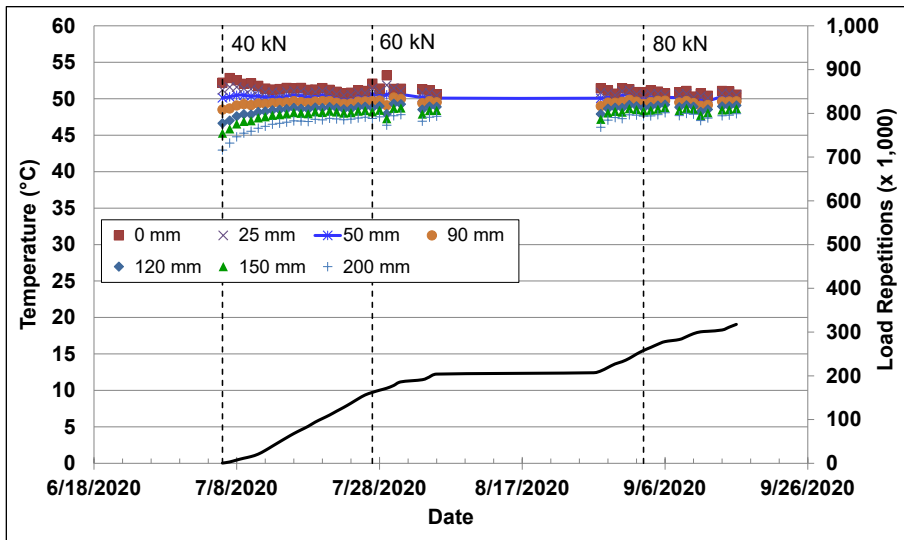
Figure 7.4: 704HB: Daily average pavement temperatures.

Table 7.1: 704HB: Summary of Air and Pavement Temperatures

Thermocouple Location	Layer	Temperature			
		Average (°C)	Std. Dev. (°C)	Average (°F)	Std. Dev. (°F)
Outside air	N/A	27.2	8.5	80.9	15.3
Inside air	N/A	42.8	2.9	109.0	5.1
Pavement surface	RHMA-G	51.2	1.7	124.2	3.1
25 mm below surface	RHMA-G	50.9	0.9	123.5	1.6
50 mm below surface	RHMA-G	50.3	0.6	122.5	1.2
90 mm below surface	Recycled	49.5	0.6	121.1	1.1
120 mm below surface	Recycled	48.7	0.6	119.6	1.1
150 mm below surface	Recycled	48.1	0.7	118.6	1.3
200 mm below surface	Aggregate base	47.1	0.9	116.8	1.6

7.4   Permanent Deformation on the Surface (Rutting)

Figure 7.5 shows the average transverse cross section measured with the laser profilometer at various stages of the test. This plot clearly shows the initial high rate of rutting and the increase in rutting and deformation over time and that most of the deformation was in the form of a depression (i.e., deformation was below the zero elevation point at the surface [see Figure 5.8]) rather than upward and outward displacement of the material above the zero elevation point.
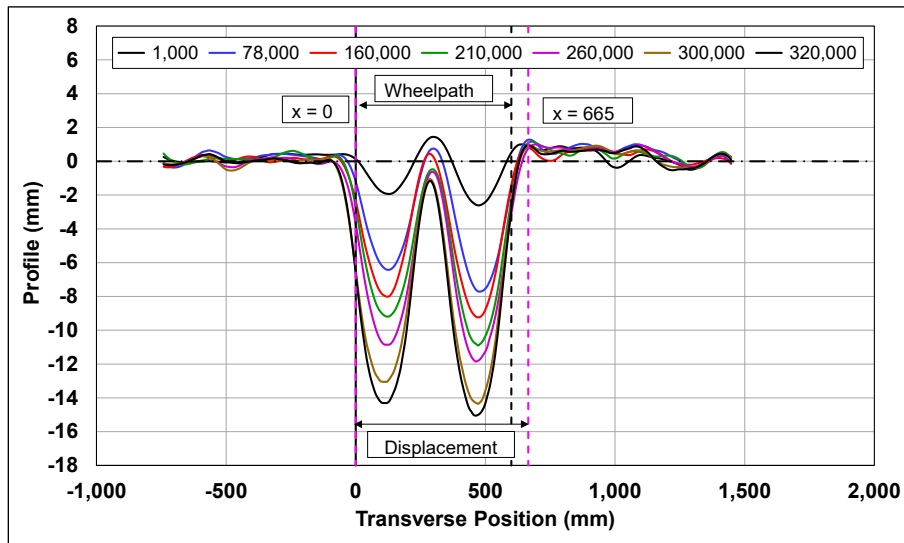
Figure 7.5: 704HB: Profilometer cross section at various load repetitions.

Figure 7.6 shows the development of permanent deformation (average maximum total rut and average deformation) with load repetitions. Error bars on the plot indicate lowest and highest measurements along the section. These error bars show that there was considerable variation in rut depth along the length of the section. The cause of this variation cannot be determined from the data alone and will be investigated during the forensic investigation when all testing is completed.

During HVS testing, rutting usually occurs at a high rate initially and then typically diminishes as trafficking progresses until reaching a steady state. This initial phase is referred to as the "embedment" phase. The embedment phase in this test, although relatively short in terms of the number of load repetitions (i.e., ±20,000), ended with a fairly significant early rut of about 7 mm (≈0.28 in.). Construction data did not provide any clear reason for this behavior (i.e., compaction quality control results were consistent with other sections, but some issues were noted with

foaming water content during early stages of CCPR material production, which may have affected the CCPR layer performance. Poor aggregate interlock in the aggregate base may also have contributed). The rate of increase of the rut depth after the embedment phase slowed considerably. The increase in the applied load to 60 kN resulted in a short embedment phase before stabilizing to rates similar to those recorded during the 40 kN testing. After the load increase to 80 kN, the rate of rut depth increased and did not change significantly until the end of the test.
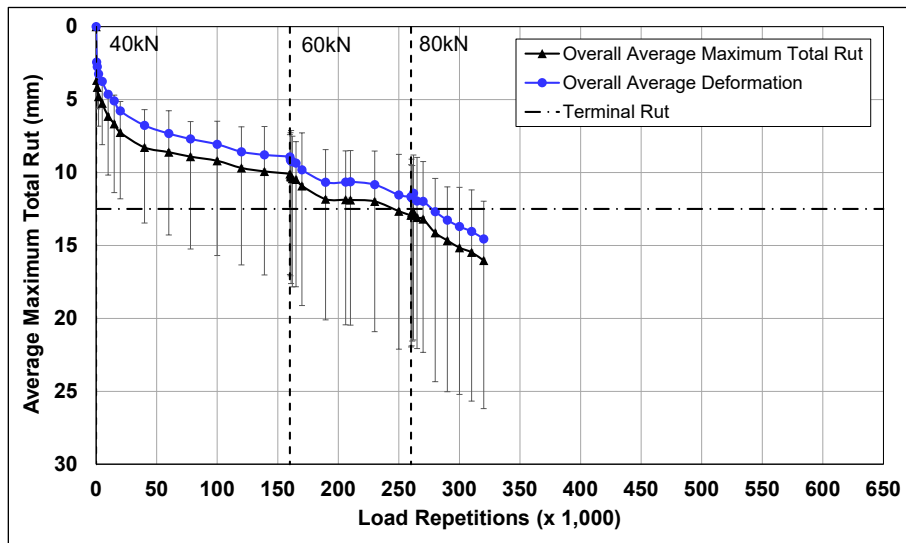
Figure 7.6: 704HB: Average maximum total rut and average deformation.

Figure 7.7 shows the average deformation and the deformation measured between Stations 3 and 7 and between Stations 8 and 13. It is clear that deformation was more severe between Stations 3 and 7, which would have influenced the variability discussed previously.

Figure 7.8 and Figure 7.9 show contour plots of the pavement surface at the start and end of the test (320,000 load repetitions). The end-of-test plot clearly shows the deeper rut at one end of the section around Station 3.

Terminal rut (12.5 mm [≈0.5 in.]) was reached after approximately 260,000 load repetitions (≈710,000 ESALs). However, since the average maximum rut is calculated from measurements at all stations (3 through 13), and the deeper rut at one end of the section influenced this average, trafficking was continued for another 60,000 additional load repetitions to further assess rutting trends under the 80 kN load.
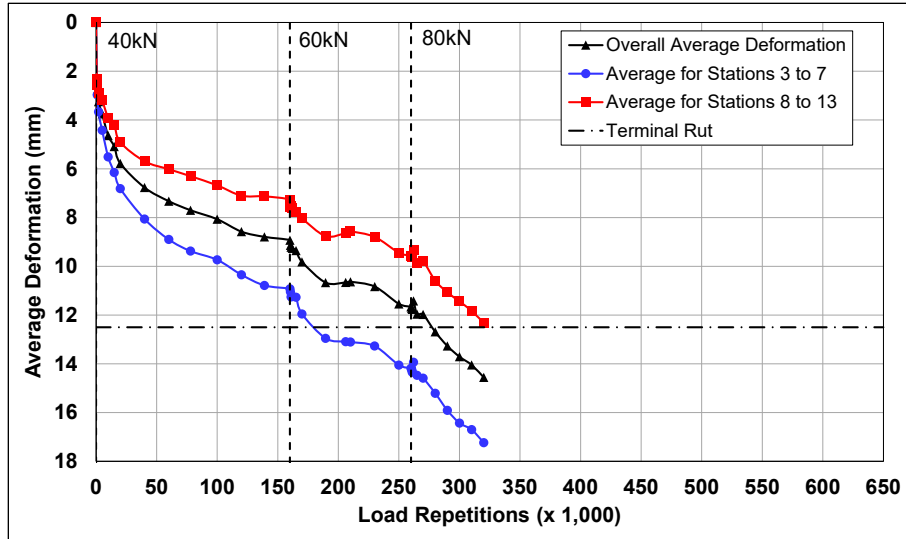
Figure 7.7: 704HB: Average deformation.
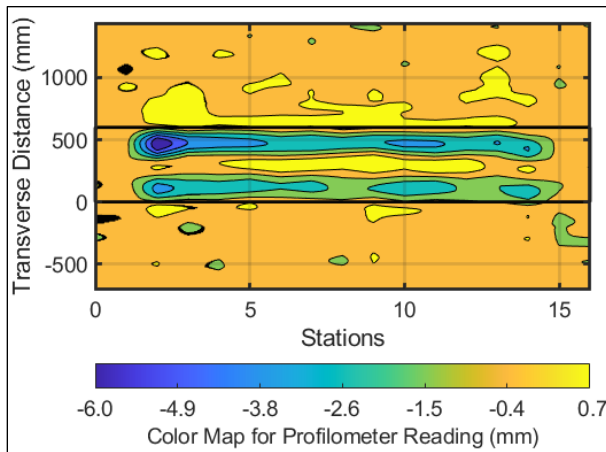
Figure 7.8: 704HB: Contour plot of permanent surface deformation at start of test.
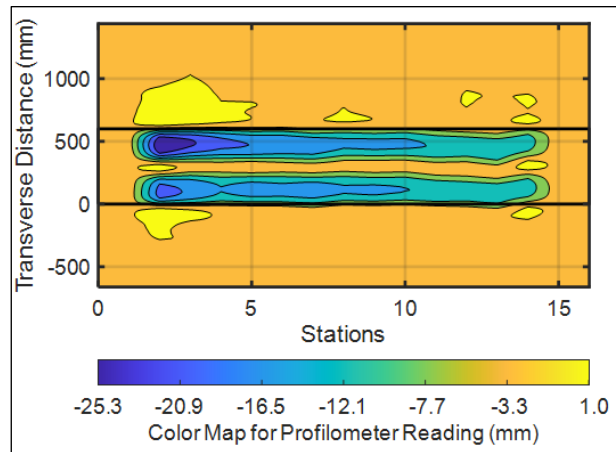
Figure 7.9: 704HB: Contour plot of permanent surface deformation at end of test.
(Note different scales in the legends.)

After completion of trafficking, the average maximum rut depth and the average deformation were 16.0 mm (≈0.63 in.) and 14.6 mm (≈0.57 in.), respectively. The maximum rut depth measured on the section was 21.7 mm (≈0.85 in.), recorded at Station 3.

7.5   Permanent Deformation in the Underlying Layers

Permanent deformation in the underlying layers, recorded with a multi-depth deflectometer (MDD) at Station 13 and compared to the surface layer (laser profilometer deformation [not total rut] measurement at Station 13), is shown in Figure 7.10. The LVDT positioned in the CCPR layer failed early in the test and could not be replaced. Note that the MDD measurements on this

section cannot be directly compared with those from the laser profilometer because the MDD was installed in the untrafficked area between the two wheelpaths of the dual wheel on this section. This instrument location can therefore only provide an indication of which layer or layers the permanent deformation occurred in and not the actual deformation in each layer, which will be assessed during forensic investigations when all testing is completed.
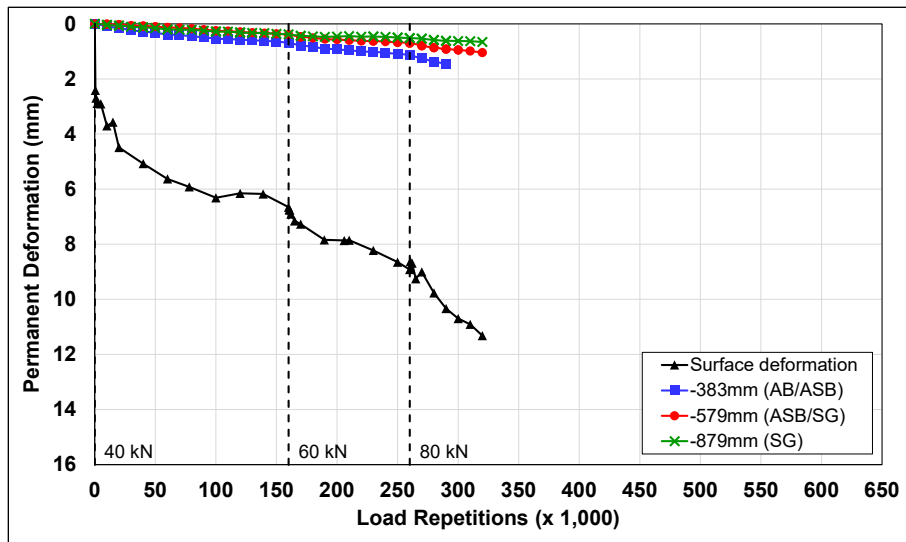
Figure 7.10: 704HB: Permanent deformation in the underlying layers.

Figure 7.10 shows that permanent deformation likely occurred predominantly in the RHMA-G, CCPR, and aggregate base layers. Although the absence of data from the damaged LVDT in the CCPR layer limits any further interpretation of the plot, data from the remaining sensors coupled with results from FWD testing (discussed in Section 7.9) indicates a potential issue in the underlying CCPR and/or aggregate base layer rather than in the RHMA-G layer. The plot clearly shows minimal permanent deformation in the aggregate subbase and subgrade. Load changes did not appear to have had a significant effect on permanent deformation in the aggregate subbase and subgrade.

7.6 Vertical Pressure at the Midpoint of the Aggregate Base Layer

Figure 7.11 shows the traffic-induced vertical pressure in the middle of the aggregate base layer. Note that vertical pressure measurements are recorded continuously during trafficking and spikes in the measurements indicate when manual measurements, which are done at creep wheel speed, were taken.

Pressure readings were stable after some initial embedment, but sensitive to load change, for the duration of the test. Increases in recorded pressures occurred after the load changes, as expected.

7.7 Deflection on the Surface (Road Surface Deflectometer)

Figure 7.12 compares elastic surface deflections measured with a road surface deflectometer (RSD) under a 40 kN half-axle load. Deflections under the 60 kN and 80 kN half-axle loads are also shown. Error bars on the 40 kN load measurements indicate lowest and highest measurements along the section for that load.
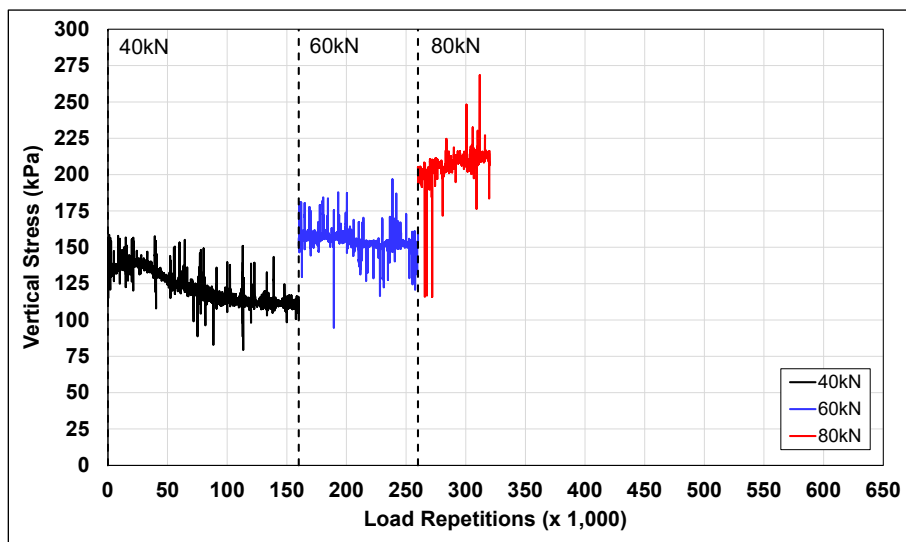
Figure 7.11: 704HB: Vertical pressure in the middle of the aggregate base layer.
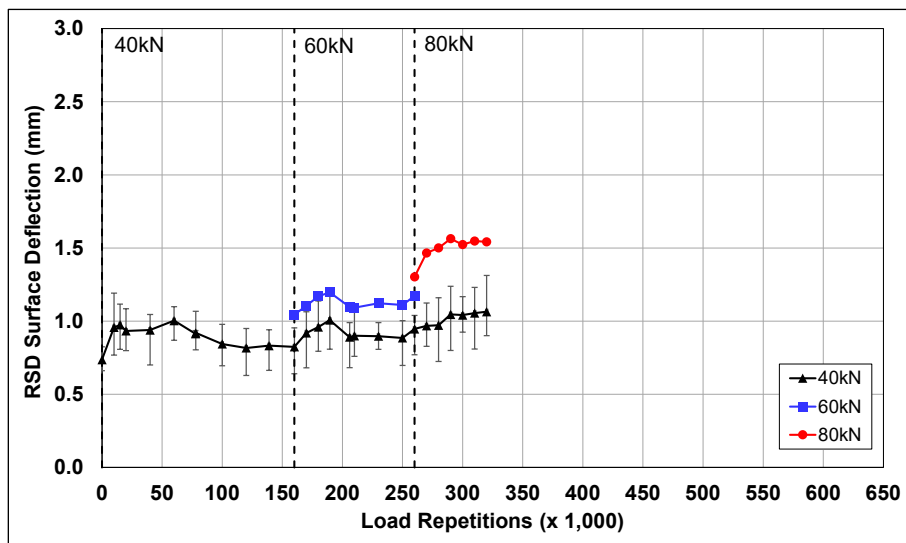
Figure 7.12: 704HB: Surface deflection (RSD).

Deflections increased during the embedment phase of each load, as expected, but appeared to stabilize after embedment under the 40 kN and 60 kN loads, indicating that no significant permanent damage occurred in the pavement for the duration of this part of the testing. After the 80 kN load change, deflections under a 40 kN load continued to increase slowly, indicating that some permanent damage was occurring in the pavement under the higher load at the time when testing was halted. Increases in absolute surface deflection were recorded on the section under the 60 kN and 80 kN loads, as expected. The error bars show that there was limited variability in stiffness along the section.

7.8 Deflection in the Underlying Layers (Multi-Depth Deflectometer)

Figure 7.13 shows the history of in-depth elastic deflections measured by the LVDTs in the multi-depth deflectometer. These readings are consistent with the surface deflections measured with the RSD shown in Figure 7.12. Deflections remained stable for the duration of testing under a 40 kN wheel load.
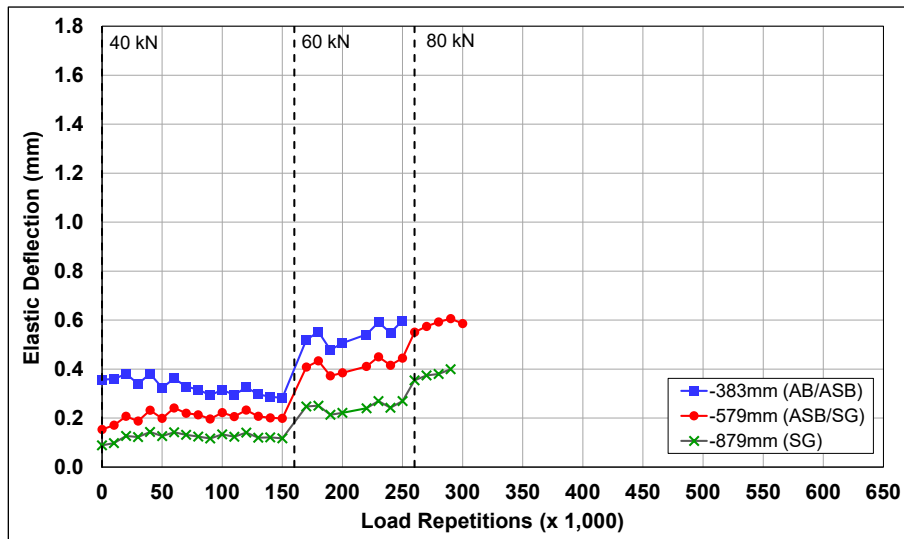
Figure 7.13: 704HB: Elastic deflection in the underlying layers.

Deflections increased with increased load, as expected, and continued to slowly increase during trafficking, indicating that only minimal damage was occurring under the heavier wheel loads in the lower levels of the pavement. Deflection decreased with increasing depth, but the LVDTs at the different depths showed similar trends over the course of the test.

7.9   Deflection in the Pavement Structure (Falling Weight Deflectometer)

Surface deflections measured with a falling weight deflectometer (FWD) on the untrafficked and trafficked areas of the section are summarized in Figure 7.14 (note that "trafficked area" and "untrafficked area" represent the FWD measurements taken on the HVS test section and adjacent to the HVS test section, respectively). Error bars represent the lowest and highest values. The results were consistent with the RSD measurements discussed previously, with the section exhibiting a small decrease in average surface deflection of about 28 microns after completion of HVS trafficking, attributed in part to the relatively low stiffness at the start of testing and a stiffness increase with densification of the material during loading. There was, however, a notable difference between the lowest and highest deflections along the section (444 microns), corresponding to the deeper rut and associated damage at one end of the section. A slight decrease in deflection was also noted in the untrafficked area, which was attributed in part to aging of the RHMA-G layer over the duration of the test (discussed in Section 13.10) and in part to continued curing of the recycled layer. Note that FWD deflections are typically lower than RSD deflections because of the difference in the loading rate and testing temperatures (i.e., FWD measures deflection at simulated highway traffic speeds over a range of temperatures, whereas RSD deflection is measured at creep speeds at a single high test temperature).
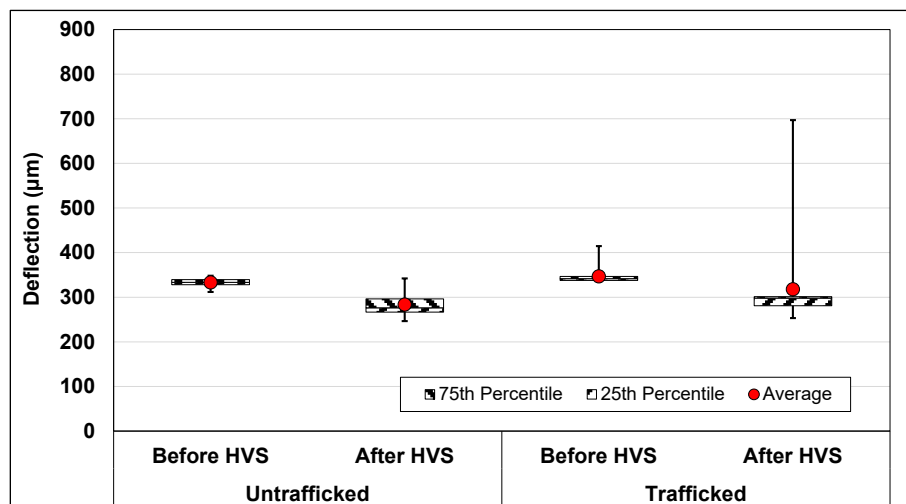

Figure 7.14: 704HB: Surface deflection (FWD).

The RHMA-G layer stiffness was backcalculated from the deflection measurements using the *CalBack* software package (see Section 5.5.5 for method followed), and the results are

summarized in Figure 7.15. Error bars represent the lowest and highest values. The average backcalculated stiffness of the RHMA-G layer (2,770 MPa) at the start of testing was lower than those recorded on RHMA-G layers tested in previous projects (around 4,300 MPa). Average stiffness increased (about 590 MPa) after HVS trafficking, with a notable difference along the length of the section (1,200 MPa to 5,400 MPa), confirming the damage at the one end. The average stiffness of the untrafficked areas at either end of the test section also increased, consistent with the deflection measurements.
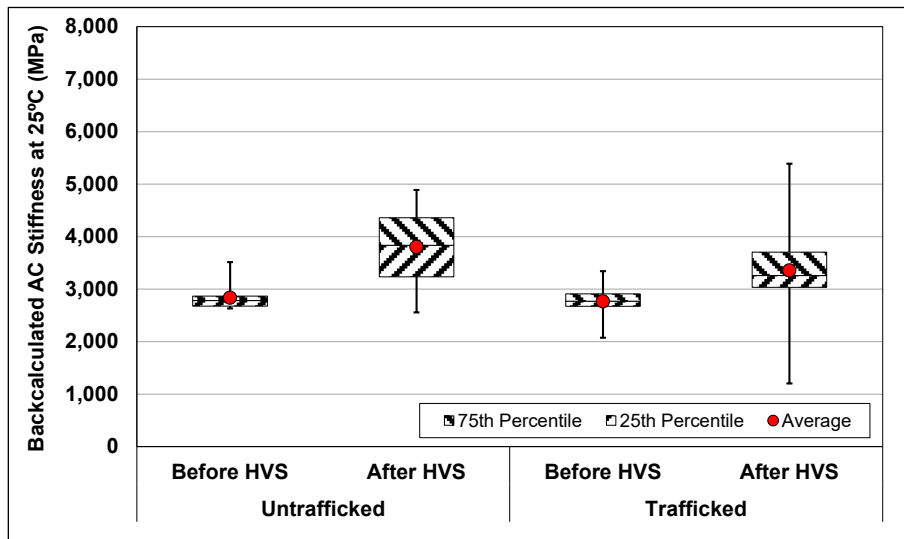
Figure 7.15: 704HB: Backcalculated stiffness of the RHMA-G layer (FWD).

7.10   Visual Assessment and Preliminary Forensic Coring

Apart from rutting, no other distresses were recorded on the test section. Photographs of the test section after HVS testing are shown in Figure 7.16 through Figure 7.19.

Cores were taken from the wheelpath at Station 13 and from the adjacent untrafficked area 600 mm (≈24 in.) from the outside edge of the wheelpath (Figure 7.20 and Figure 7.21, respectively). No distresses or debonding were noted on the cores. Thickness and air-void content of the RHMA-G layer were measured on both cores (Table 7.2) and indicate that although there was no difference in air-void content between the wheelpath and the untrafficked area, approximately 6 mm (0.24 in.) of rutting/densification was recorded in the wheelpath, confirming the observations from the MDD results.
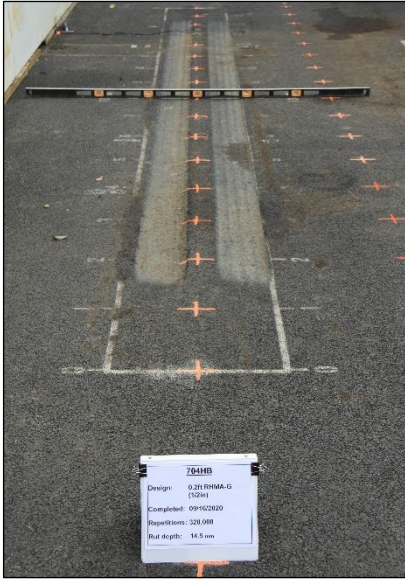
Figure 7.16: 704HB: Test section view from Station 0.
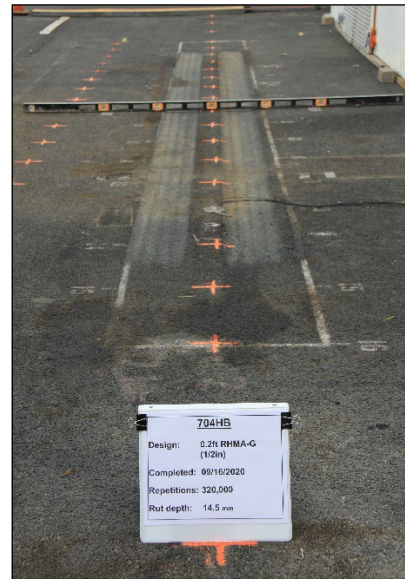
Figure 7.17: 704HB: Test section view from Station 16.

Figure 7.18: 704HB: View of rut at Station 8.

Figure 7.19: 704HB: Close-up view of surface at Station 8.

Figure 7.20: 704HB: Core taken in wheelpath.
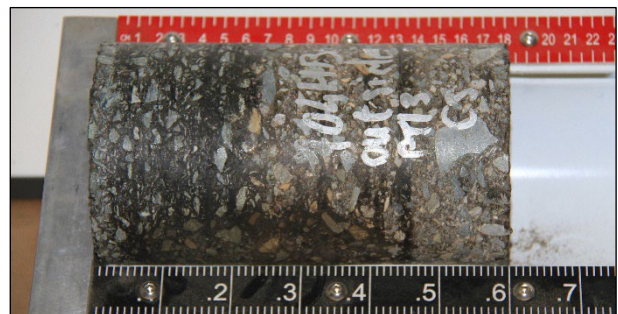
Figure 7.21: 704HB: Core taken 600 mm from edge of wheelpath.

Table 7.2: 704HB: Thickness and Air-Void Content Measurements from Cores

Property	Wheelpath	Untrafficked	Difference
RHMA-G thickness (mm [in.])	55 [2.17]	61 [2.40]	6 [0.24]
RHMA-G air-void content (%)	4.7	4.6	0.1

Blank page

8. SECTION 703HB: 0.4 ft. RHMA-G (1/2 in.) NO RAP

8.1 Test Summary

Loading commenced with a 40 kN half-axle load on September 24, 2020, and ended with an 80 kN load on December 06, 2020. A total of 400,000 load repetitions were applied and 61 datasets were collected. Load was increased from 40 kN to 60 kN after 160,000 load repetitions and then to 80 kN after 260,000 load repetitions. The HVS loading history for Section 703HB is shown in Figure 8.1. No breakdowns occurred on this test, but trafficking was suspended during public holidays in November.
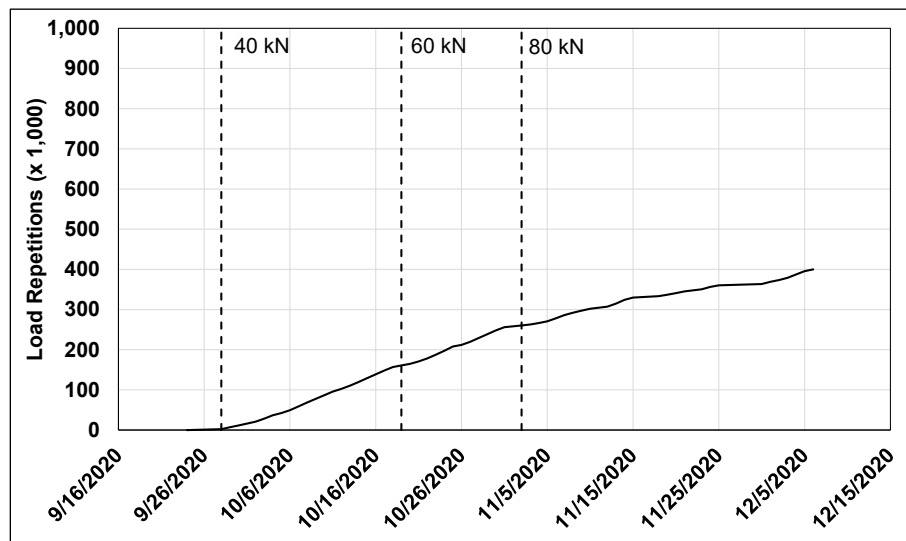
Figure 8.1: 703HB: HVS loading history.

8.2 Air Temperatures

8.2.1 Outside Air Temperatures

Daily 24-hour average outside air temperatures, measured with thermocouples attached to either side of the HVS environmental chamber (i.e., in direct sunlight), are summarized in Figure 8.2. Vertical error bars on each point on the graph show the daily temperature range. Temperatures ranged from 7.9°C to 48.9°C (≈46°F to 120°F) during the course of HVS testing, with a daily 24-hour average of 27.0°C (≈81°F), an average minimum of 18.9°C (≈66°F), and an average maximum of 37.4°C (≈99°F).
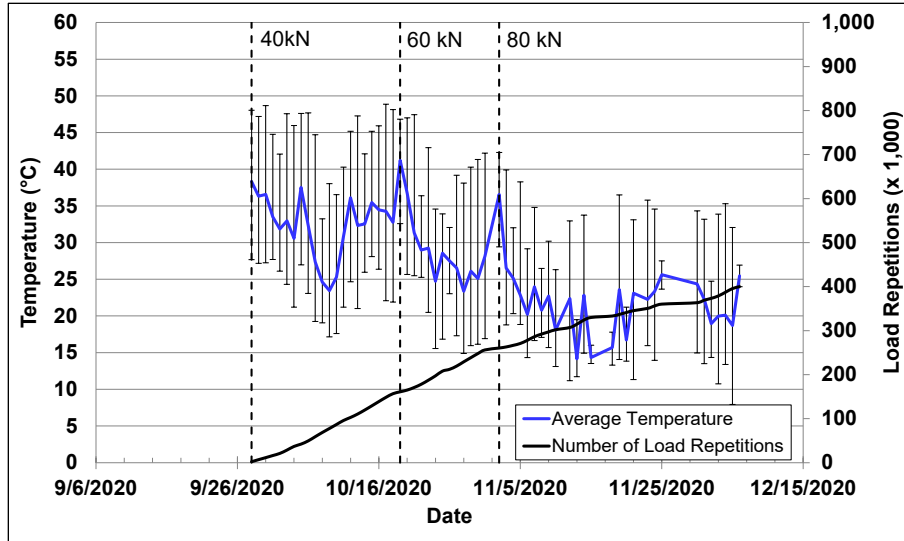
Figure 8.2: 703HB: Daily average air temperatures outside the environmental chamber.

8.2.2 Air Temperatures Inside the Environmental Chamber

The daily 24-hour average air temperatures, measured with thermocouples attached to either side of the HVS environmental chamber above the heaters and calculated from the hourly temperatures recorded during HVS operations, are shown in Figure 8.3. Vertical error bars on each point on the graph show the daily temperature range. During the test, air temperatures inside the environmental chamber ranged from 24.9°C to 49.5°C (≈77°F to 121°F) with an average of 38.6°C (≈102°F) and a standard deviation of 3.8°C (≈6.8°F). Air temperature was automatically adjusted with heater settings to maintain a pavement temperature of 50±2°C at a pavement depth of 50 mm (≈2.0 in.). The recorded pavement temperatures discussed in Section 8.3 indicate that the inside air temperatures were adjusted appropriately to maintain the required pavement temperature.

8.3 Pavement Temperatures

Daily 24-hour averages of the air, surface, and in-depth temperatures of the RHMA-G and recycled layers are shown in Figure 8.3 and listed in Table 8.1. Pavement temperatures were constant and in the target range (50±2°C at a pavement depth of 50 mm) in the RHMA-G layer. Temperatures decreased with increasing depth in the underlying layers, as expected.
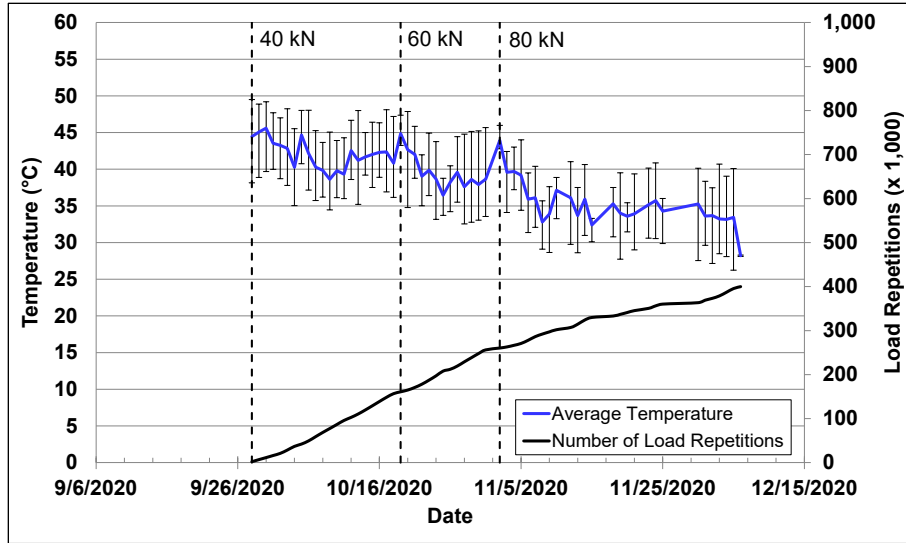
Figure 8.3: 703HB: Daily average air temperatures inside the environmental chamber.
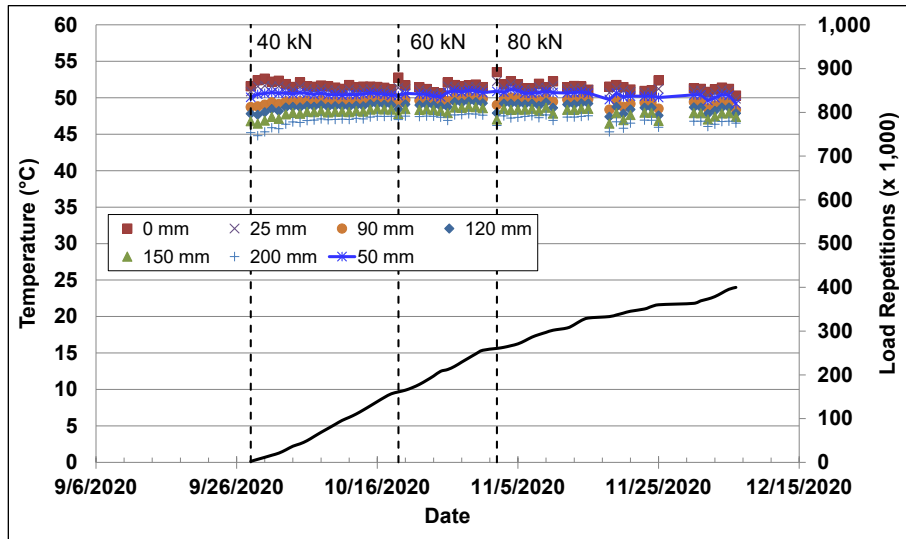
Figure 8.4: 703HB: Daily average pavement temperatures.

Table 8.1: 703HB: Summary of Air and Pavement Temperatures

Thermocouple Location	Layer	Temperature			
		Average (°C)	Std. Dev. (°C)	Average (°F)	Std. Dev. (°F)
Outside air	N/A	27.0	6.5	80.6	11.7
Inside air	N/A	38.6	3.8	101.5	6.8
Pavement surface	RHMA-G	51.6	0.5	124.9	0.9
25 mm below surface	RHMA-G	51.2	0.4	124.2	0.7
50 mm below surface	RHMA-G	50.5	0.3	122.9	0.5
90 mm below surface	RHMA-G	49.5	0.4	121.1	0.7
120 mm below surface	RHMA-G	48.7	0.5	119.7	0.9
150 mm below surface	RHMA-G	48.0	0.6	118.4	1.1
200 mm below surface	Recycled	46.9	0.7	116.4	1.3

8.4   Permanent Deformation on the Surface (Rutting)

Figure 8.5 shows the average transverse cross section measured with the laser profilometer at various stages of the test. This plot clearly shows the initial higher rate of rutting and the increase in rutting and deformation over time and that most of the deformation was in the form of a depression (i.e., deformation was below the zero elevation point at the surface [see Figure 5.8]). Minor upward and outward displacement of the material above the zero elevation point occurred after the load increase to 60 kN.
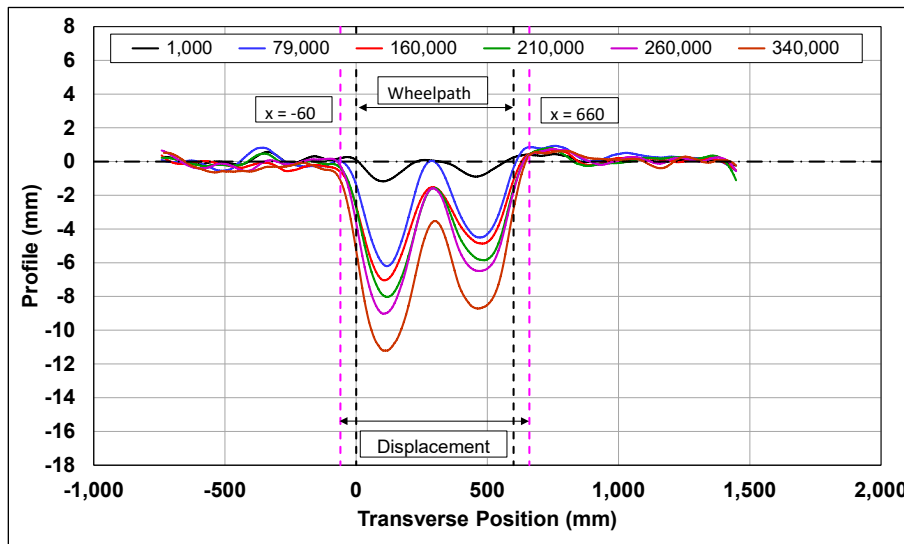
Figure 8.5: 703HB: Profilometer cross section at various load repetitions.

Figure 8.6 shows the development of permanent deformation (average maximum total rut and average deformation) with load repetitions. Error bars on the average maximum total rut line indicate lowest and highest measurements along the section. These error bars indicate some variation along the section but notably less than that measured on the control (Section 704HB). The embedment phase in this test occurred over a similar number of load repetitions to Section 704HB (i.e., ±20,000), but ended with a rut depth of about 4 mm (≈0.16 in.), considerably less that the 7 mm (≈0.28 in.) recorded on Section 704HB. This difference was attributed in part to the thicker RHMA-G layer.

The rate of increase of the rut depth after the embedment phase slowed considerably. Increases in the applied loads to 60 kN and 80 kN resulted in short embedment phases before stabilizing to rates similar to those recorded during the 40 kN testing. This slower rut rate compared to

Section 704HB was attributed in part to the thicker RHMA-G layer (120 mm [0.4 ft.] on this section compared to 60 mm [0.2 ft.] on the control section).
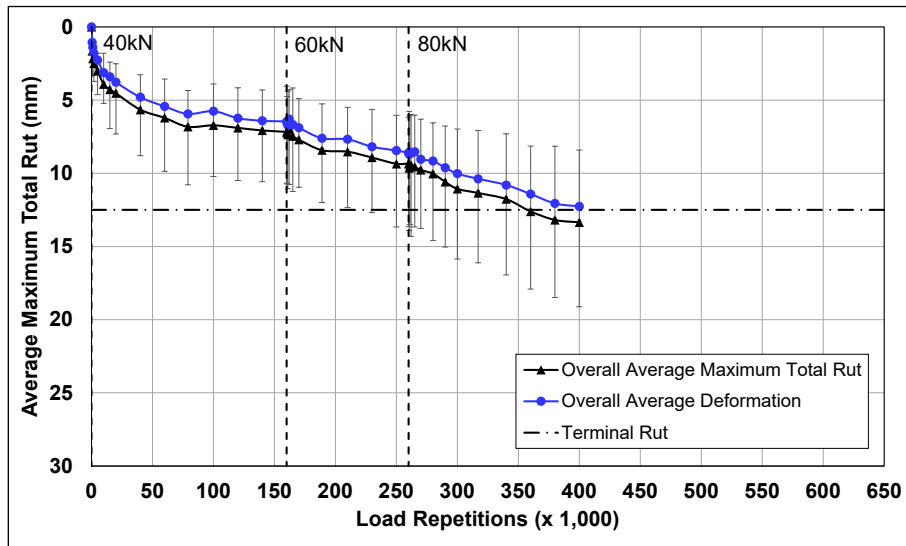
Figure 8.6: 703HB: Average maximum total rut and average deformation.

Figure 8.7 shows the average deformation and the deformation measured between Stations 3 and 7 and between Stations 8 and 13. The average rut depth was deeper between Stations 8 and 13, opposite to Section 704HB, but the difference between the rut depths on the two subsections was similar, indicating similar variability along the length of the section.
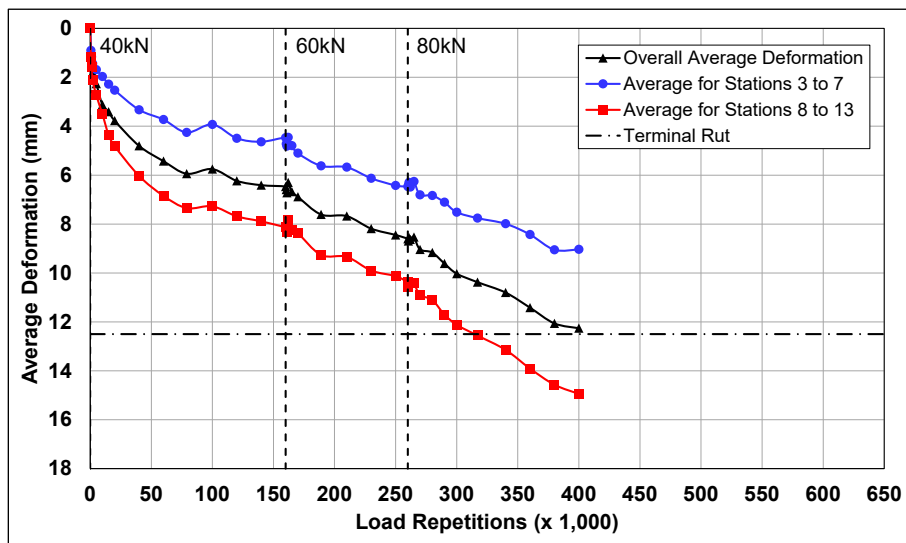
Figure 8.7: 703HB: Average deformation.

Figure 8.8 and Figure 8.9 show contour plots of the pavement surface at the start and end of the test (400,000 load repetitions). The end-of-test plot shows the deeper rut between Stations 8

and 13. Terminal rut (12.5 mm [≈0.5 in.]) was reached after 400,000 load repetitions (≈3.28 million ESALs). Trafficking is often continued until the rut depth at all locations is at or close to the terminal rut on the track to further assess rutting trends, but this was not feasible on this test. After completion of trafficking, the average maximum rut depth and the average deformation were 13.3 mm (≈0.52 in.) and 12.3 mm (≈0.48 in.), respectively. The maximum rut depth measured on the section was 16.7 mm (≈0.66 in.), recorded at Station 11.
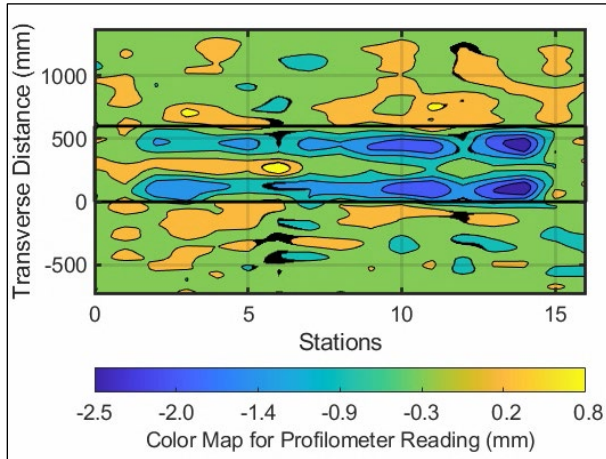
Figure 8.8: 703HB: Contour plot of permanent surface deformation at start of test.
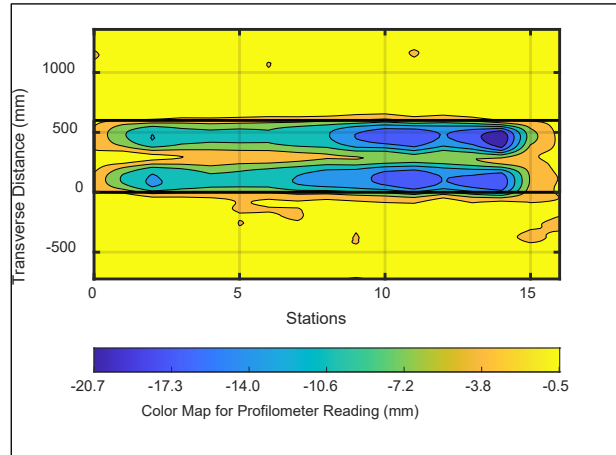
Figure 8.9: 703HB: Contour plot of permanent surface deformation at end of test.
(Note different scales in the legends.)

8.5   Permanent Deformation in the Underlying Layers

No multi-depth deflectometer (MDD) permanent deformation data was recorded on this test section.

8.6   Vertical Pressure at the Midpoint of the Aggregate Base Layer

Figure 8.10 shows the traffic-induced vertical pressure in the middle of the aggregate base layer. Note that vertical pressure measurements are recorded continuously during trafficking, and spikes in the measurements indicate when manual measurements, which are done at creep wheel speed, were taken.

Vertical pressure readings were stable after some initial embedment, but sensitive to load change, for the duration of the test. Increases in recorded pressures occurred after the load changes, as expected. There was an approximate 15 kPa increase in vertical stress between 335,000 and 345,000 load repetitions during trafficking with the 80 kN wheel load. There was no

observed reason for this increase. The results were generally consistent with those measured on Section 704HB.
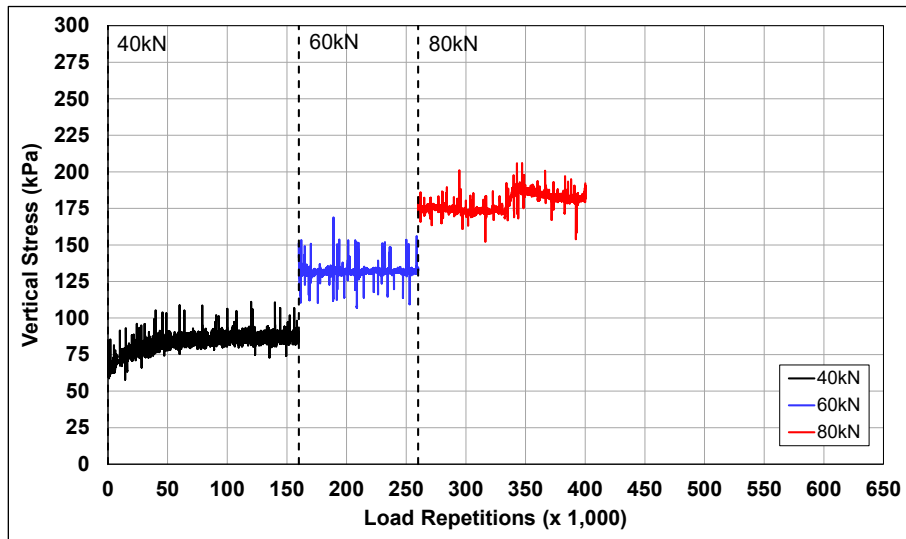
Figure 8.10: 703HB: Vertical pressure in the middle of the aggregate base layer.

8.7 Deflection on the Surface (Road Surface Deflectometer)

Figure 8.11 compares elastic surface deflections measured with a road surface deflectometer (RSD) under a 40 kN half-axle load. Deflections under the 60 kN and 80 kN loads are also shown.
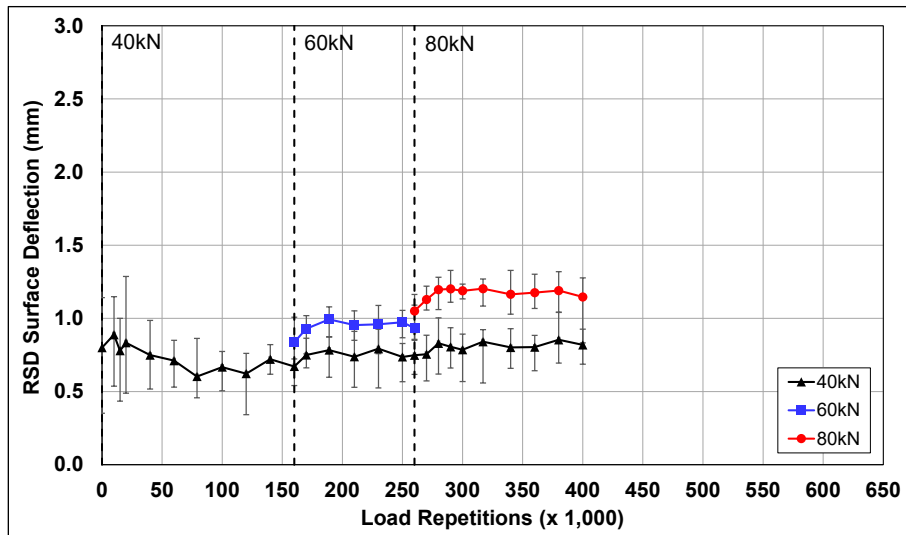
Figure 8.11: 703HB: Surface deflection (RSD).

Deflections increased during the embedment phase of each load. Although deflections appeared to stabilize after embedment under each load, deflection measured under the 40 kN load continued to increase, indicating that some permanent damage was occurring in the pavement

under the 60 kN and 80 kN loads. Increases in absolute surface deflection were recorded on the section under the 60 kN and 80 kN loads, as expected. Error bars on the plot indicate lowest and highest measurements along the section under the 40 kN load. These error bars indicate some variability in the early tests and then limited variability along the section for the remainder of the test.

Deflections were lower than those measured on Section 704HB at all wheel loads, which was attributed to the thicker RHMA-G layer. At the end of the test, deflections on this section were 0.2 mm lower than on Section 704HB under the 40 kN load and 0.4 mm under the 80 kN load.

8.8 Deflection in the Underlying Layers (Multi-Depth Deflectometer)

No multi-depth deflectometer (MDD) deflection data was recorded on this test section.

8.9 Deflection in the Pavement Structure (Falling Weight Deflectometer)

Surface deflections measured with a falling weight deflectometer (FWD) on the untrafficked and trafficked areas of the section are summarized in Figure 8.12 ("trafficked area" and "untrafficked area" represent the FWD measurements taken on the HVS test section and adjacent to the HVS test section, respectively). Error bars represent the lowest and highest values.
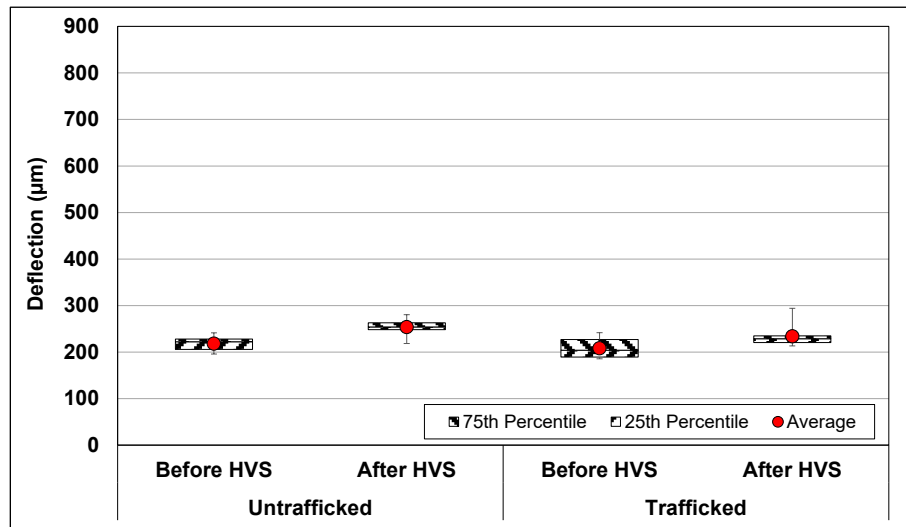
Figure 8.12: 703HB: Surface deflection (FWD).

The results were consistent with the RSD measurements discussed above, with the section exhibiting a small increase in surface deflection of about 26 microns after completion of HVS trafficking. Note that FWD deflections are typically lower than RSD deflections because of the

difference in the loading rate and testing temperatures (i.e., FWD measures deflection at simulated highway traffic speeds over a range of temperatures, whereas RSD deflection is measured at creep speeds at a single high temperature).

The RHMA-G layer stiffness was backcalculated from the deflection measurements using the *CalBack* software package (see Section 5.5.5 for method followed), and the results are summarized in Figure 8.13. Error bars represent the lowest and highest values.
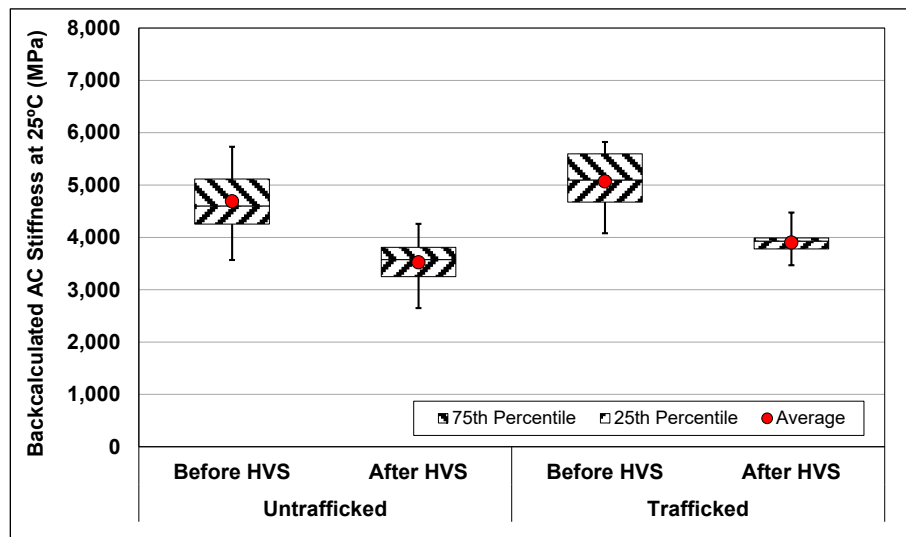
Figure 8.13: 703HB: Backcalculated stiffness of the RHMA-G layer (FWD).

The average backcalculated stiffness of the RHMA-G layer (5,070 MPa) at the start of testing was higher than those on RHMA-G layers tested in previous projects (around 4,300 MPa) and notably higher than that measured on Section 704HB. However, the average stiffness decreased by about 1,170 MPa, indicating that HVS trafficking did cause some damage in the RHMA-G layer. The stiffness of the untrafficked areas at either end of the test section also decreased, which was not expected. The reason for this decrease is not clear and will be further evaluated when forensic investigations are undertaken after completion of all testing on the track.

8.10   Visual Assessment and Preliminary Forensic Coring

Apart from rutting, no other distress was recorded on the section. Photographs of the test section after HVS testing are shown in Figure 8.14 through Figure 8.17.
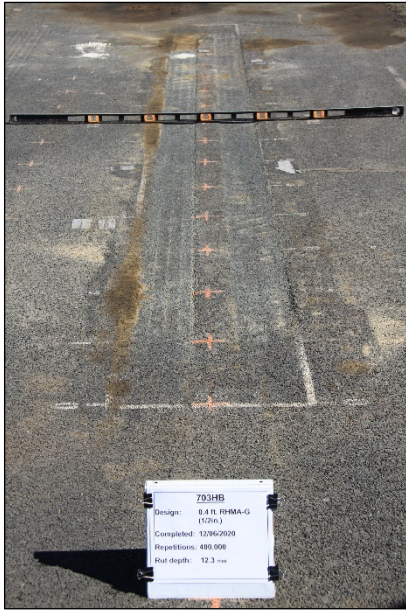
Figure 8.14: 703HB: Test section view from Station 0.

Figure 8.15: 703HB: Test section view from Station 16.

Figure 8.16: 703HB: View of rut at Station 8.
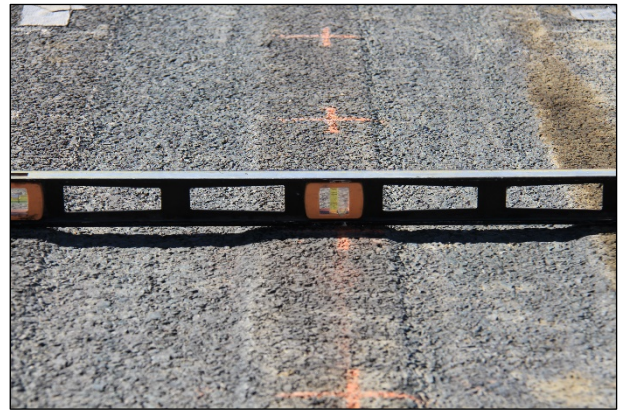
Figure 8.17: 703HB: Close-up view of test section surface at Station 8.

Cores were taken from the wheelpath at Station 13, and from the adjacent untrafficked area 600 mm (≈24 in.) from the outside edge of the wheelpath (Figure 8.18 and Figure 8.19, respectively). No distresses or debonding were noted on the cores. Thickness and air-void content of the RHMA-G layer were measured on both cores (Table 8.2). There was no difference in air-void content between the trafficked and untrafficked areas, and only a 3 mm (≈0.12 in.) and 1 mm (≈0.04 in.) difference in thickness in the top and bottom lifts of RHMA-G, respectively, indicating that limited densification occurred in the wheelpaths. This implies that rutting was likely in the underlying CCPR or aggregate base layers, which will be assessed during the forensic investigation when all testing on the track has been completed.
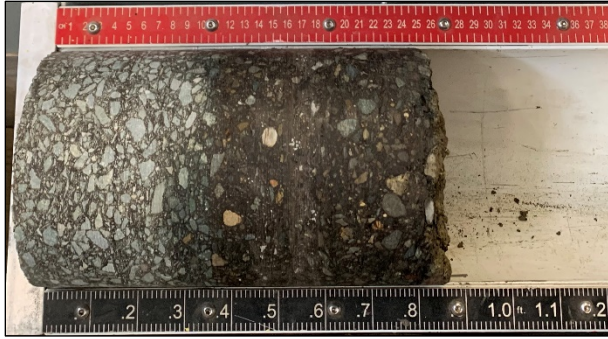
Figure 8.18: 703HB: Core taken in wheelpath.

Figure 8.19: 703HB: Core taken 600 mm from edge of wheelpath.

Table 8.2: 703HB: Thickness and Air-Void Content Measurements from Cores

Property	Layer	Wheelpath	Untrafficked	Difference
RHMA-G thickness (mm [in.])	Top	61 [2.40]	64 [2.52]	3 [0.12]
	Bottom	57 [2.24]	58 [2.28]	1 [0.04]
RHMA-G air-void content (%)	Top	7.0	6.8	No difference
	Bottom	5.1	5.1	No difference

Blank page

9. SECTION 701HC: 0.2 ft. RHMA-G (1/2 in.) WITH RAP

9.1 Test Summary

Loading commenced with a 40 kN half-axle load on September 23, 2019, and ended with an 80 kN load on July 23, 2020. A total of 300,000 load repetitions were applied and 39 datasets were collected. Load was increased from 40 kN to 60 kN after 160,000 load repetitions, and then to 80 kN after 260,000 load repetitions. The HVS loading history for Section 701HC is shown in Figure 9.1. Trafficking on this section was severely impacted, first because of a three-month breakdown resulting from a major hydraulic system failure, followed by a mandated four-month COVID-19 shutdown. The test can be repeated on the additional section if deemed appropriate based on the findings of the second-level analysis of laboratory and HVS test results on other sections *(2)*.
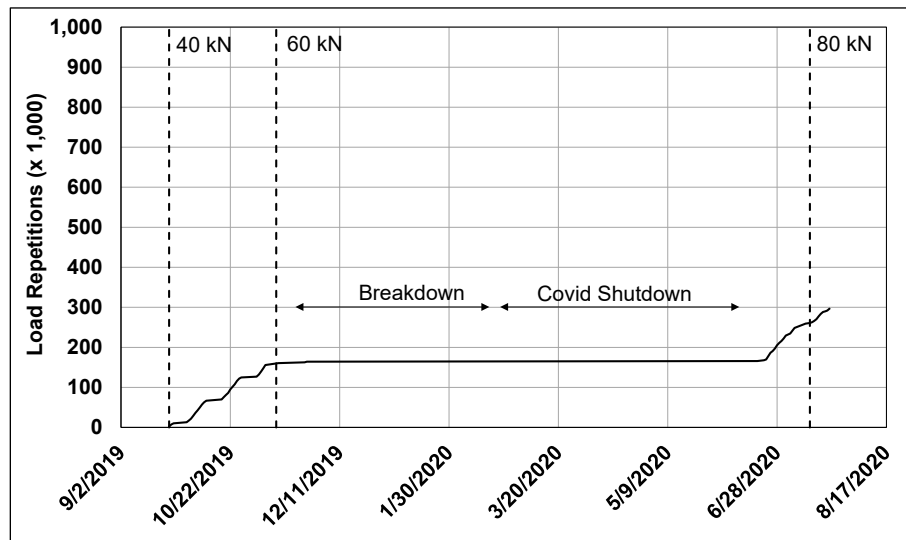
Figure 9.1: 701HC: HVS loading history.

9.2 Air Temperatures

9.2.1 Outside Air Temperatures

Daily 24-hour average outside air temperatures, measured with thermocouples attached to either side of the HVS environmental chamber (i.e., in direct sunlight), are summarized in Figure 9.2. Vertical error bars on each point on the graph show the daily temperature range. Temperatures ranged from 5.9°C to 49.7°C (≈43°F to 121°F) during the course of HVS testing,

with a daily 24-hour average of 25.8°C (≈78°F), an average minimum of 18.7°C (≈66°F), and an average maximum of 37.2°C (≈99°F).
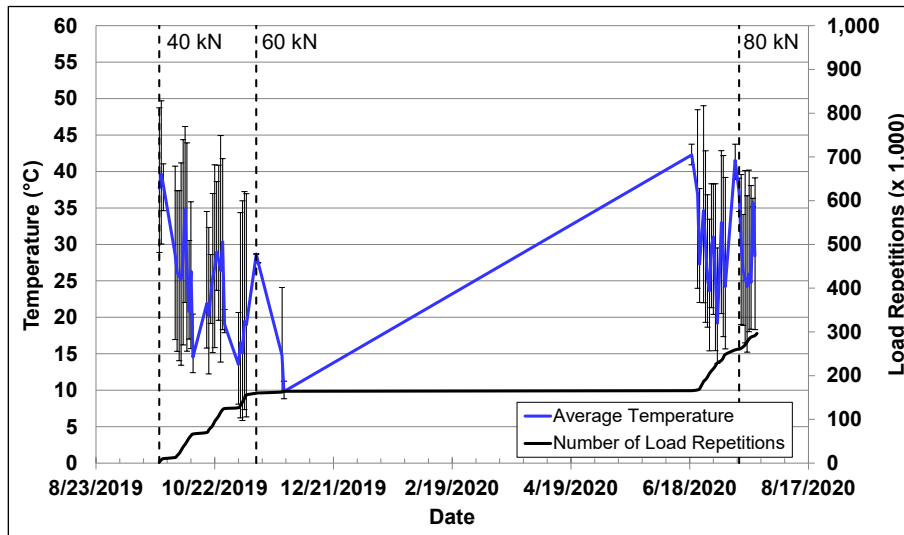
Figure 9.2: 701HC: Daily average air temperatures outside the environmental chamber.

9.2.2 Air Temperatures Inside the Environmental Chamber

The daily 24-hour average air temperatures, measured with thermocouples attached to either side of the HVS environmental chamber above the heaters and calculated from the hourly temperatures recorded during HVS operations, are shown in Figure 9.3. Vertical error bars on each point on the graph show the daily temperature range. During the test, air temperatures inside the environmental chamber ranged from 21.0°C to 52.0°C (≈70°F to 126°F) with an average of 38.1°C (≈100.6°F) and a standard deviation of 5.7°C (≈10.3°F). Air temperature was automatically adjusted with heater settings to maintain a pavement temperature of 50±2°C at a pavement depth of 50 mm. The recorded pavement temperatures discussed in Section 9.3 indicate that the inside air temperatures were adjusted appropriately to maintain the required pavement temperature.

9.3 Pavement Temperatures

Daily 24-hour averages of the air, surface, and in-depth temperatures of the RHMA-G and recycled layers are shown in Figure 9.4 and listed in Table 9.1. Pavement temperatures were constant and in the target range (50±2°C at a pavement depth of 50 mm) in the RHMA-G layer. Temperatures decreased with increasing depth in the underlying layers, as expected.
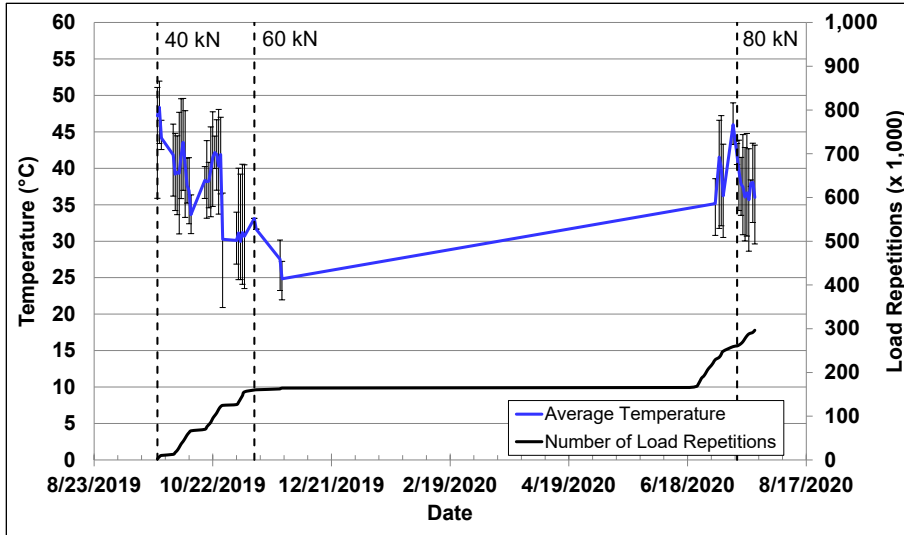
Figure 9.3: 701HC: Daily average air temperatures inside the environmental chamber.
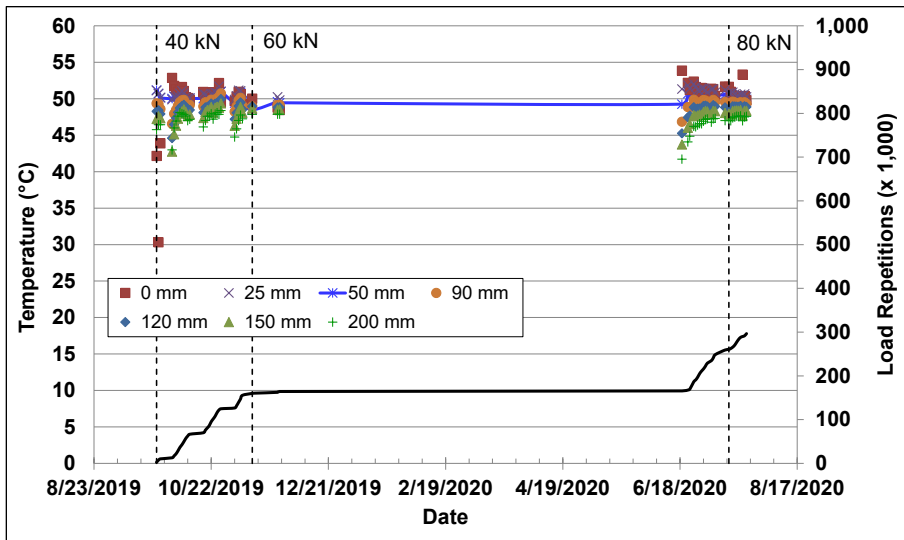
Figure 9.4: 701HC: Daily average pavement temperatures.

Table 9.1: 701HC: Summary of Air and Pavement Temperatures

Thermocouple Location	Layer	Temperature			
		Average (°C)	Std. Dev. (°C)	Average (°F)	Std. Dev. (°F)
Outside air	N/A	25.7	9.4	78.2	16.9
Inside air	N/A	38.1	5.7	100.6	10.3
Pavement surface	RHMA-G	50.1	6.4	122.2	11.4
25 mm below surface	RHMA-G	50.7	1.3	123.3	2.4
50 mm below surface	RHMA-G	50.4	0.9	122.7	1.6
90 mm below surface	Recycled	49.4	0.9	121.0	1.5
120 mm below surface	Recycled	48.7	0.9	119.6	1.7
150 mm below surface	Recycled	48.0	1.1	118.3	2.0
200 mm below surface	Aggregate base	47.1	1.2	116.8	2.2

9.4 Permanent Deformation on the Surface (Rutting)

Figure 9.5 shows the average transverse cross section measured with the laser profilometer at various stages of the test. This plot clearly shows the initial higher rate of rutting and increase in rutting and deformation over time and that most of the deformation was in the form of a depression (i.e., deformation was below the zero elevation point at the surface [see Figure 5.8]). Minor upward and outward displacement of the material above the zero elevation point occurred during the last approximately 20,000 load repetitions after the load increase to 80 kN (i.e., between 280,000 and 300,000 load repetitions).
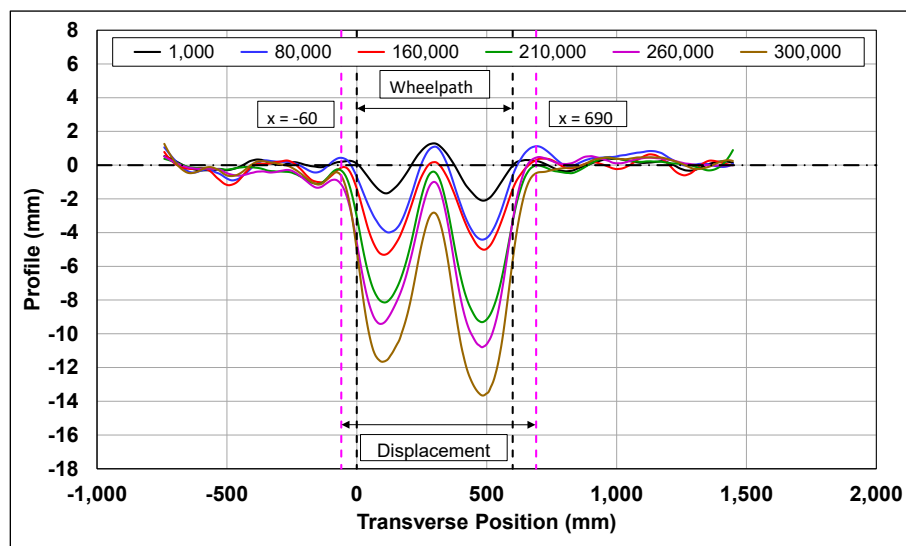
Figure 9.5: 701HC: Profilometer cross section at various load repetitions.

Figure 9.6 shows the development of permanent deformation (average maximum total rut and average deformation) with load repetitions. Error bars on the average maximum total rut indicate lowest and highest measurements along the section. These error bars indicate some variation along the section but less than that measured on the control (Section 704HB). The embedment phase in this test occurred over a similar number of load repetitions to Section 704HB (i.e., ±20,000) but ended with a rut depth of about 4 mm (≈0.16 in.), consistent with Section 703HB, but considerably less than the 7 mm (≈0.28 in.) recorded on Section 704HB. The reason for this difference is not clear, especially given that this section was tested before Section 704HB and was therefore subjected to less aging. However, apart from the potential issues noted in Chapter 8 the presence of the RAP may have stiffened the mix. The rate of increase of the rut depth after the embedment phase slowed considerably. The increase in the applied load to 60 kN

resulted in a short embedment phase, followed by a steady rate of increase that was faster than that recorded during the 40 kN testing. This faster-than-typical increase in rut rate was likely caused by the hydraulic oil spill. After the load increase to 80 kN, the rate of rut depth increased again and did not change significantly until the end of the test.
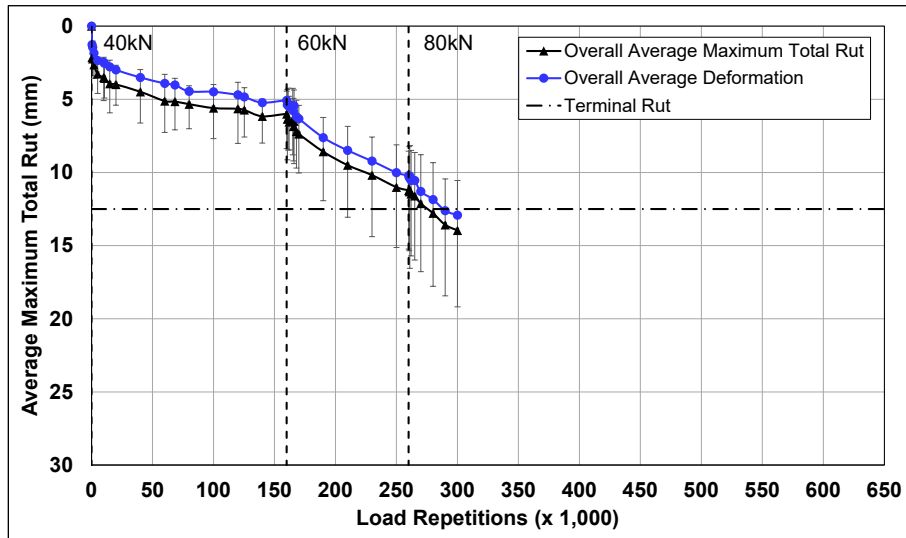
Figure 9.6: 701HC: Average maximum total rut and average deformation.

Figure 9.7 shows the average deformation and the deformation measured between Stations 3 and 7 and between Stations 8 and 13. Some variation along the length of the section was apparent, with higher levels of deformation between Stations 8 and 13 than between Stations 3 and 7. However, less variation was recorded on this test than on Section 704HB.
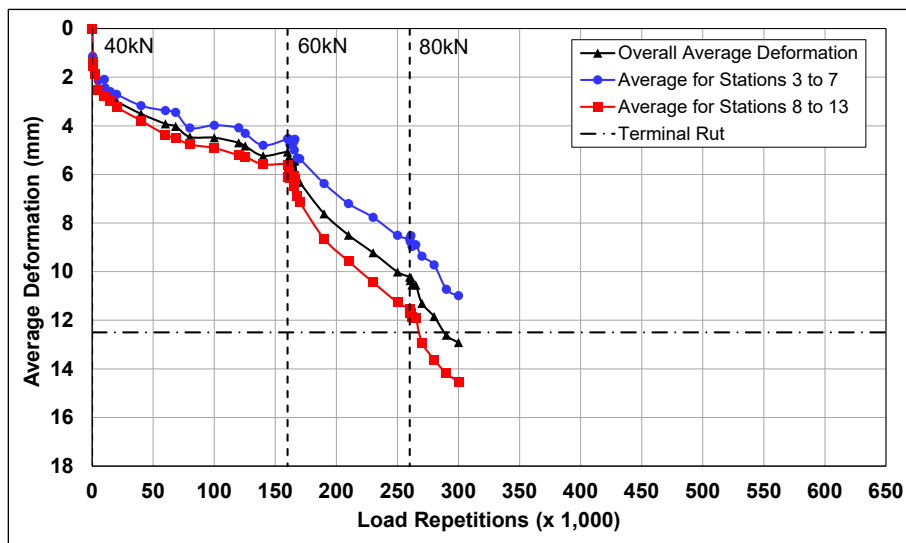
Figure 9.7: 701HC: Average deformation.

Figure 9.8 and Figure 9.9 show contour plots of the pavement surface at the start and end of the test (300,000 load repetitions). The end-of-test plot clearly shows the deeper rut at one end of the section.
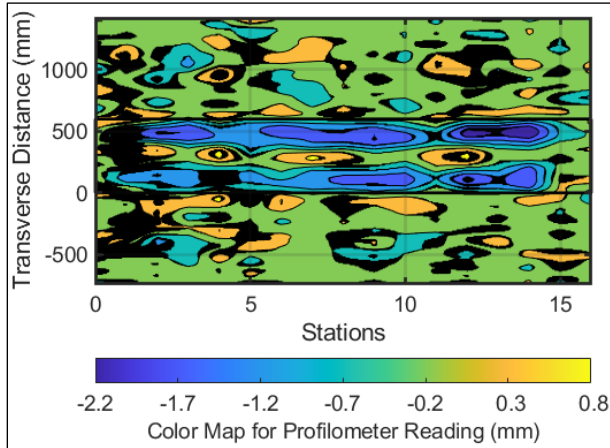
Figure 9.8: 701HC: Contour plot of permanent surface deformation at start of test.
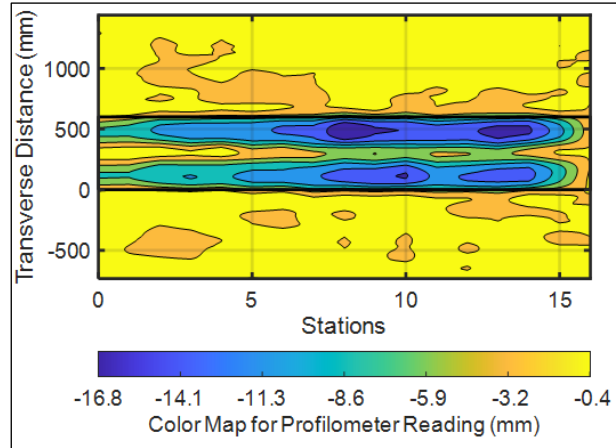
Figure 9.9: 701HC: Contour plot of permanent surface deformation at end of test.
(Note different scales in the legends.)

Terminal rut (12.5 mm [≈0.5 in.]) was reached after approximately 285,000 load repetitions (≈1,077,000 ESALs). However, since the average maximum rut is calculated from measurements at Stations 3 through 13, and the deeper rut at one end of the section influenced this average, trafficking was continued for another 15,000 additional load repetitions to further assess rutting trends under the 80 kN load.

After completion of trafficking, the average maximum rut depth and the average deformation were 14.0 mm (≈0.55 in.) and 12.9 mm (≈0.51 in.), respectively. The maximum rut depth measured on the section was 16.9 mm (≈0.67 in.), recorded at Station 8.

9.5   Permanent Deformation in the Underlying Layers

Permanent deformation in the underlying layers, recorded with a multi-depth deflectometer (MDD) at Station 13 and compared to the surface layer (laser profilometer deformation [not total rut] measurement at Station 13), is shown in Figure 9.10. Note that the MDD measurements cannot be directly compared with those from the laser profilometer because the MDD on this section was installed in the untrafficked area between the two wheelpaths of the dual wheel on this section. This instrument location can therefore only provide an indication of which layer or

layers the permanent deformation occurred in and not the actual deformation in each layer, which will be assessed during forensic investigations when all testing is completed.

Figure 9.10 shows that permanent deformation occurred primarily in the RHMA-G layer (likely a result of the oil spill), with less in the CCPR and aggregate base layers. Minimal permanent deformation in the aggregate subbase and subgrade was recorded. There was a notable increase in permanent deformation in all of the layers after the load change to 60 kN.
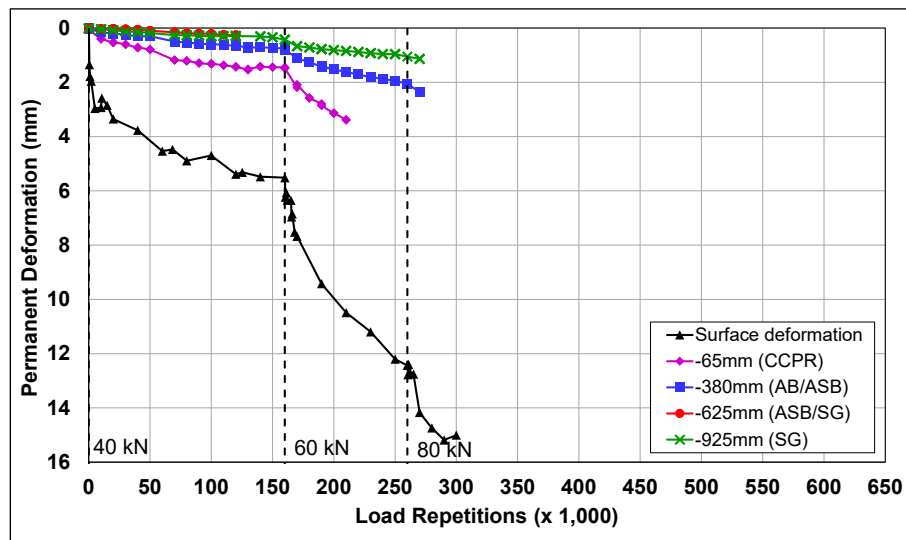
Figure 9.10: 701HC: Permanent deformation in the underlying layers.

9.6 Vertical Pressure at the Midpoint of the Aggregate Base Layer

Figure 9.11 shows the traffic-induced vertical pressure in the middle of the aggregate base layer. Note that vertical pressure measurements are recorded continuously during trafficking and spikes in the measurements indicate when manual measurements, which are done at creep wheel speed, were taken.

Vertical pressure readings were stable after some initial embedment, but sensitive to load change, for the duration of the test. Increases in recorded pressures occurred after the load changes, as expected. The results were consistent with those measured on Section 704HB.

9.7 Deflection on the Surface (Road Surface Deflectometer)

Figure 9.12 compares elastic surface deflections measured with a road surface deflectometer (RSD) under a 40 kN half-axle load. Deflections under the 60 kN and 80 kN loads are also shown.
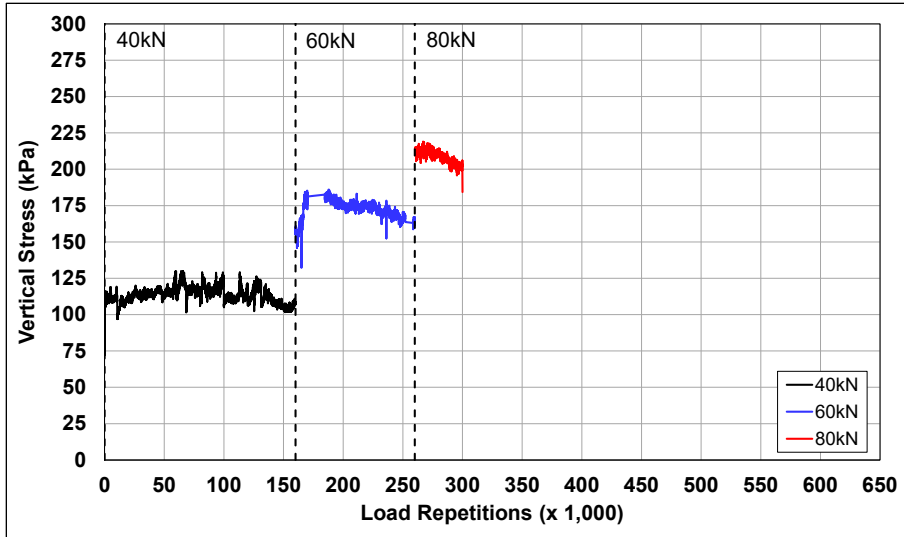
Figure 9.11: 701HC: Vertical pressure in the middle of the aggregate base layer.
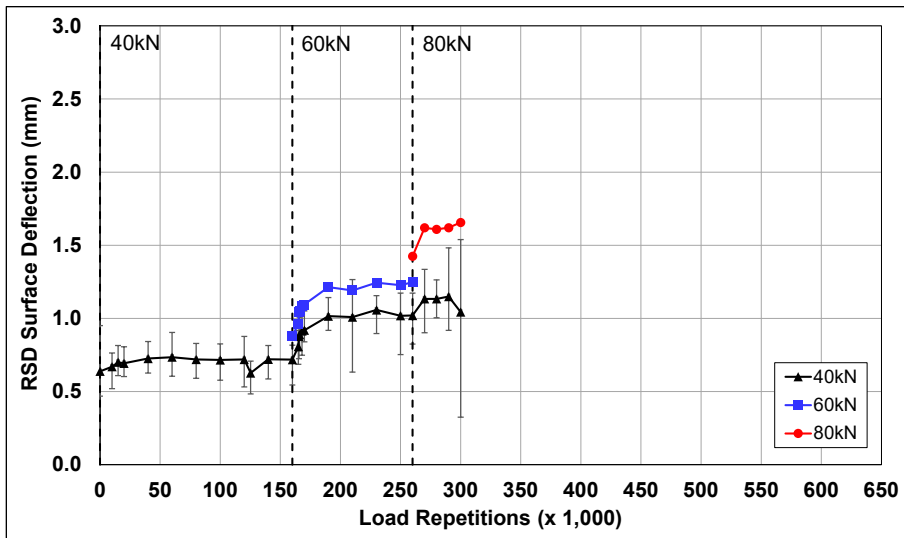
Figure 9.12: 701HC: Surface deflection (RSD).

Deflections increased during the embedment phase of each load. Although deflections appeared to stabilize after the embedment phase under each load, deflection measured under the 40 kN load continued to increase, indicating that some permanent damage was occurring in the pavement under the 60 kN and 80 kN loads. Increases in absolute surface deflection were recorded on the section under the 60 kN and 80 kN loads, as expected and similar to those recorded on Section 704HB. Error bars on the plot indicate lowest and highest measurements along the section under a 40 kN load. These error bars indicate limited variability along the section during the 40 kN load testing but increases in variability at the higher wheel loads during the latter part of the test. This was likely a result of the hydraulic oil spill.

Deflections measured in the early part of the test under the 40 kN load were lower than those measured on the control section (704HB). This was attributed in part to early stiffening of the mix resulting from blending of the recycled and virgin binders. Deflections in the latter part of the test were consistent with those measured on the control.

9.8 Deflection in the Underlying Layers (Multi-Depth Deflectometer)

Figure 9.13 shows the history of in-depth elastic deflections measured by the LVDTs in the multi-depth deflectometer. These readings are consistent with the surface deflections measured with the RSD shown in Figure 9.12. Deflections in all layers remained stable for the duration of testing under a 40 kN wheel load. Deflections increased with increased load, as expected, and continued to increase at a very slow rate during trafficking, indicating that minimal damage was occurring in the underlying layers under the heavier wheel loads. Deflection decreased with increasing depth, but the LVDTs at the different depths all showed similar trends over the course of the test. Note that the LVDTs may have been effected by the hydraulic oil spill.
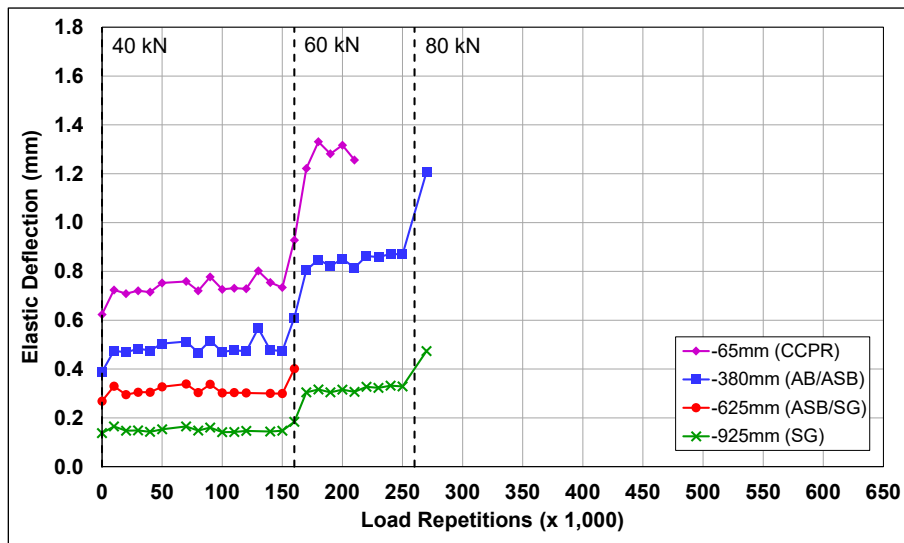
Figure 9.13: 701HC: Elastic deflection in the underlying layers.

9.9 Deflection in the Pavement Structure (Falling Weight Deflectometer)

Surface deflections measured with a falling weight deflectometer (FWD) on the untrafficked and trafficked areas of the section are summarized in Figure 9.14 ("trafficked area" and "untrafficked area" represent the FWD measurements taken on the HVS test section and adjacent to the HVS test section, respectively). Error bars represent the lowest and highest values. The results were

consistent with the RSD measurements discussed above, with the section exhibiting a small increase in surface deflection of about 145 microns after completion of HVS trafficking, indicating that some damage occurred in the section during trafficking. No significant change in deflection was noted in the untrafficked area. Note that FWD deflections are typically lower than RSD deflections because of the difference in the loading rate and testing temperatures (i.e., FWD measures deflection at simulated highway traffic speeds over a range of temperatures, whereas RSD deflection is measured at creep speeds at a single high temperature).
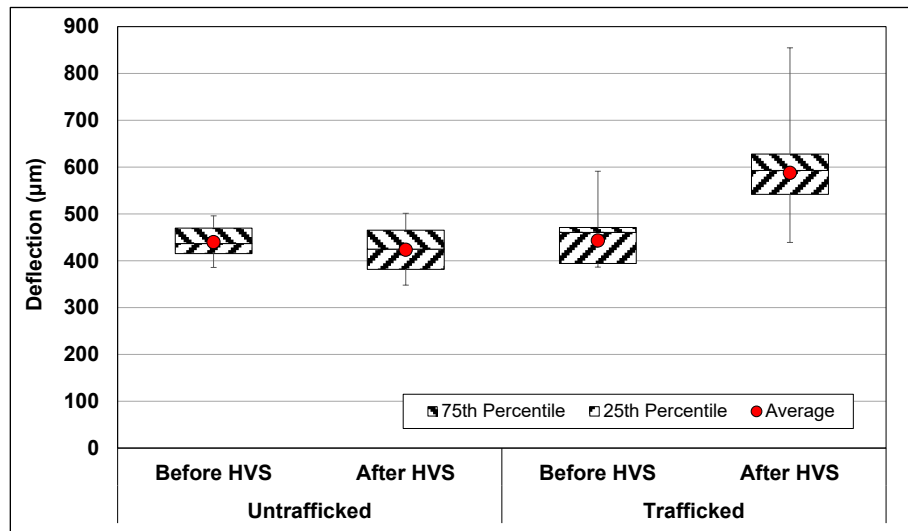
Figure 9.14: 701HC: Surface deflection (FWD).

The RHMA-G layer stiffness was backcalculated from the deflection measurements using the *CalBack* software package (see Section 5.5.5 for method followed), and the results are summarized in Figure 9.15. Error bars represent the lowest and highest values. The average backcalculated stiffness of the RHMA-G layer (3,653 MPa) at the start of testing was marginally lower than that recorded on RHMA-G layers tested in previous projects (around 4,300 MPa) but marginally higher than that measured on Section 704HB. This was attributed in part to the presence of small amounts of stiffer reclaimed asphalt binder in the mix. Stiffness decreased by about 690 MPa during HVS trafficking, indicating that the trafficking and/or hydraulic oil spill caused some damage in the RHMA-G layer. The stiffness of the untrafficked areas at either end of the test section also increased over the duration of the test (from 3,401 MPa to 4,076 MPa), further supporting the observation that small amounts of reclaimed asphalt binder had blended

with the virgin binder over time. The untrafficked areas were not affected by the hydraulic oil spill.
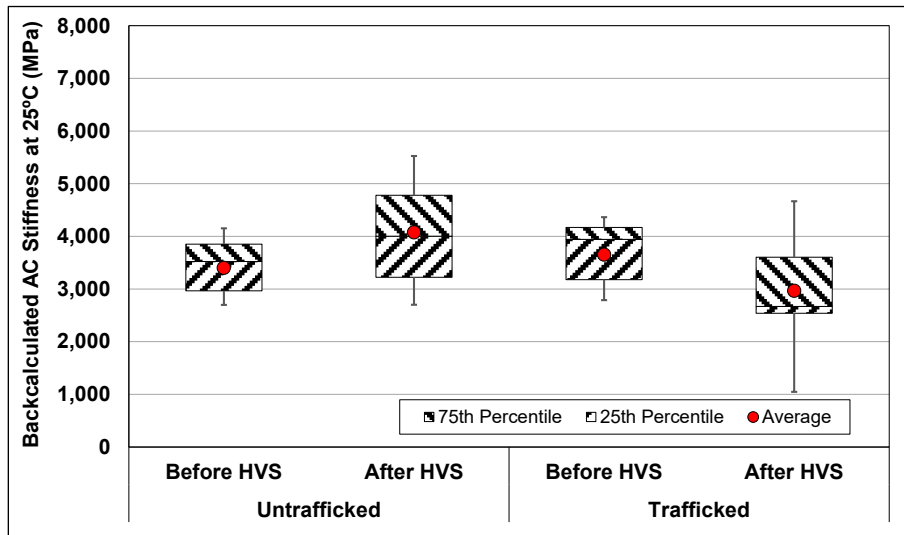
Figure 9.15: 701HC: Backcalculated stiffness of the RHMA-G layer (FWD).

9.10 Visual Assessment and Preliminary Forensic Coring

Apart from rutting, no other distresses were recorded on the section. Photographs of the test section after HVS testing are shown in Figure 9.16 through Figure 9.19.

Cores were taken from the wheelpath at Station 13 and from the adjacent untrafficked area 600 mm (≈24 in.) from the outside edge of the wheelpath (Figure 9.20 and Figure 9.21, respectively). No distresses or debonding were noted on the cores. Thickness and air-void content of the RHMA-G layer were measured on both cores (Table 9.2) and results indicate that although there was a small difference in air-void content between the wheelpath and the untrafficked area (0.8%), approximately 5 mm (0.20 in.) of rutting/densification was recorded in the wheelpath, confirming the observations from the profilometer MDD results.

Table 9.2: 701HC: Thickness and Air-Void Content Measurements from Cores

Property	Wheelpath	Untrafficked	Difference
RHMA-G thickness (mm [in.])	53 [2.09]	58 [2.28]	5 [0.20]
RHMA-G air-void content (%)	5.9	6.7	0.8
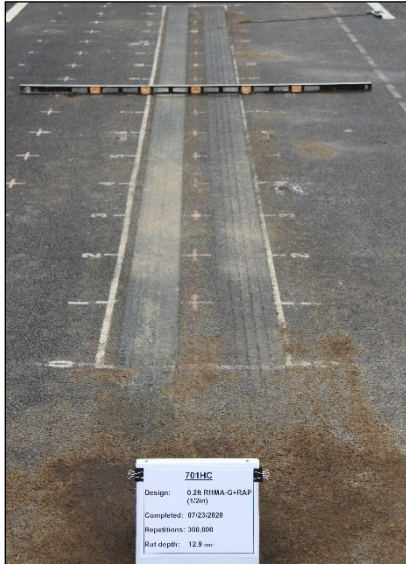
Figure 9.16: 701HC: Test section view from Station 0.

Figure 9.17: 701HC: Test section view from Station 16.

Figure 9.18: 701HC: View of rut at Station 8.

Figure 9.19: 701HC: Close-up view of test section surface at Station 8.

Figure 9.20: 701HC: Core taken in wheelpath.
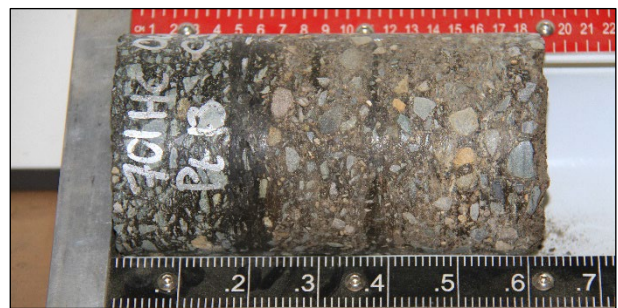
Figure 9.21: 701HC: Core taken 600 mm from edge of wheelpath.

10. SECTION 698HC: 0.2 ft. RHMA-G (3/4 in.) NO RAP

10.1 Test Summary

Loading commenced with a 40 kN half-axle load on July 6, 2020, and ended with an 80 kN load on September 18, 2020. A total of 600,000 load repetitions were applied and 50 datasets were collected. Load was increased from 40 kN to 60 kN after 160,000 load repetitions and then to 80 kN after 260,000 load repetitions. The HVS loading history for Section 698HC is shown in Figure 10.1. A 10-day breakdown resulting from a hydraulic system failure occurred between August 8 and August 17, a second 15-day breakdown resulting from an operating system failure occurred between October 2 and October 17, and a third 17-day breakdown resulting from another but different hydraulic system failure occurred between October 26 and November 11. The test was terminated just before reaching the rutting failure criterion (12.5 mm [0.5 in.]) due to ongoing hydraulic system issues. No oil spills occurred on the test section.
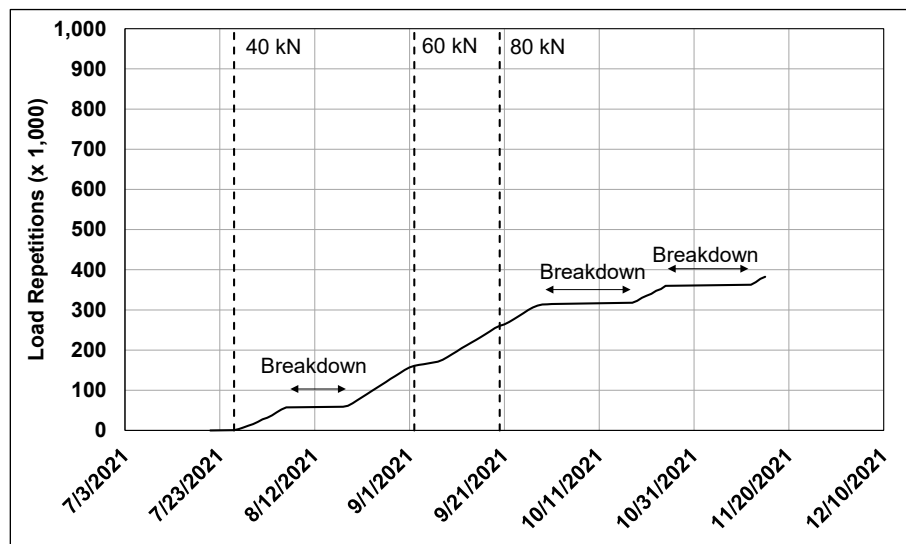
Figure 10.1: 698HC: HVS loading history.

10.2 Air Temperatures

10.2.1 Outside Air Temperatures

Daily 24-hour average outside air temperatures, measured with thermocouples attached to either side of the HVS environmental chamber (i.e., in direct sunlight), are summarized in Figure 10.2. Vertical error bars on each point on the graph show the daily temperature range. Temperatures ranged from 5.4°C to 48.7°C (≈42°F to 120°F) during the course of HVS testing,

with a daily 24-hour average of 24.8°C (≈77°F), an average minimum of 16.7°C (≈62°F), and an average maximum of 35.1°C (≈95°F).
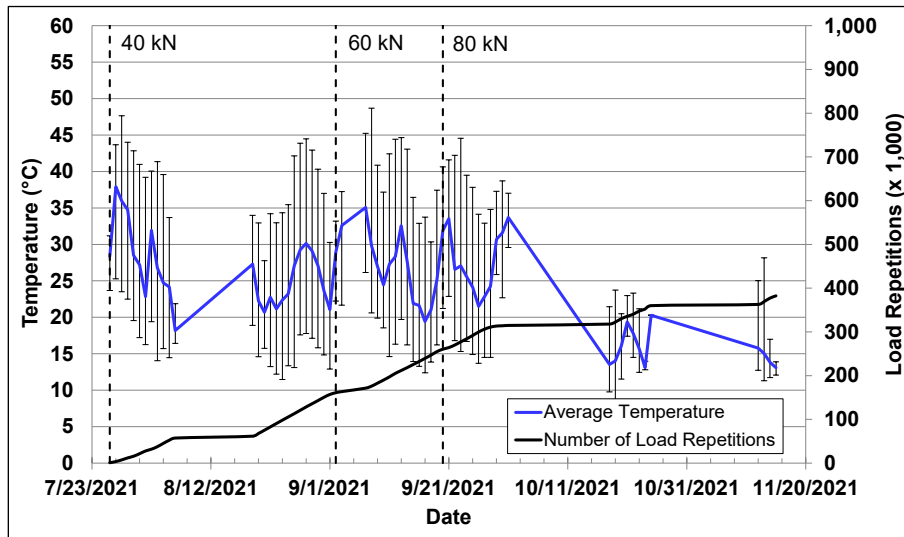
Figure 10.2: 698HC: Daily average air temperatures outside the environmental chamber.

10.2.2 Air Temperatures Inside the Environmental Chamber

The daily 24-hour average air temperatures, measured with thermocouples attached to either side of the HVS environmental chamber above the heaters and calculated from the hourly temperatures recorded during HVS operations, are shown in Figure 10.3. Vertical error bars on each point on the graph show the daily temperature range. During the test, air temperatures inside the environmental chamber ranged from 22.3°C to 49.7°C (≈72°F to 122°F) with an average of 37.8°C (≈100°F) and a standard deviation of 3.2°C (≈5.8°F). Air temperature was automatically adjusted with heater settings to maintain a pavement temperature of 50±2°C at a pavement depth of 50 mm (≈2.0 in.). The recorded pavement temperatures discussed in Section 10.3 indicate that the inside air temperatures were adjusted appropriately to maintain the required pavement temperature.

10.3 Pavement Temperatures

Daily 24-hour averages of the air, surface, and in-depth temperatures of the RHMA-G and recycled layers are shown in Figure 10.4 and listed in Table 10.1. Pavement temperatures were constant and in the target range (50±2°C at a pavement depth of 50 mm) in the RHMA-G layer. Temperatures decreased with increasing depth in the underlying layers, as expected.
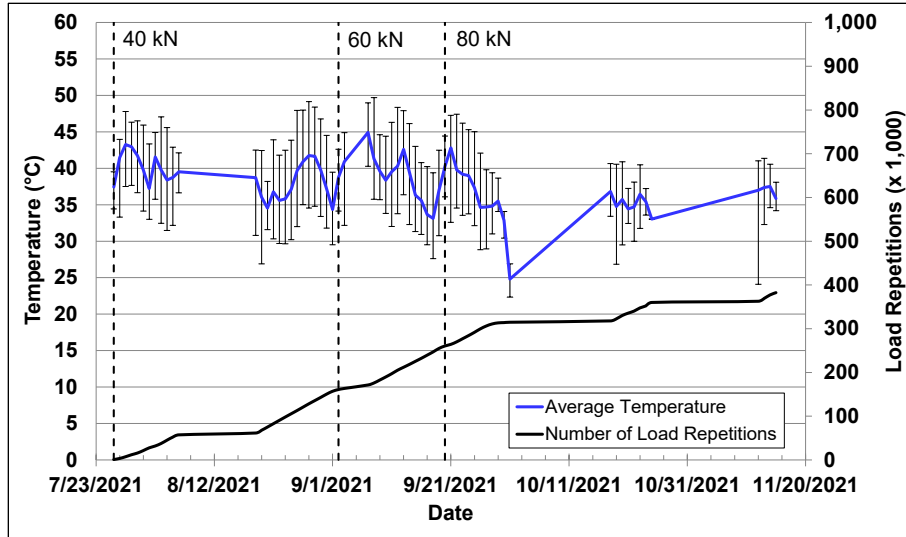
Figure 10.3: 698HC: Daily average air temperatures inside the environmental chamber.
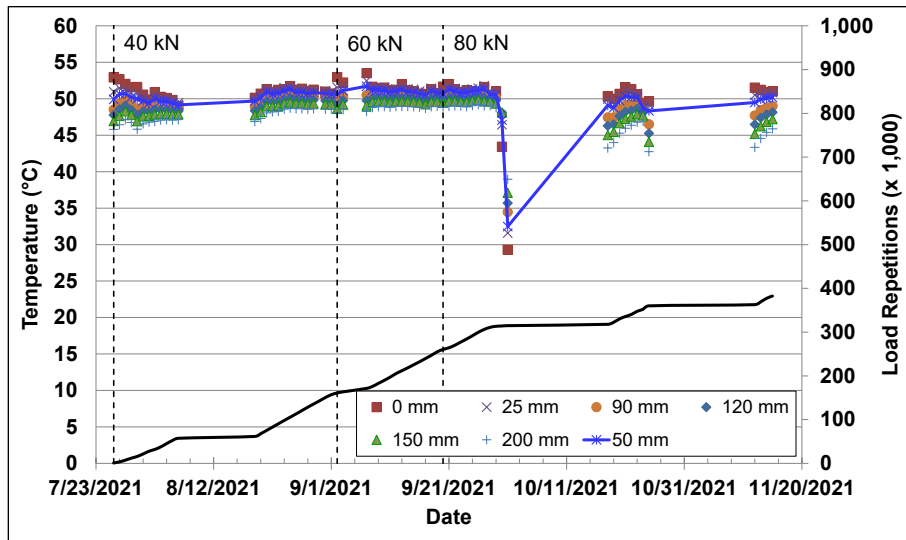
Figure 10.4: 698HC: Daily average pavement temperatures.

Table 10.1: 698HC: Summary of Air and Pavement Temperatures

Thermocouple Location	Layer	Temperature			
		Average (°C)	Std. Dev. (°C)	Average (°F)	Std. Dev. (°F)
Outside air	N/A	24.3	8.9	75.7	16.0
Inside air	N/A	38.0	4.3	100.4	7.8
Pavement surface	RHMA-G	51.0	2.9	123.8	5.3
25 mm below surface	RHMA-G	50.9	1.4	123.7	2.6
50 mm below surface	RHMA-G	50.5	1.3	122.9	2.3
90 mm below surface	Recycled	49.8	1.3	121.6	2.3
120 mm below surface	Recycled	49.2	1.3	120.6	2.4
150 mm below surface	Recycled	48.6	1.5	119.5	2.6
200 mm below surface	Recycled	47.8	1.7	118.0	3.0

10.4   Permanent Deformation on the Surface (Rutting)

Figure 10.5 shows the average transverse cross section measured with the laser profilometer at various stages of the test. This plot clearly shows the initial higher rate of rutting and the increase in rutting and deformation over time and that most of the deformation was in the form of a depression (i.e., deformation was below the zero elevation point at the surface [see Figure 5.8]). Minor upward and outward displacement of the material above the zero elevation point occurred after the load increase to 60 kN.
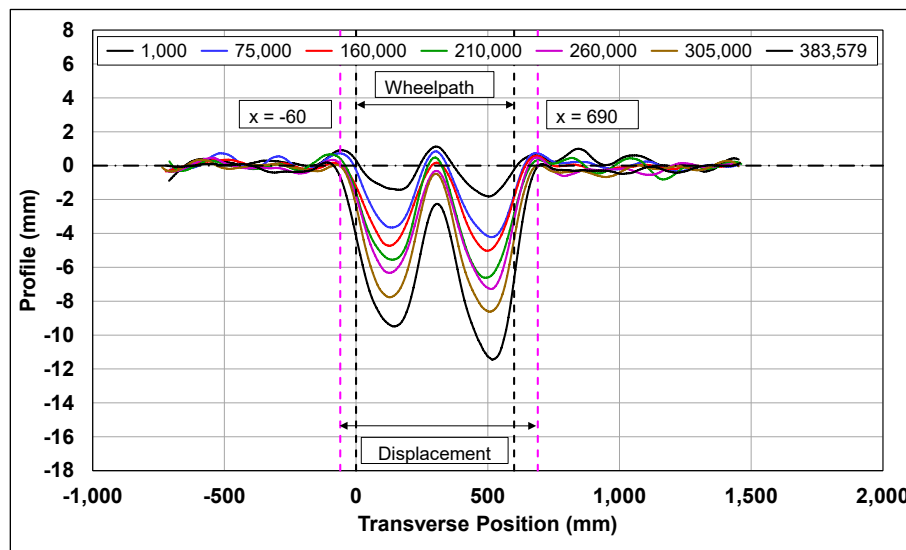
Figure 10.5: 698HC: Profilometer cross section at various load repetitions.

Figure 10.6 shows the development of permanent deformation (average maximum total rut and average deformation) with load repetitions. Error bars on the average maximum total rut line indicate lowest and highest measurements along the section. These error bars indicate some limited variation along the section and considerably less than that measured on Section 704HB. The embedment phase in this test occurred over a similar number of load repetitions to Section 704HB (i.e., ±20,000) but ended with a rut depth of about 4 mm (≈0.16 in.), considerably less that the 7 mm (≈0.28 in.) recorded on Section 704HB. This was attributed in part to the larger nominal maximum aggregate size and partly to the age of the section when tested.

The rate of increase of the rut depth after the embedment phase slowed considerably. Increases in the applied loads to 60 kN and 80 kN resulted in short embedment phases before stabilizing to rates similar to those recorded during the 40 kN testing.
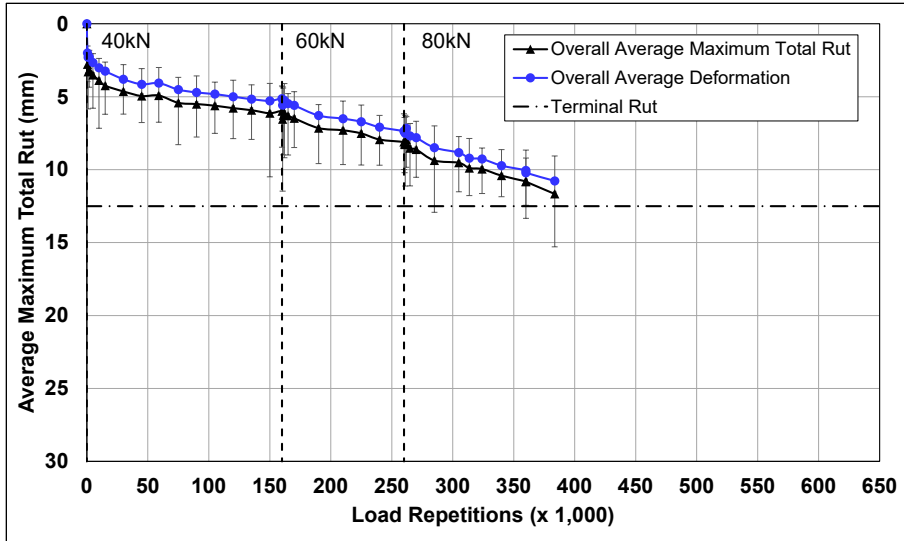
Figure 10.6: 698HC: Average maximum total rut and average deformation.

Figure 10.7 shows the average deformation and the deformation measured between Stations 3 and 7 and between Stations 8 and 13. The difference in average rut depth between the two subsections was very small, indicating only minor variability along the length of the section.
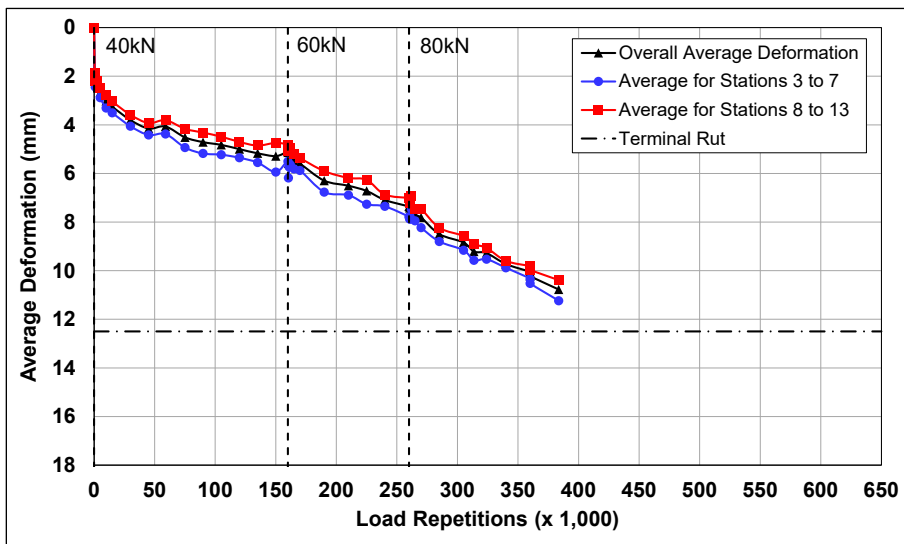
Figure 10.7: 698HC: Average deformation.

Figure 10.8 and Figure 10.9 show contour plots of the pavement surface at the start and end of the test (384,000 load repetitions). The end-of-test plot shows the relative uniformity along the length of the test section. After completion of trafficking, the average maximum rut depth and the average deformation were 11.7 mm (≈0.46 in.) and 10.8 mm (≈0.43 in.), respectively. The maximum rut depth measured on the section was 12.7 mm (≈0.50 in.), recorded at Station 8.

Note that testing was stopped just prior to reaching terminal rut depth due to equipment problems.
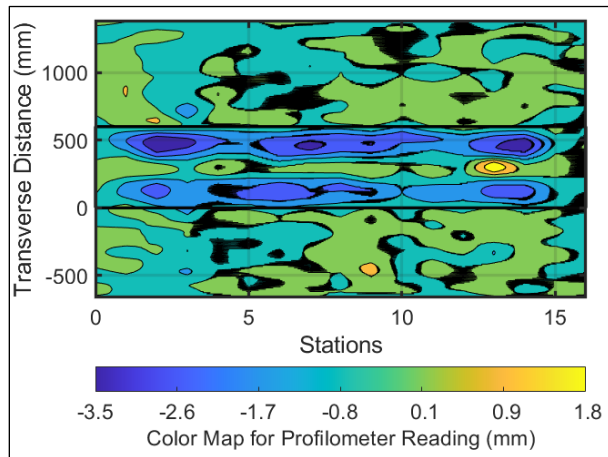
Figure 10.8: 698HC: Contour plot of permanent surface deformation at start of test.
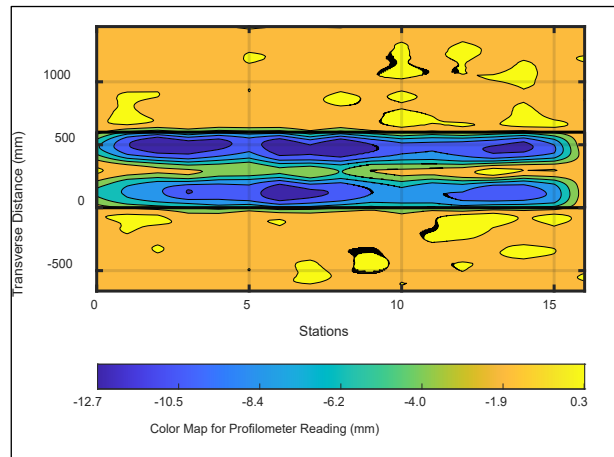
Figure 10.9: 698HC: Contour plot of permanent surface deformation at end of test.
(Note different scales in the legends.)

10.5   Permanent Deformation in the Underlying Layers

Permanent deformation in the underlying layers, recorded with multi-depth deflectometers (MDD) at Station 3 (in a wheelpath) and Station 13 (between wheelpaths) and compared to the surface layer (laser profilometer deformation [not total rut] measurements at Station 3 and Station 13), is shown in Figure 10.10 and Figure 10.11, respectively. Note that the MDD measurements at Station 13 cannot be directly compared with those from the laser profilometer because the MDD was installed in the untrafficked area between the wheelpaths. This instrument location can therefore only provide an indication of which layer or layers the permanent deformation occurred in and not the actual deformation in each layer.

Figure 10.10 (MDD in the wheelpath) shows that permanent deformation occurred primarily in the RHMA-G and CCPR layers. This differs from the results shown in Figure 10.11 and from the other sections (MDD between the wheelpaths), which show more deformation in the RHMA-G layer and less in the CCPR layer. Both plots show decreasing levels of permanent deformation in the aggregate base and aggregate subbase layers, and minimal permanent deformation in the subgrade. Notable increases in permanent deformation in the layers was not observed after the load changes.
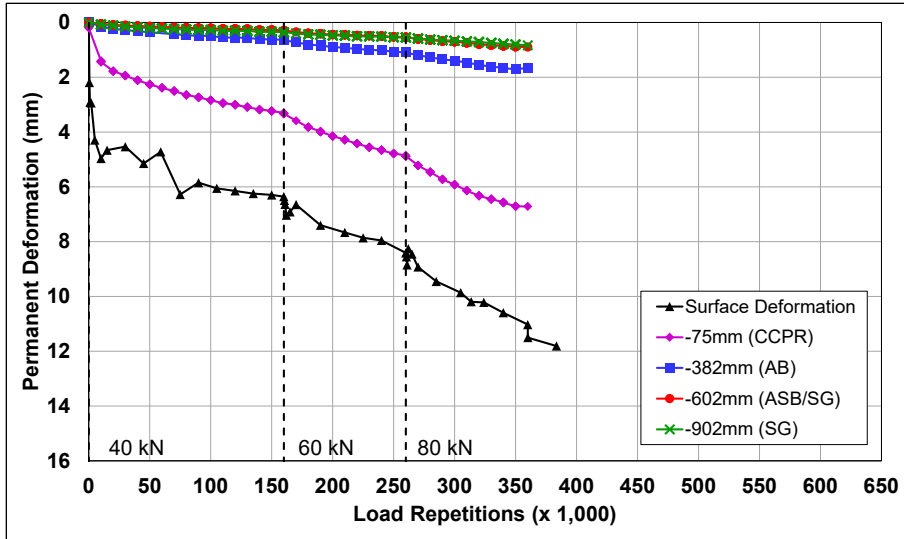
Figure 10.10: 698HC: Station 3: Permanent deformation in the underlying layers.
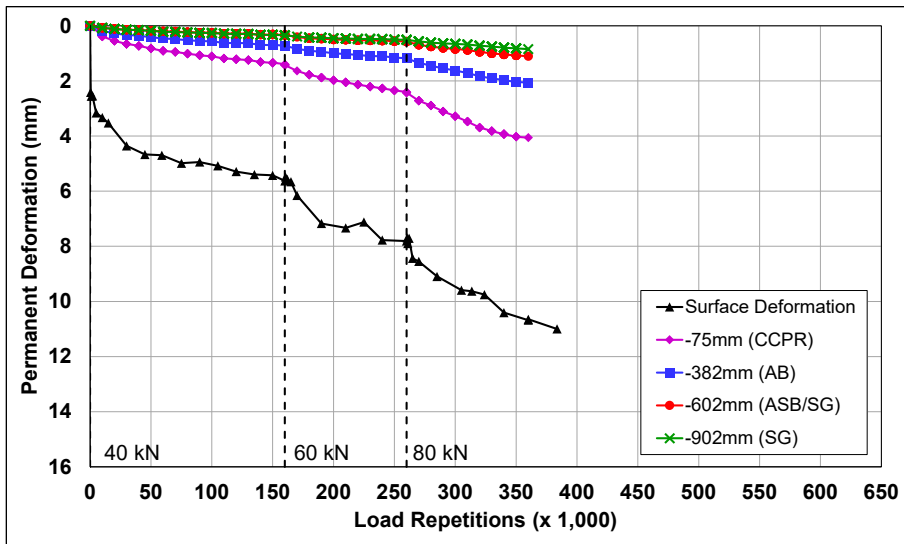
Figure 10.11: 698HC: Station 13: Permanent deformation in the underlying layers.

10.6 Vertical Pressure at the Midpoint of the Aggregate Base Layer

Figure 10.12 shows the traffic-induced vertical pressure in the middle of the aggregate base layer. Note that vertical pressure measurements are recorded continuously during trafficking and spikes in the measurements indicate when manual measurements, which are done at creep wheel speed, were taken.

Vertical pressure readings were stable after some initial embedment, but sensitive to load change, for the duration of the test. Increases in recorded pressures occurred after the load changes, as expected. The results were consistent with those measured on Section 704HB.
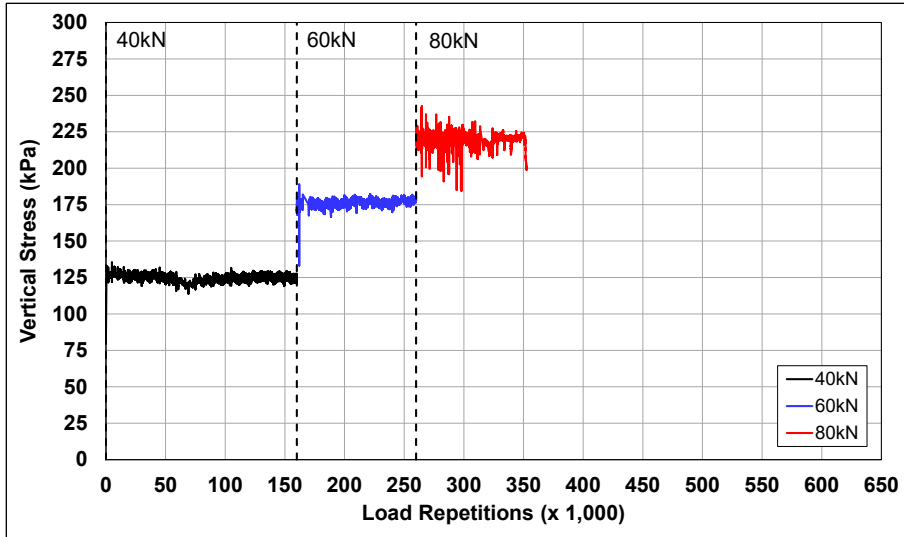
Figure 10.12: 698HC: Vertical pressure in the middle of the aggregate base layer.

10.7   Deflection on the Surface (Road Surface Deflectometer)

Figure 10.13 compares elastic surface deflections measured with a road surface deflectometer (RSD) under a 40 kN half-axle load. Deflections under the 60 kN and 80 kN loads are also shown.
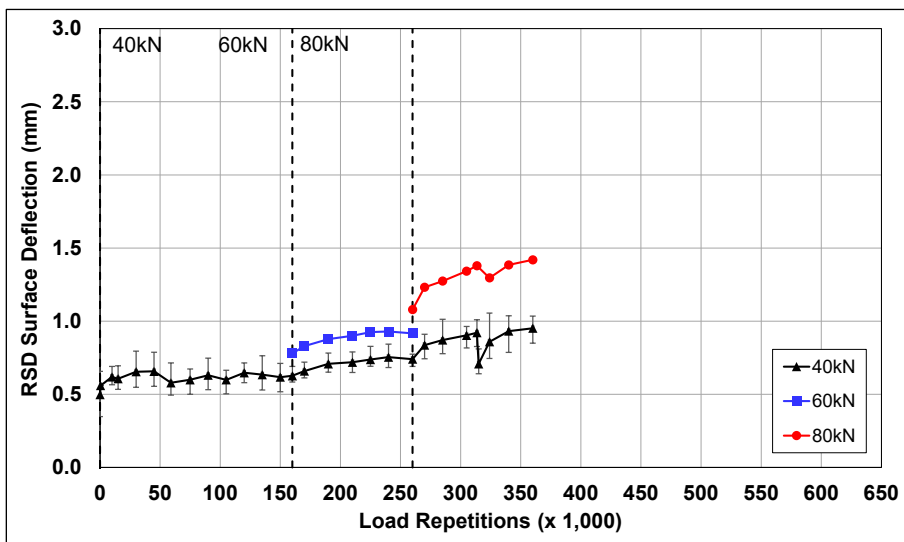
Figure 10.13: 698HC: Surface deflection (RSD).

Deflections increased during the embedment phase of each load. Although deflections appeared to stabilize after embedment under each load, deflection measured under the 40 kN load continued to increase, indicating that some permanent damage was occurring in the pavement under the 60 kN and 80 kN loads. Increases in absolute surface deflection were recorded on the section under the 60 kN and 80 kN loads, as expected. Error bars on the plot indicate lowest and

highest measurements along the section under the 40 kN load. These error bars indicate limited variability along the section during the 40 kN load testing.

Deflections measured in the early part of the test under the 40 kN load were lower than those measured on Section 704HB. This was attributed in part to the larger NMAS and partly to the longer period between construction and starting the test, during which some additional aging of the RHMA-G layer would have occurred. Deflections in the latter part of the test were consistent with those measured on Section 704HB.

10.8   Deflection in the Underlying Layers (Multi-Depth Deflectometer)

Figure 10.14 and Figure 10.15 show the history of in-depth elastic deflections measured by the LVDTs in the multi-depth deflectometers at Station 3 (in the wheelpath) and Station 13 (between the wheelpaths). The deflections measured were similar at both locations. These readings are consistent with the surface deflections measured with the RSD shown in Figure 10.13. There was a small increase in deflection at all levels during the initial embedment phase, after which deflections were stable for the remainder of the 40 kN wheel load trafficking. Deflections increased with increased load, as expected. They remained constant at all levels during the 60 kN wheel load tests, but continued to increase in the CCPR layer during the 80 kN wheel load tests. Deflection decreased with increasing depth, but the LVDTs at the different depths all showed similar trends over the course of the test.
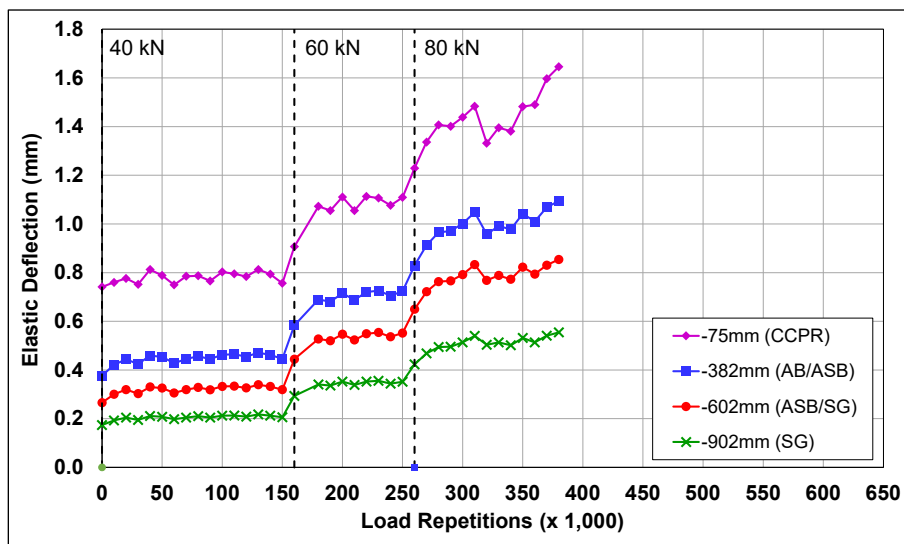

Figure 10.14: 698HC: Station 3: Elastic deflection in the underlying layers.
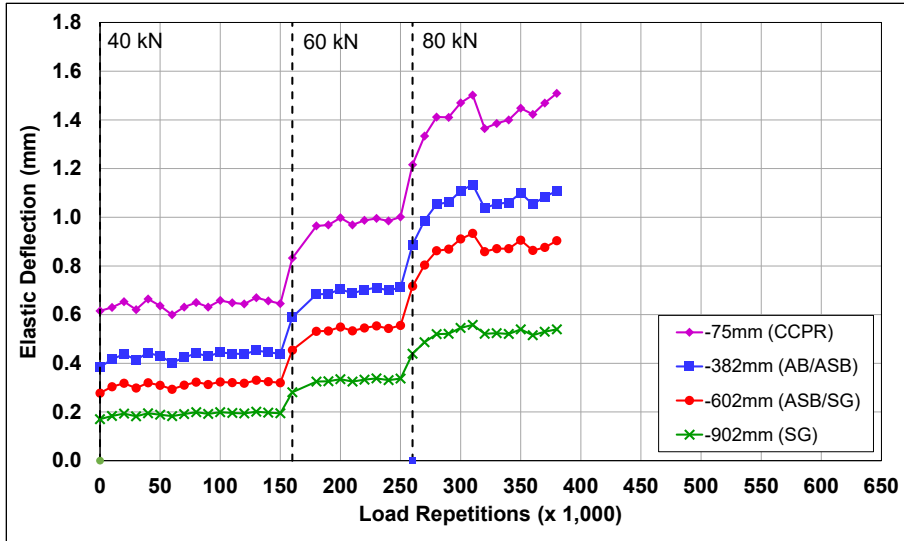
Figure 10.15: 698HC: Station 13: Elastic deflection in the underlying layers.

10.9   Deflection in the Pavement Structure (Falling Weight Deflectometer)

Surface deflections measured with a falling weight deflectometer (FWD) on the untrafficked and trafficked areas of the section are summarized in Figure 10.16 ("trafficked area" and "untrafficked area" represent the FWD measurements taken on the HVS test section and adjacent to the HVS test section, respectively). Error bars represent the lowest and highest values.
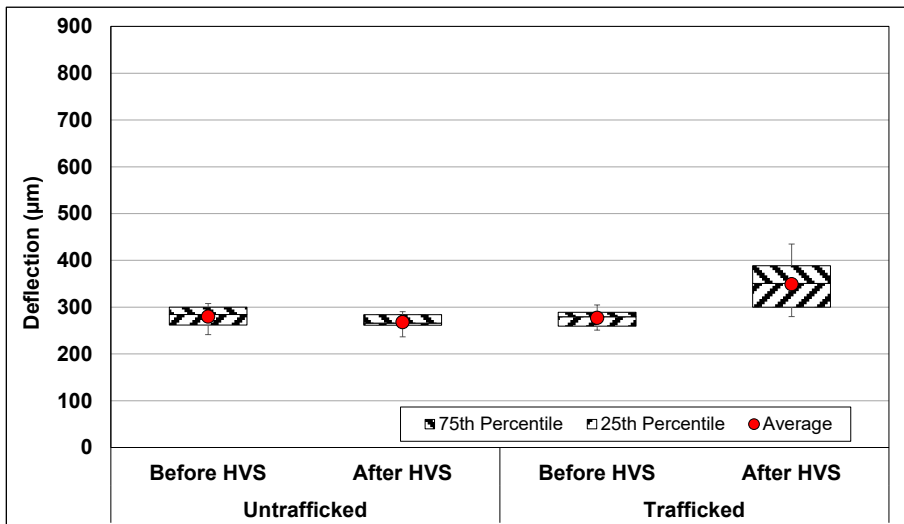
Figure 10.16: 698HC: Surface deflection (FWD).

The results were consistent with the RSD measurements discussed above, with the section exhibiting an increase in average surface deflection of about 72 microns after completion of HVS

trafficking. There was no change in deflection over time in the untrafficked area. Note that FWD deflections are typically lower than RSD deflections because of the difference in the loading rate and testing temperatures (i.e., FWD measures deflection at simulated highway traffic speeds over a range of temperatures, whereas RSD deflection is measured at creep speeds at a single high test temperature).

The RHMA-G layer stiffness was backcalculated from the deflection measurements using the *CalBack* software package (see Section 5.5.5 for method followed), and the results are summarized in Figure 10.17. Error bars represent the lowest and highest values. The average backcalculated stiffness of the RHMA-G layer (5,600 MPa) at the start of testing was considerably higher than those recorded on RHMA-G layers tested in previous projects (around 4,300 MPa) and higher than that measured on Section 704HB. The average stiffness decreased by about 1,618 MPa during HVS trafficking, indicating that the trafficking caused some damage in the RHMA-G layer. The stiffness of the untrafficked areas at either end of the test section remained essentially unchanged.
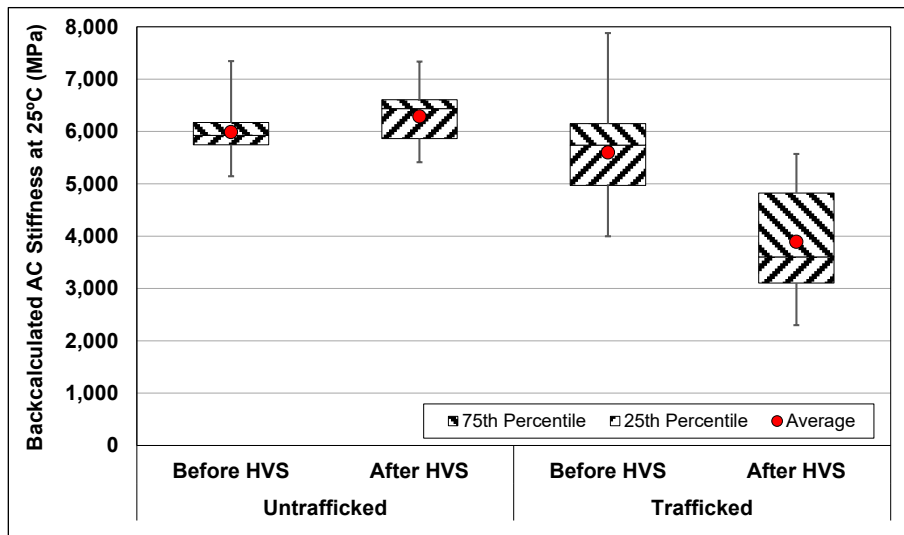
Figure 10.17: 698HC: Backcalculated stiffness of the RHMA-G layer (FWD).

10.10 Visual Assessment and Preliminary Forensic Coring

Apart from rutting, no other distress was recorded on the section. Photographs of the test section after HVS testing are shown in Figure 10.18 through Figure 10.21.

Cores were taken from the wheelpath at Station 13, and from the adjacent untrafficked area 600 mm (≈24 in.) from the outside edge of the wheelpath (Figure 10.22 and Figure 10.23, respectively). No distresses or debonding were noted on the cores. Thickness and air-void content for the RHMA-G layer were measured on both cores (Table 10.2). There was no difference in wheelpath air-void content between the two cores. The RHMA-G layer in the wheelpath was 5 mm (≈0.2 in.) thinner that the RHMA-G layer in the untrafficked area, indicating that some rutting and densification had occurred in this layer. These observations were consistent with the MDD results.
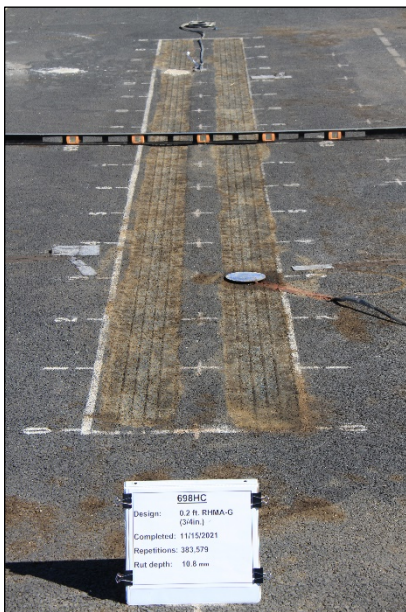
Figure 10.18: 698HC: Test section view from Station 0.
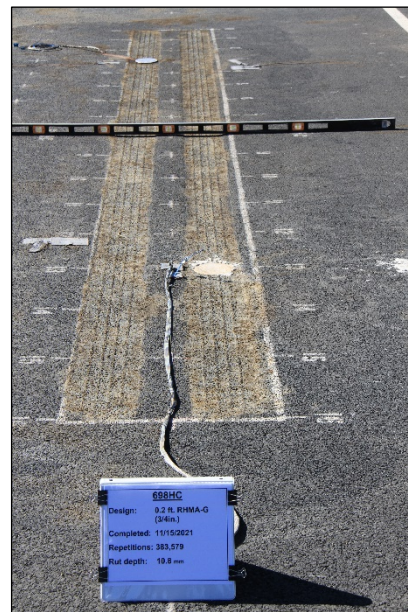
Figure 10.19: 698HC: Test section view from Station 16.

Figure 10.20: 698HC: View of rut at Station 8.

Figure 10.21: 698HC: Close-up view of test section surface at Station 8.
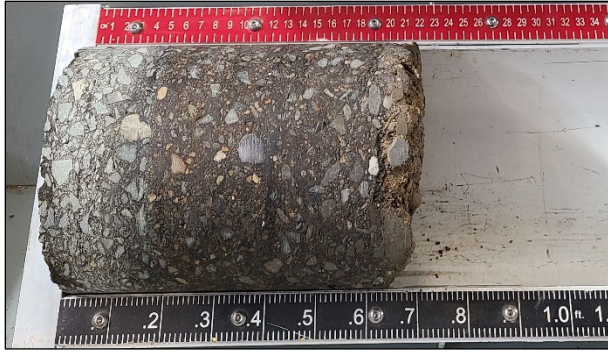
Figure 10.22: 698HC: Core taken in wheelpath.
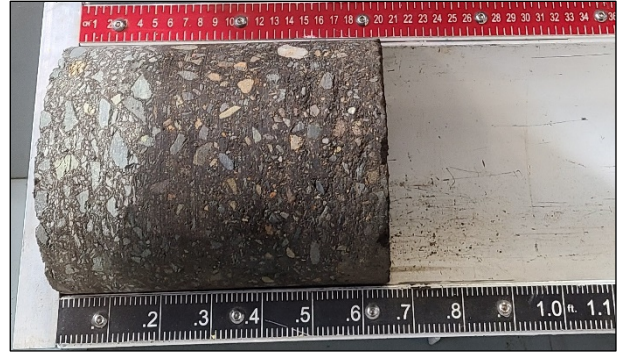
Figure 10.23: 698HC: Core taken 600 mm from edge of wheelpath.

Table 10.2: 698HC: Thickness and Air-Void Content Measurements from Cores

Property	Wheelpath	Untrafficked	Difference
RHMA-G thickness (mm [in.])	61 [2.40]	66 [2.60]	5 [0.20]
RHMA-G air-void content (%)	5.0	5.2	No difference

Blank page

11. SECTION 700HB: 0.5 ft. RHMA-G (3/4 in.) WITH RAP

11.1 Test Summary

Loading commenced with a 40 kN half-axle load on July 6, 2020, and ended with an 80 kN load on September 18, 2020. A total of 600,000 load repetitions were applied and 50 datasets were collected. Load was increased from 40 kN to 60 kN after 160,000 load repetitions and then to 80 kN after 260,000 load repetitions. The HVS loading history for Section 700HB is shown in Figure 11.1. A 15-day breakdown resulting from a hydraulic system failure occurred between August 25 and September 6 and a second 10-day breakdown resulting from an operating system failure occurred between September 26 and October 5.
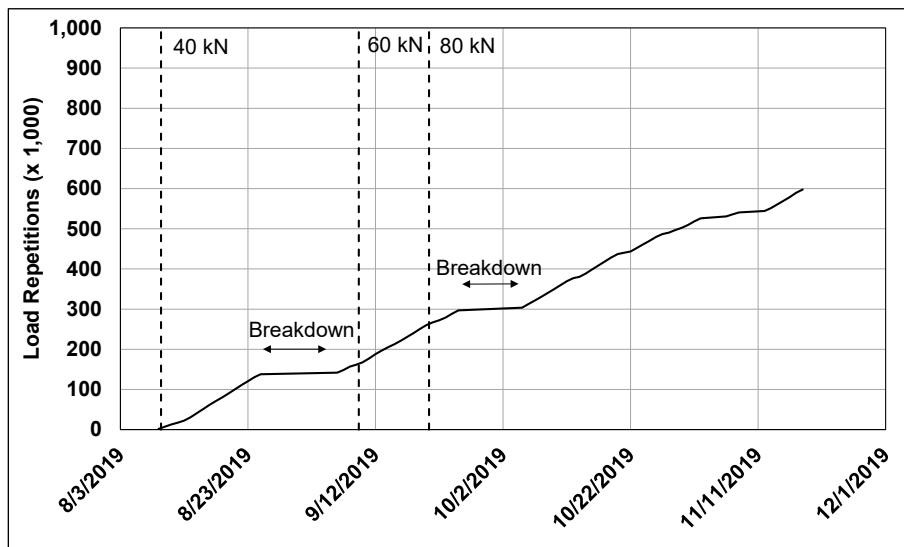
Figure 11.1: 700HB: HVS loading history.

11.2 Air Temperatures

11.2.1 Outside Air Temperatures

Daily 24-hour average outside air temperatures, measured with thermocouples attached to either side of the HVS environmental chamber (i.e., in direct sunlight), are summarized in Figure 11.2. Vertical error bars on each point on the graph show the daily temperature range. Temperatures ranged from 5.2°C to 50.3°C (≈41°F to 123°F) during the course of HVS testing, with a daily 24-hour average of 27.5°C (≈82°F), an average minimum of 18.5°C (≈65°F), and an average maximum of 38.4°C (≈101°F).
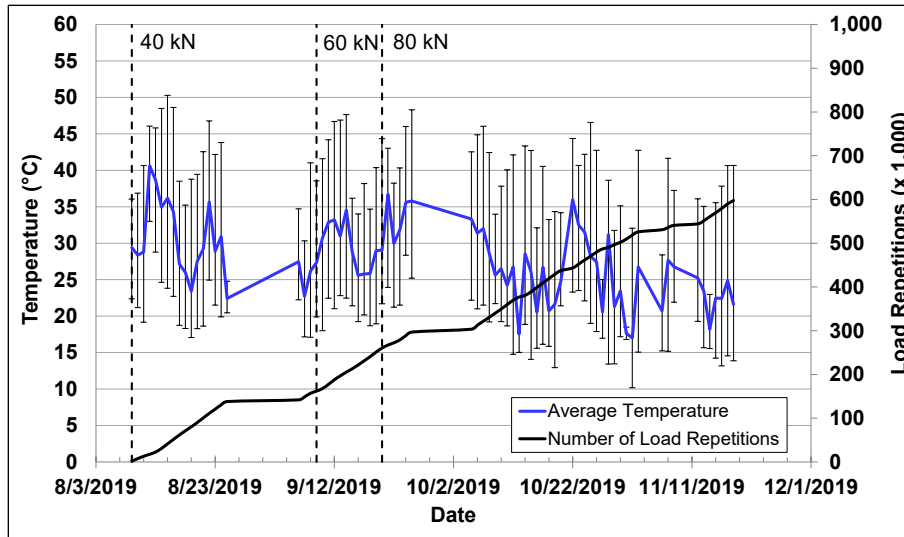
Figure 11.2: 700HB: Daily average air temperatures outside the environmental chamber.

11.2.2 Air Temperatures Inside the Environmental Chamber

The daily 24-hour average air temperatures, measured with thermocouples attached to either side of the HVS environmental chamber above the heaters and calculated from the hourly temperatures recorded during HVS operations, are shown in Figure 11.3. Vertical error bars on each point on the graph show the daily temperature range. During the test, air temperatures inside the environmental chamber ranged from 12.0°C to 52.0°C (≈54°F to 126°F) with an average of 43.5°C (≈110°F) and a standard deviation of 3.7°C (≈6.7°F). Air temperature was automatically adjusted with heater settings to maintain a pavement temperature of 50±2°C at a pavement depth of 50 mm (≈2.0 in.). The recorded pavement temperatures discussed in Section 11.3 indicate that the inside air temperatures were adjusted appropriately to maintain the required pavement temperature.

11.3 Pavement Temperatures

Daily 24-hour averages of the air, surface, and in-depth temperatures of the RHMA-G and recycled layers are shown in Figure 11.4 and listed in Table 11.1. Pavement temperatures were constant and in the target range (50±2°C at a pavement depth of 50 mm) in the RHMA-G layer. Temperatures decreased with increasing depth in the underlying layers, as expected.

UCPRC-RR-2022-05
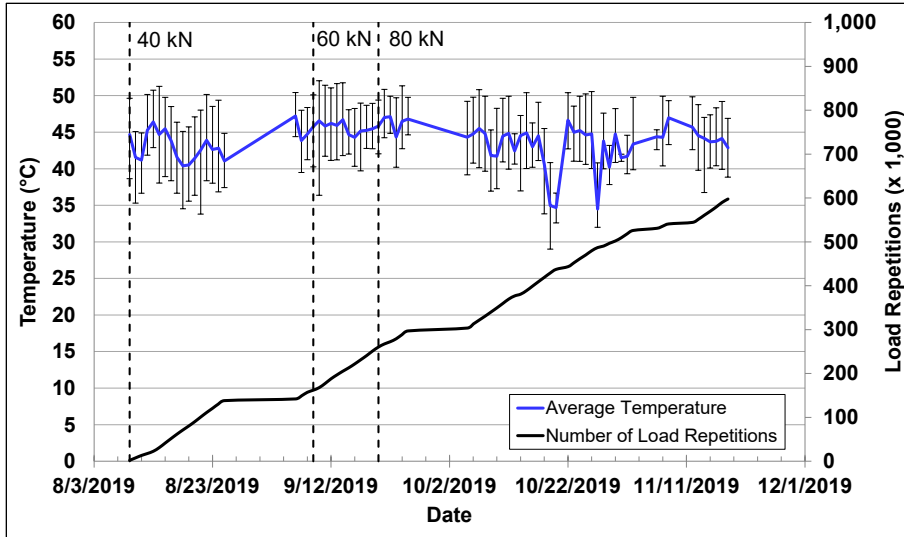
Figure 11.3: 700HB: Daily average air temperatures inside the environmental chamber.
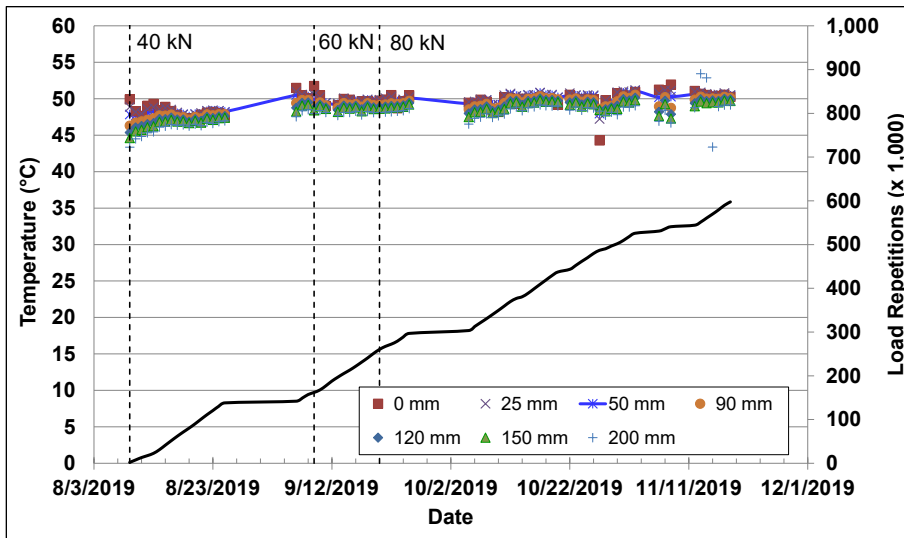
Figure 11.4: 700HB: Daily average pavement temperatures.

Table 11.1: 700HB: Summary of Air and Pavement Temperatures

Thermocouple Location	Layer	Temperature			
		Average (°C)	Std. Dev. (°C)	Average (°F)	Std. Dev. (°F)
Outside air	N/A	27.5	8.7	81.5	15.7
Inside air	N/A	43.5	3.7	110.3	6.7
Pavement surface	RHMA-G	49.3	3.0	120.7	5.5
25 mm below surface	RHMA-G	49.5	2.6	121.1	4.7
50 mm below surface	RHMA-G	49.3	2.6	120.8	4.7
90 mm below surface	RHMA-G	48.7	2.7	119.7	4.8
120 mm below surface	RHMA-G	48.4	2.7	119.0	4.9
150 mm below surface	RHMA-G	48.0	2.7	118.4	4.9
200 mm below surface	Recycled	47.4	3.9	117.4	7.1

11.4   Permanent Deformation on the Surface (Rutting)

Figure 11.5 shows the average transverse cross section measured with the laser profilometer at various stages of the test. This plot clearly shows the initial higher rate of rutting and the increase in rutting and deformation over time and that most of the deformation was in the form of a depression (i.e., deformation was below the zero elevation point at the surface [see Figure 5.8]). Minor upward and outward displacement of the material above the zero elevation point occurred after the load increase to 60 kN.
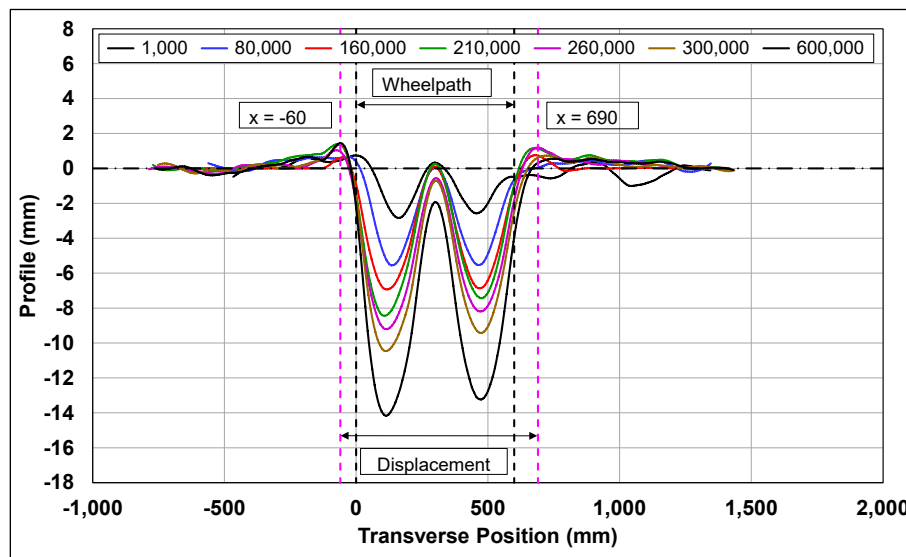
Figure 11.5: 700HB: Profilometer cross section at various load repetitions.

Figure 11.6 shows the development of permanent deformation (average maximum total rut and average deformation) with load repetitions. Error bars on the average maximum total rut line indicate lowest and highest measurements along the section. These error bars indicate some variation along the section but less than that measured on Section 704HB and marginally more than that measured on Section 698HC (19 mm NMAS control). The embedment phase in this test occurred over a similar number of load repetitions to Section 704HB and Section 698HC (i.e., ±20,000) but ended with a rut depth of about 4 mm (≈0.16 in.), considerably less that the 7 mm (≈0.28 in.) recorded on Section 704HB. This was attributed in part to the thicker RHMA-G layers, the larger nominal maximum aggregate size, and/or the use of RAP in the mix on this section.

The rate of increase of the rut depth after the embedment phase slowed considerably. Increases in the applied loads to 60 kN and 80 kN resulted in short embedment phases before stabilizing

to rates similar to those recorded during the 40 kN testing. This slower rut rate compared to Section 704HB was attributed primarily to the much thicker RHMA-G layer (150 mm [0.5 ft.] on this section compared to 60 mm [0.2 ft.] on Section 704HB). However, the rut rate on this section was marginally faster than that recorded on Section 698HC, indicating that thickness and presence of RAP did not improve rutting resistance when comparing these two sections, whereas age may have had an effect given that Section 698HC was tested 24 months after Section 700HB.
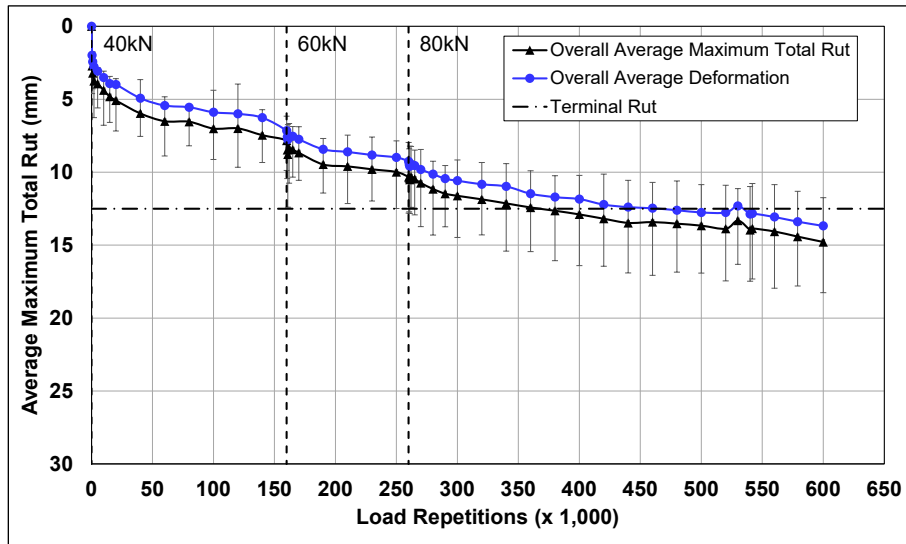
Figure 11.6: 700HB: Average maximum total rut and average deformation.

Figure 11.7 shows the average deformation and the deformation measured between Stations 3 and 7 and between Stations 8 and 13. The average rut depth was marginally deeper between Stations 8 and 13, with the difference between the rut depths on the two subsections less than on Section 704HB, indicating less variability along the length of the section.

Figure 11.8 and Figure 11.9 show contour plots of the pavement surface at the start and end of the test (600,000 load repetitions). The end-of-test plot shows the deeper rut between Stations 8 and 13. Terminal rut (12.5 mm [≈0.5 in.]) was reached after approximately 370,000 load repetitions (≈2.73 million ESALs). However, trafficking was continued for another 230,000 additional load repetitions to further assess rutting trends on this thicker RHMA-G layer under the 80 kN load. After completion of trafficking, the average maximum rut depth and the average deformation were 14.8 mm (≈0.58 in.) and 13.7 mm (≈0.54 in.), respectively. The maximum rut depth measured on the section was 15.8 mm (≈0.85 in.), recorded at Station 11.
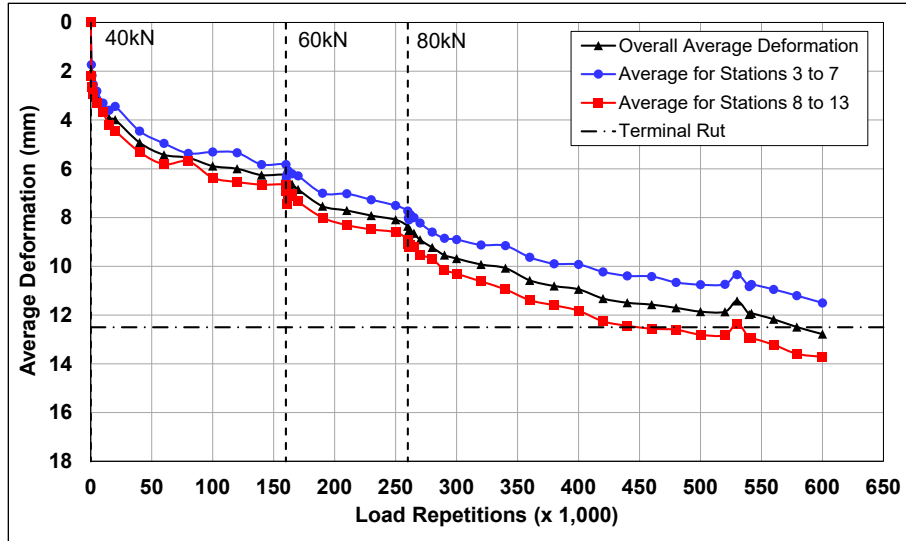
Figure 11.7: 700HB: Average deformation.
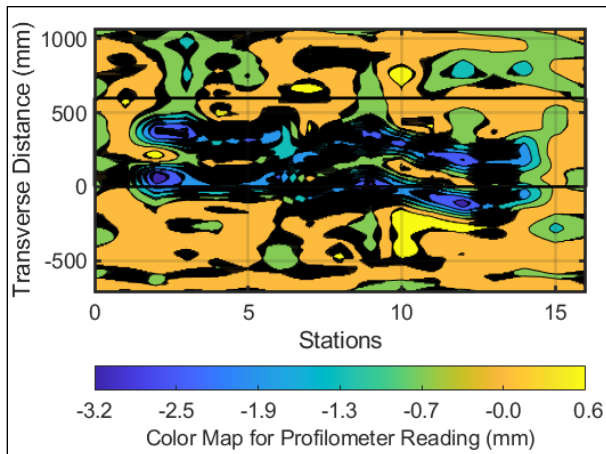
Figure 11.8: 700HB: Contour plot of permanent surface deformation at start of test.
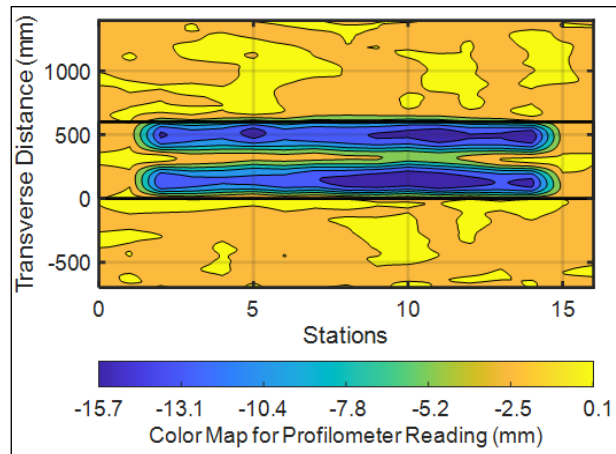
Figure 11.9: 700HB: Contour plot of permanent surface deformation at end of test.
(Note different scales in the legends.)

11.5 Permanent Deformation in the Underlying Layers

Permanent deformation in the underlying layers, recorded with a multi-depth deflectometer (MDD) at Station 13 and compared to the surface layer (laser profilometer deformation [not total rut] measurement at Station 13), is shown in Figure 11.10. The LVDTs appeared to have had better survivability on this test compared to the tests on Section 704HB. Note that the MDD measurements cannot be directly compared with those from the laser profilometer because the MDD on this section was installed in the untrafficked area between the wheelpaths. This instrument location can therefore only provide an indication of which layer or layers the

permanent deformation occurred in and not the actual deformation in each layer, which will be assessed during forensic investigations when all testing is completed.
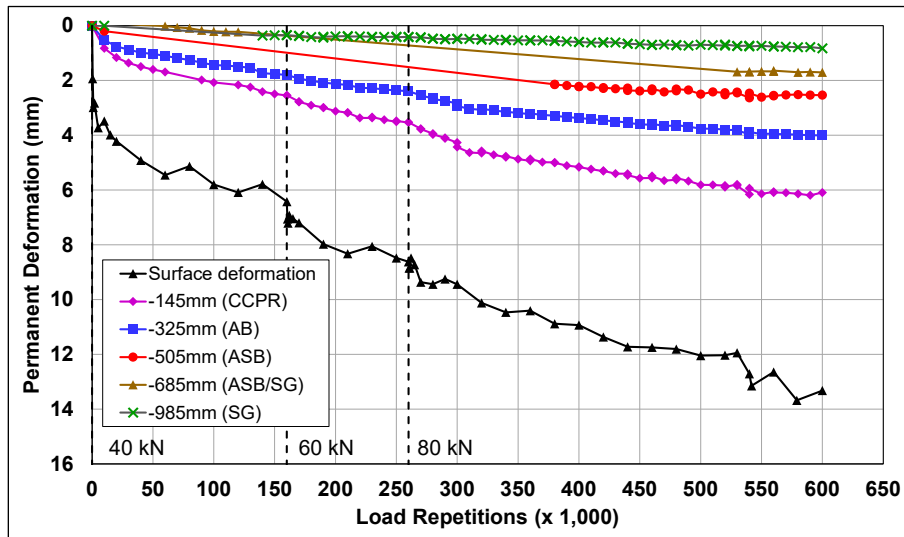
Figure 11.10: 700HB: Permanent deformation in the underlying layers.

Figure 11.10 shows that permanent deformation occurred primarily in the RHMA-G layer, consistent with other tests, with decreasing levels of permanent deformation in the CCPR, aggregate base, and aggregate subbase layers. Minimal permanent deformation was recorded in the subgrade. Notable increases in permanent deformation in the layers was not observed after the load changes, which was attributed in part to the thicker RHMA-G layer on this section.

11.6   Vertical Pressure at the Midpoint of the Aggregate Base Layer

Figure 11.11 shows the traffic-induced vertical pressure in the middle of the aggregate base layer. Note that vertical pressure measurements are recorded continuously during trafficking and spikes in the measurements indicate when manual measurements, which are done at creep wheel speed, were taken.

Vertical pressure readings were stable after some initial embedment, but sensitive to load change, for the duration of the test. Increases in recorded pressures occurred after the load changes, as expected. The results were consistent with those measured on Section 704HB and Section 698HC.
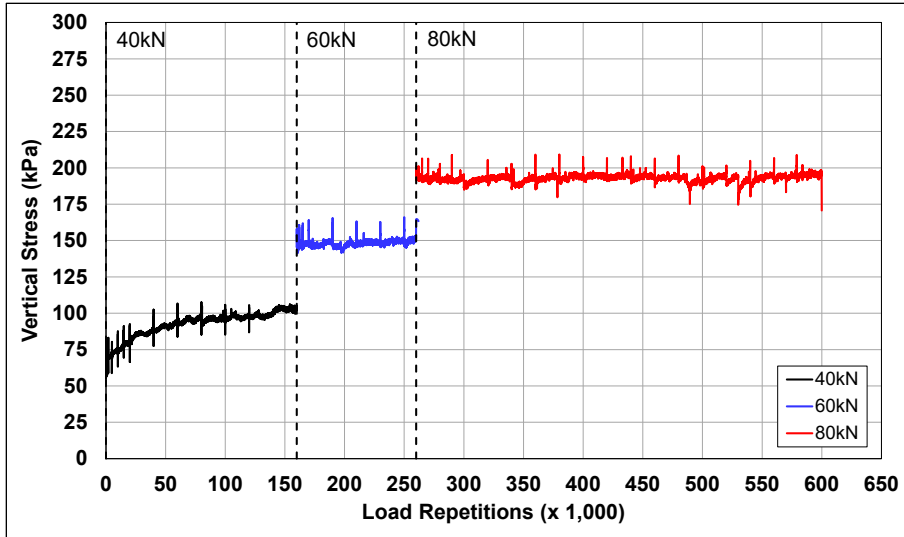
Figure 11.11: 700HB: Vertical pressure in the middle of the aggregate base layer.

11.7 Deflection on the Surface (Road Surface Deflectometer)

Figure 11.12 compares elastic surface deflections measured with a road surface deflectometer (RSD) under a 40 kN half-axle load. Deflections under the 60 kN and 80 kN loads are also shown.
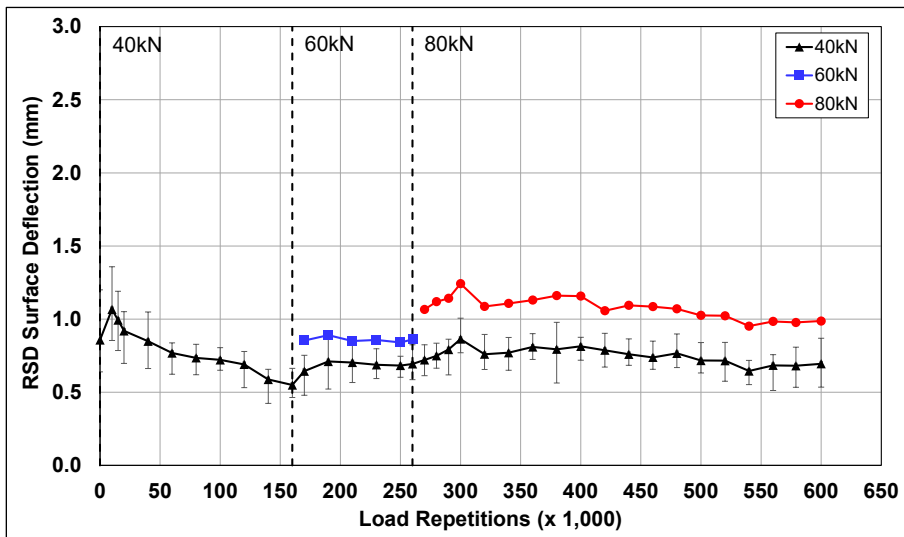
Figure 11.12: 700HB: Surface deflection (RSD).

Deflections increased during the embedment phase of each load but stabilized thereafter at all load levels, indicating that only limited permanent damage was occurring in the pavement under the 60 kN and 80 kN loads, which was attributed to the thicker pavement. This trend was different to those observed on Section 704HB and Section 698HC, where deflections continued to increase under the 40 kN load. Increases in absolute surface deflection were recorded on the

section under the 60 kN and 80 kN loads, as expected. Error bars on the plot indicate lowest and highest measurements along the section under the 40 kN load. There was limited variability for the duration of the test.

Deflections measured in the early part of the test under the 40 kN load were lower than those measured on Section 704HB (attributed to the thicker RHMA-G layer) but higher than those recorded on Section 698HC (attributed to age of the section at time of testing). Deflections in the latter part of the test were consistent with those measured on Section 704HB and marginally lower than those recorded on Section 698HC.

11.8   Deflection in the Underlying Layers (Multi-Depth Deflectometer)

Figure 11.13 shows the history of in-depth elastic deflections measured by the LVDTs in the multi-depth deflectometer. These readings are consistent with the surface deflections measured with the RSD shown in Figure 11.12.
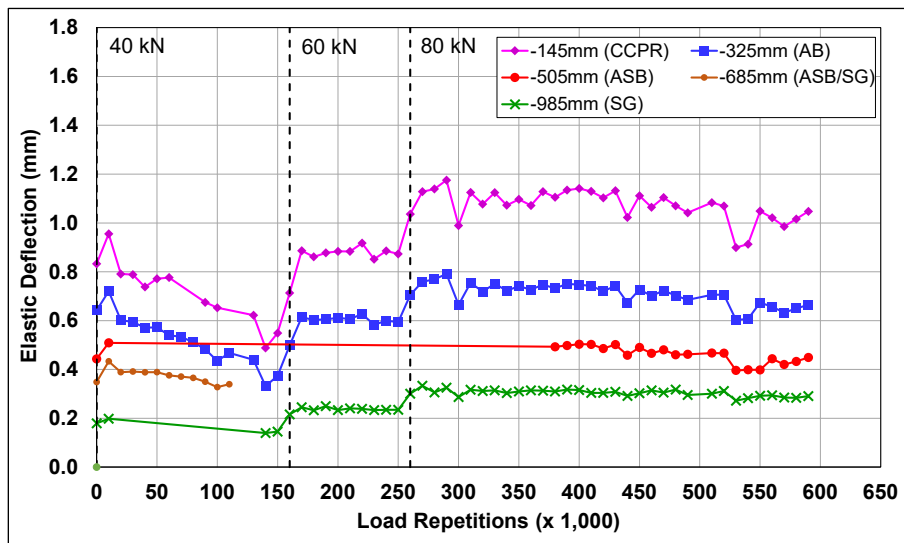
Figure 11.13: 700HB: Elastic deflection in the underlying layers.

Deflections decreased during the 40 kN wheel load trafficking suggesting some stiffening/densification in the layers attributable to HVS trafficking as well as the additional confinement provided by the thicker RHMA-G layer. Deflections increased with increased load, as expected, but then remained essentially the same for the duration of testing at that load, indicating that minimal damage was occurring in the underlying layers under the heavier wheel

loads. Deflection decreased with increasing depth, but the LVDTs at the different depths all showed similar trends over the course of the test.

Deflections under 40 and 60 kN wheel loads were consistent with those recorded on Section 704HB and Section 698HC. However, under the 80 kN wheel load, the deflections recorded on Section 698 HC were notably higher.

11.9 Deflection in the Pavement Structure (Falling Weight Deflectometer)

Surface deflections measured with a falling weight deflectometer (FWD) on the untrafficked and trafficked areas of the section are summarized in Figure 11.14 ("trafficked area" and "untrafficked area" represent the FWD measurements taken on the HVS test section and adjacent to the HVS test section, respectively). Error bars represent the lowest and highest values. The results were consistent with the RSD measurements discussed above, with the section exhibiting a small decrease in surface deflection of about 135 microns after completion of HVS trafficking. This was attributed in part to blending of the aged reclaimed asphalt binder with the virgin asphalt rubber binder over time, given that a similar decrease in deflection was measured in the untrafficked area. Note that FWD deflections are typically lower than RSD deflections because of the difference in the loading rate and testing temperatures (i.e., FWD measures deflection at simulated highway traffic speeds over a range of temperatures, whereas RSD deflection is measured at creep speeds at a single high test temperature).
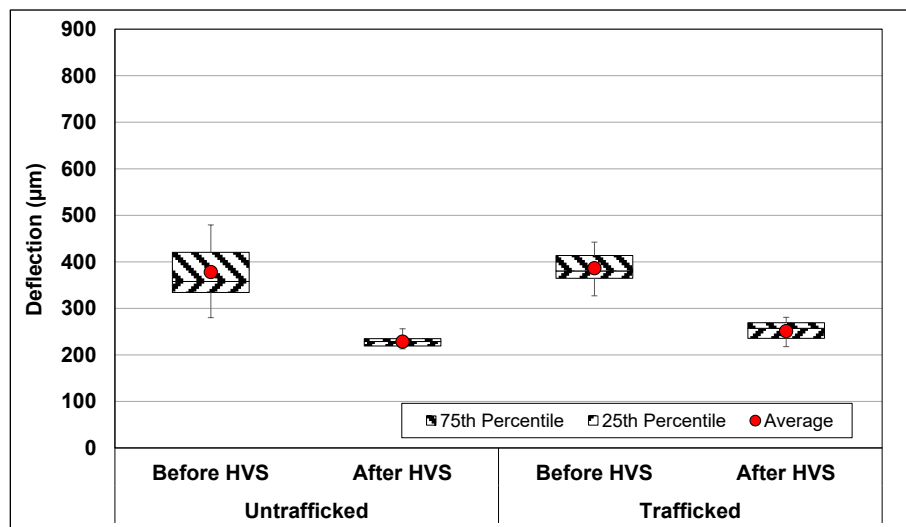
Figure 11.14: 700HB: Surface deflection (FWD).

The RHMA-G layer stiffness was backcalculated from the deflection measurements using the *CalBack* software package (see Section 5.5.5 for method followed), and the results are summarized in Figure 11.15. Error bars represent the lowest and highest values. The average backcalculated stiffness of the RHMA-G layer (2,746 MPa) at the start of testing was considerably lower than those recorded on RHMA-G layers tested in previous projects (around 4,300 MPa) and lower than those measured on Section 704HB and Section 698HC. However, the average stiffness increased by about 1,630 MPa during HVS trafficking, indicating that the trafficking did not cause any damage in the RHMA-G layer, or that damage was masked by an increase in stiffness due to blending of the reclaimed asphalt and asphalt rubber binders over time (note that the mix used in the first lift had close to zero silo time, while the mix used in the second lift was stored for close to eight hours before placement). The stiffness of the untrafficked areas at either end of the test section also increased by a similar amount during the test (from 2,829 MPa to 4,621 MPa), further supporting the observation that some blending had occurred between the reclaimed and virgin asphalt binders after placement of the first lift.
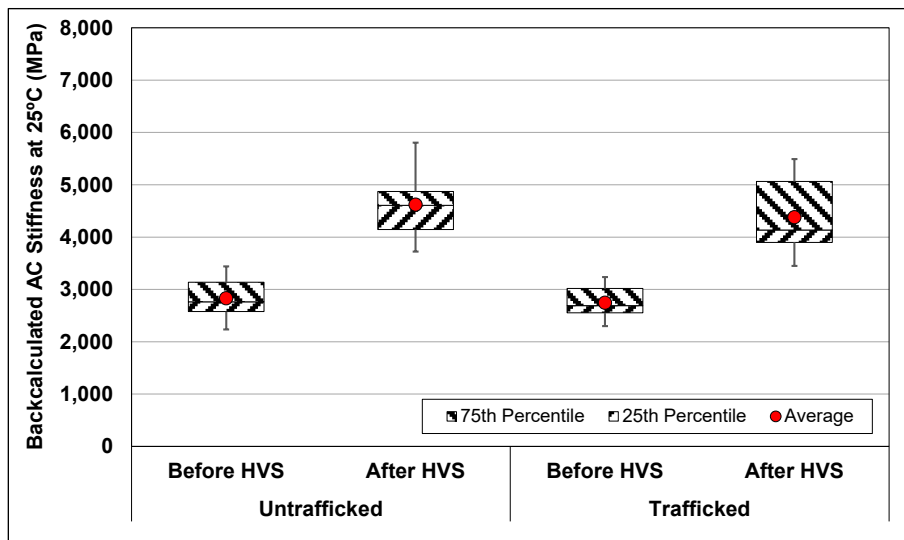
Figure 11.15: 700HB: Backcalculated stiffness of the RHMA-G layer (FWD).

11.10 Visual Assessment and Preliminary Forensic Coring

Apart from rutting, no other distress was recorded on the section. Photographs of the test section after HVS testing are shown in Figure 11.16 through Figure 11.19. Cores were taken from the wheelpath at Station 13, and from the adjacent untrafficked area 600 mm (≈24 in.) from the outside edge of the wheelpath (Figure 11.20 and Figure 11.21, respectively). No distresses or

debonding were noted on the cores. Thickness and air-void content of the RHMA-G layers were measured on both cores (Table 11.2), but some damage on the bottom lift of the core sampled from the untrafficked area caused during cutting prevented determination of an air-void content.

In the top layers, the wheelpath air-void content was 1.8% lower than the untrafficked area and the core was 119 mm (≈0.43 in.) thinner, indicating that considerable rutting and densification had occurred in the top layer. The difference in thickness between the bottom layers on the two cores was 2 mm (0.08 in.). These observations were consistent with the MDD results.

Figure 11.16: 700HB: Test section view from Station 0.

Figure 11.17: 700HB: Test section view from Station 16.

Figure 11.18: 700HB: View of rut at Station 8.

Figure 11.19: 700HB: Close-up view of test section surface at Station 8.

Figure 11.20: 700HB: Core taken in wheelpath.
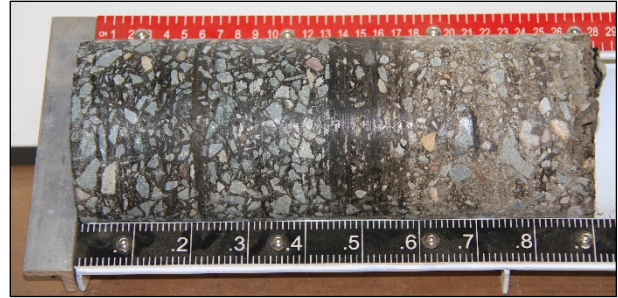
Figure 11.21: 700HB: Core taken 600 mm from edge of wheelpath.

Table 11.2: 700HB: Thickness and Air-Void Content Measurements from Cores

Property	Layer	Wheelpath	Untrafficked	Difference
RHMA-G thickness (mm [in.])	Top	59 [2.32]	70 [2.76]	11 [0.43]
	Bottom	71 [2.80]	73 [2.87]	2 [0.08]
RHMA-G air-void content (%)	Top	3.8	5.6	1.8
	Bottom	3.3	Core damaged	N/A

Blank page

12.   HEAVY VEHICLE SIMULATOR TEST RESULT SUMMARY

12.1   Introduction

Five of the seven planned first phase Heavy Vehicle Simulator (HVS) tests on four different RHMA-G mixes with different lift thicknesses have been completed in the first phase of this study, which focused on assessing rutting resistance. The following tests, in order of testing, were completed:

- Section 700HB: 0.5 ft. (150 mm) RHMA-G, with 3/4 in. NMAS with 10% RAP aggregate replacement. Tested between August and November, 2019.
- Section 701HC: 0.2 ft. (60 mm) RHMA-G, with 1/2 in. NMAS with 10% RAP aggregate replacement. Tested between September 2019 and July 2020.
- Section 704HB: 0.2 ft. (60 mm) RHMA-G, with 1/2 in. NMAS and no RAP (Control Section). Tested between July and September 2020.
- Section 703HB: 0.4 ft. (120 mm) RHMA-G, with 1/2 in. NMAS and no RAP. Tested between September and December 2020.
- Section 698HC: 0.2 ft. (60 mm) RHMA-G, with 3/4 in. nominal maximum aggregate size (NMAS) and no RAP. Tested between July and November 2021.

The following two sections were planned, but not tested:

- Section 699Hx: 0.5 ft. (150 mm) RHMA-G, with 3/4 in. NMAS and no RAP.
- Section 702Hx: 0.4 ft. (120 mm) RHMA-G, with 1/2 in. NMAS with 10% RAP aggregate replacement.

Testing focused on early rutting performance and started in August 2019 and continued, with interruptions, until November 2021. Interruptions included the programmed overhaul of the hydraulic systems on both machines, which in turn were interrupted by the COVID-19 pandemic and subsequent prolonged supply chain issues that resulted in significant delays in receiving critical spare parts. Testing on the remaining two tests was postponed indefinitely due to time and funding constraints and because initial second-level analyses, documented in a separate report *(2)*, indicated that sufficient data had been collected from the tested sections to make informed decisions about the expected performance of thicker RHMA-G layers and RHMA-G layers produced with RAP as replacement aggregate.

A range of daily 24-hour average temperatures was experienced over the two-year testing period; however, pavement temperatures remained constant in the target range throughout HVS trafficking. None of the sections were tested during prolonged rainfall and no sections were tested when surface water was present.

12.2 Rutting Performance

Rutting behavior on the five sections is compared in Figure 12.1 and Figure 12.2. The following observations were made:

- Terminal rut (12.5 mm [0.5 in.]) was reached on four of the five sections. Testing was stopped just prior to reaching terminal rut on one section (698HC) due to hydraulic system issues, and rut rate to terminal rut was extrapolated where appropriate.

- Four of the five sections showed similar trends, consistent with other HVS tests, with an early embedment phase of less than 5 mm. One test (704HB, control) had a considerably deeper embedment phase, and terminal rut was reached with the lowest number of load repetitions. The reason for this difference in performance is not clear from the data, although some observations during track construction and testing may have contributed. Although testing was interrupted due to a hydraulic system failure, no hydraulic oil spilled on the section. Comparisons of multi-depth deflectometer data from the other sections indicate that there may have been a problem in the aggregate base layer (shearing of materials due to uncrushed rounded aggregate) and/or in the CCPR layer (Section 704HB was located where the first CCPR-FA material was placed when higher-than-design foaming water contents were noted and while settings on the plant were still being dialed in). A forensic investigation will be conducted once all testing on the track is complete.

- On Section 701HC, rutting behavior was consistent with the other sections during testing with a 40 kN wheel load, but after the load increase to 60 kN, the rate of rut depth increased considerably, and terminal rut was reached earlier than expected. This was attributed to a hydraulic system failure (ruptured metal pipe with no indication of distress) that resulted in oil spilling on the section immediately after the load change. Hydraulic oil is known to soften asphalt binder and although the oil was cleaned off immediately after the spill and an absorbent material was applied for a period after the cleanup and before restarting trafficking, the sudden change in rut rate appears to have been caused by the oil spill.

- The 0.4 ft. 1/2 in. mix section with no RAP (703HB) performed similar to the 0.5 ft. 3/4 in. section with RAP (700HB), indicating that RAP as aggregate replacement did not appear to have a significant influence on rutting performance on these two thicker sections.

Section 703HB was tested about 12 months after Section 700HB, and this initial aging may have had a small influence on the results.
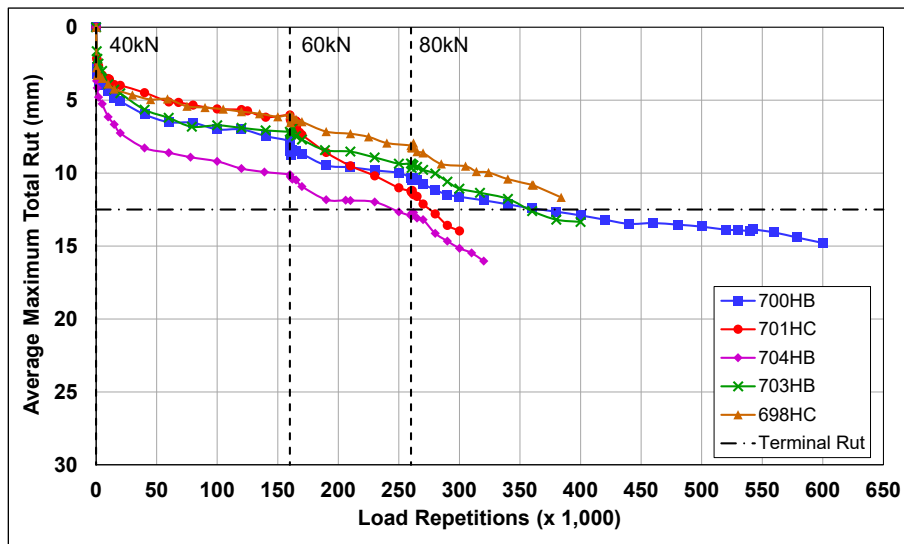
Figure 12.1: Average maximum rut for all sections.
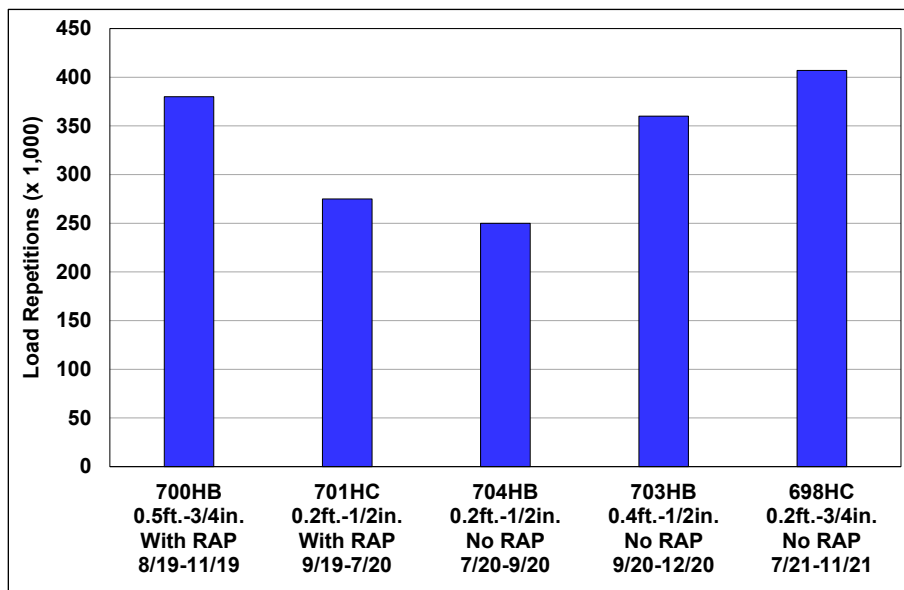
Figure 12.2: Load repetitions to terminal rut (12.5 mm [0.5 in.]).
(Note Section 698HC test was stopped at 384,000 repetitions. Terminal rut on this section was extrapolated for this plot.)

- The slowest rate of rut-depth change was recorded on Section 698HC. However, this test was conducted two years after Section 700HB and 701HC and approximately one year after Section 704HB and Section 703HB. Aging of the layer during this period may therefore have stiffened the mix, which in turn improved the rutting resistance (see discussion about stiffness change over time in Section 13.10).

- Prior to the oil spill on Section 701HC, rutting performance on this section and Section 698HC was the same, indicating that nominal maximum aggregate size and RAP as aggregate replacement did not appear to have a notable influence on rutting performance on these two tests.
- No cracking or other distresses were observed on any of the test sections.

12.3   Surface Deflection (Road Surface Deflectometer)

Surface deflections measured on each section with a road surface deflectometer (RSD) when the terminal rut was reached are compared in Figure 12.3. Note that deflection is measured between the dual wheels, not in the actual wheelpath. The following observations were made:

- The highest deflection was measured on Section 701HC, where a hydraulic oil spill occurred after the load change to 60 kN. This indicates that the oil probably softened the mix, which explains the change in rutting behavior after the spill.
- Deflections on the sections with two lifts of RHMA-G (700HB and 703HB) were lower than those recorded on the sections with one lift, as expected.
- Nominal maximum aggregate size and the presence of RAP as aggregate replacement did not appear to have any notable influence on surface deflection.
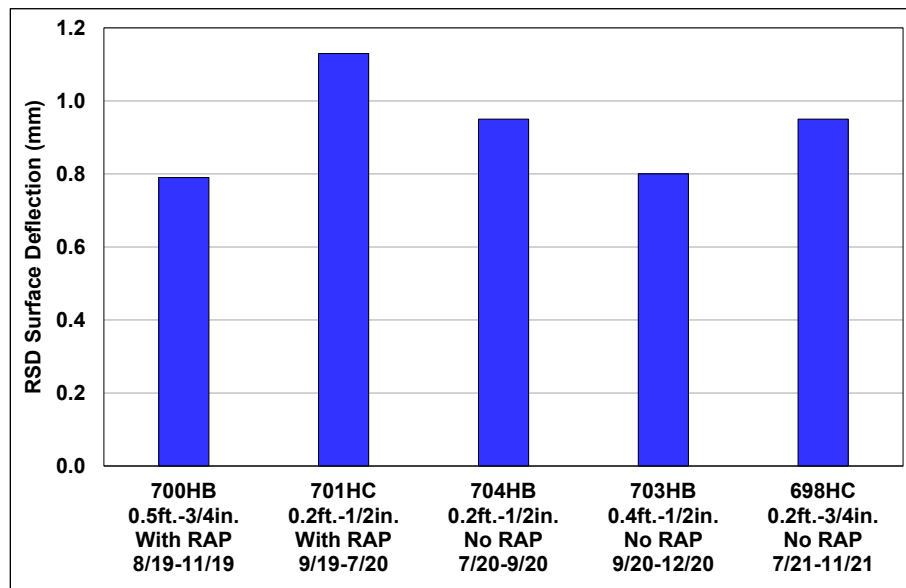
Figure 12.3: Surface deflection (RSD) at terminal rut for all sections.

12.4   Pavement Deflection (Falling Weight Deflectometer)

Pavement deflections measured on each section with an FWD 30 days after construction of the test track and before and after HVS testing on each section are compared in Figure 12.4.
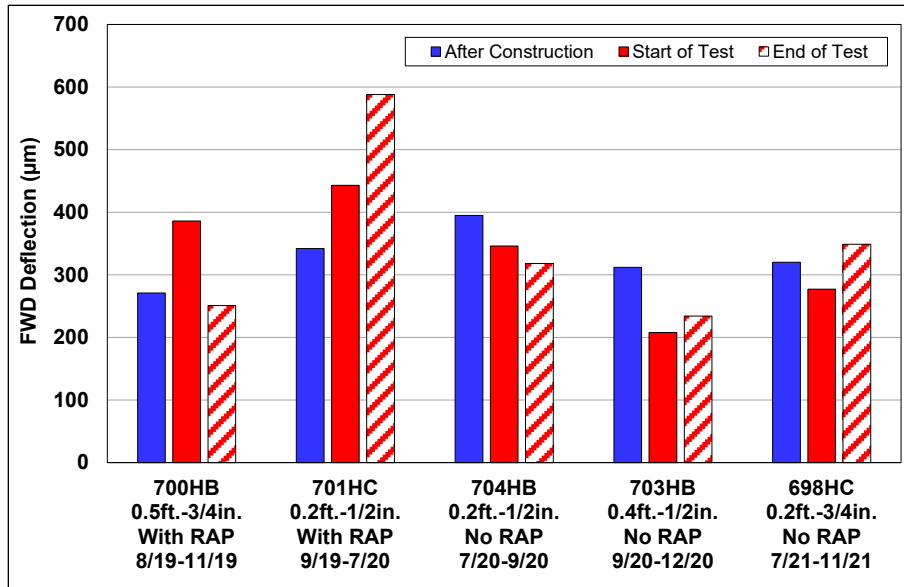
Figure 12.4: Pavement deflection (FWD) for all sections.

The following observations were made:

- Deflections after construction were generally consistent, ranging from 291 µm (700HB) to 395 µm (704HB), with no clear trends distinguishing the different mixes. The highest rate of rut depth increase was recorded on Section 704HB.

- After HVS testing, the highest deflection was measured on Section 701HC consistent with the measurements with the RSD. There was a notable difference in the deflections measured on this section before and after HVS testing, an indication that considerable damage was caused to the RHMA-G layer during trafficking as a result of the oil spill.

- Deflections after HVS testing on the sections with two lifts of RHMA-G (700HB and 703HB) were lower than those recorded on the sections with one lift, as expected. Deflections on Section 700HB appeared to have reduced during testing (stiffening of the mix through diffusion of small amounts of RAP binder possibly countered the effect of damage by trafficking) but remained essentially constant on Section 703HB. The lowest before-and-after deflections were recorded on Section 703HB.

- Differences in nominal maximum aggregate size and the presence of RAP as aggregate replacement did not appear to have any notable influence on pavement deflection.

12.5 RHMA-G Layer Stiffness (Falling Weight Deflectometer)

Stiffnesses of the RHMA-G layer backcalculated from FWD deflection measurements 30 days after construction and before and after HVS testing are compared in Figure 12.5. The results were consistent with the deflection measurements (i.e., stiffness decreased with increasing deflection).
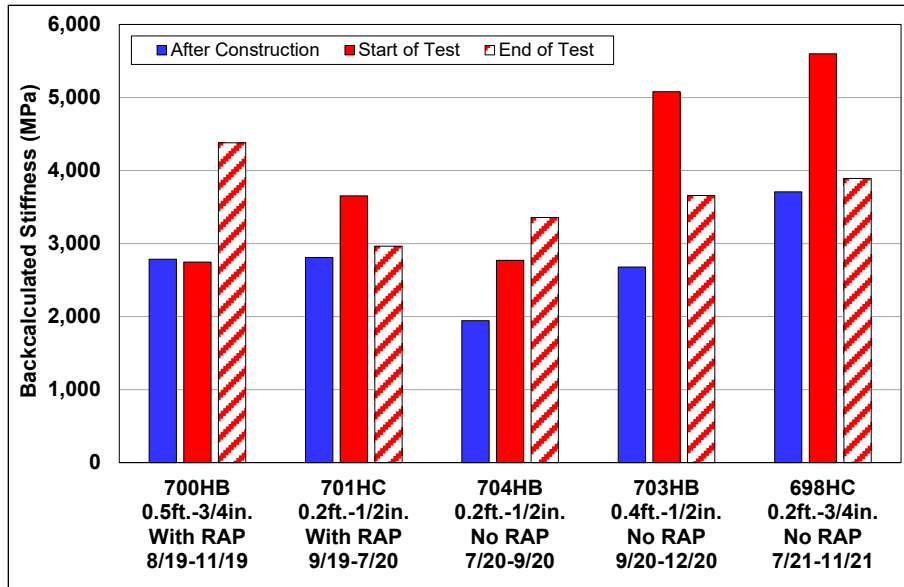
Figure 12.5: Backcalculated RHMA-G layer stiffness (FWD) for all sections.

The following observations were made:

- Stiffnesses after construction ranged from 1.943 MPa (704HB) to 3,709 MPa (698HC), with no clear trends distinguishing the different mixes.

- Stiffnesses increased in the period between construction and the start of HVS testing on all sections except Section 700HB, indicating the influence of aging of the RHMA-G layer over time.

- After HVS testing, the lowest stiffness was measured on Section 701HC, consistent with the deflection measurements and with damage attributed primarily to the oil spill.

- Stiffnesses after HVS testing on the sections with two lifts of RHMA-G (700HB and 703HB) were mostly higher than those recorded on the sections with one lift with the exception of Section 698HC, which was tested later than the other sections. Stiffness increased on Section 700HB during testing (attributed in part to stiffening of the mix through diffusion of small amounts of RAP binder which potentially countered the effect of damage by trafficking) but decreased on Section 703HB (i.e., some damage caused by HVS trafficking). The highest stiffness after HVS testing was recorded on Section 700HB.

- Differences in nominal maximum aggregate size and the presence of RAP as aggregate replacement did not appear to have any notable influence on pavement stiffness other than the observations on Section 700HB, with the interval between construction and HVS testing appearing to have a larger influence.

13. LABORATORY TEST RESULTS

13.1   Introduction

This chapter covers a first-level analysis of preliminary laboratory testing results for the four mixes used on the test track. Test specimens were prepared from mix sampled from the silos at the plant. Samples were taken after the trucks had been loaded with mix used in the first lift on each cell, except for the 3/4 in. mix with RAP, which was sampled when the trucks were loading material for the second lift (approximately eight hours of silo storage). Mix was stored in sealed metal buckets in a temperature controlled room (25°C [77°F]) until they were tested. The following tests were conducted:

- Mix stiffness: axial and flexural dynamic modulus
- Rutting performance and moisture sensitivity: Hamburg wheel track (HWT)
- Rutting performance: unconfined repeated load triaxial
- Cracking performance: four-point bending beam fatigue and semicircular bend (SCB)

13.2   Testing Plan

The testing factorial is summarized in Table 13.1.

Table 13.1: Tests Performed on Plant-Produced Mixes

Test	Replicates	Air Voids (%)[a]	Test Variables
Axial dynamic modulus - AASHTO T 378	3	7.0±0.5	• 1 temperature sequence (4, 20, 45°C) • 1 stress level • No confining pressure
Flexural dynamic modulus - AASHTO T 321	2	7.0±0.5	• 3 temperatures (10, 20, 30°C) • 2 strain levels (100 µstrain at 10 and 20°C; 200 µstrain at 30°C)
Hamburg wheel track - AASHTO T 324	2	7.0±0.5	• 1 temperature (50°C)
Flow number from repeated load triaxial results - AASHTO T 378	3	7.0±0.5	• 1 temperature (52°C) • 1 deviator stress (480 kPa [70 psi]) • 1 contact stress (30 kPa [4 psi]) • No confining pressure
Beam fatigue - AASHTO T 321	3	7.0±0.5	• 1 temperature (20°C) • 3 strain ranges (high, medium, low) based on the mix stiffness • 1 frequency (10 Hz)
Semicircular Beam (SCB) test - AASHTO T 393	3	7.0±0.5	• 1 temperature (25°C)

13.2.1 Performance Testing Specimen Preparation

Specimen preparation details for the different tests were as follows:

- Asphalt mix performance tester (AMPT) tests were conducted on specimens with 100 mm (≈4 in.) diameter and 150 mm (≈6 in.) height, cored from 150 mm and 175 mm (≈7 in.) gyratory-compacted specimens.
- Beam specimens were cut from ingots compacted with a dual steel-drum roller. The beams were 380 mm (≈15 in.) in length, 50 mm (≈2 in.) in height, and 63 mm (≈2.5 in.) in width.
- Hamburg wheel track specimens were cut from gyratory-compacted specimens with 150 mm diameter and 60 mm (≈2.4 in.) height.
- Semicircular bend specimens were cut from gyratory-compacted specimens with 150 mm diameter and 175 mm height. Two 50 mm thick discs were cut from the compacted specimen, from which four SCB specimens were cut. A 15×1.5 mm notch was cut into each SCB specimen.

13.2.2 Mix Testing Details

Specimen Air Void Contents

Air-void contents were determined according to AASHTO T 269. Bulk specific gravity was determined using both saturated surface-dry (AASHTO T 166) and automatic vacuum sealing methods (AASHTO T 331).

Mix Stiffness: Axial Dynamic Modulus

Tests to determine dynamic modulus ($E*$) and phase angle of the RHMA-G mixes were performed using an AMPT at 10, 1, and 0.1 Hz when testing at 4°C and 20°C (39°F and 68°F) and at 10, 1, 0.1, and 0.01 Hz when testing at 45°C (113°F). In this test, the specimen is subjected to a haversine axial-compressive load with fixed amplitude under controlled-strain conditions. The axial deformation of the specimen during cyclic loading is measured using three linear variable displacement transducers (LVDTs) mounted around the specimen 120° apart. The dynamic modulus is calculated by dividing the peak stress (σ_{max}) by the peak strain (ε_{max}) during each loading cycle. Three replicate specimens from each mix were tested.

Dynamic modulus master curves were developed using Equation 13.1 through Equation 13.3. The measured modulus values were used to construct master curves at the reference temperature of 20°C by fitting the data to the sigmoidal function shown in Equation 13.1. The testing frequencies at any testing temperature were converted to the reduced frequency at the

reference temperature using the time-temperature superposition principle (Equation 13.2) with the aid of the Arrhenius shift factor (Equation 13.3).

$$log(|G^*(f_r)|) = \delta + \frac{\alpha}{1+e^{\beta+\gamma \times log(f_r)}}$$ (13.1)

where: δ, α, β, and γ are sigmoidal function parameters
f_r is the reduced frequency at reference temperature T_r (°C)

$$log(f_r) = log(a_T(T)) + log(f)$$ (13.2)

where: f is the testing frequency at testing temperature T (°C)

$$log(a_T(T)) = \frac{E_a}{Ln(10) \times R}(\frac{1}{T} - \frac{1}{T_r})$$ (13.3)

where: aT(T) is the shift factor value for temperature T (°K)
E_a is an activation energy term (Joules [J]/mol)
R is the universal gas constant (J/(mol·K)
T_r is the reference temperature (°K)

The parameters of the sigmoidal function as well as the activation energy term in the Arrhenius shift factor equation were estimated using the *Solver* feature in *Microsoft Excel* by minimizing the sum of square error between predicted and measured values.

Mix Stiffness: Flexural Dynamic Modulus

Four-point-bending beam frequency sweep tests were conducted to measure the stiffness (flexural dynamic modulus) of the RHMA-G beams under different frequencies and various temperatures. Two replicates were tested at temperatures of 10°C, 20°C, and 30°C and over frequencies of 15, 10, 5, 2, 1, 0.5, 0.2, 0.1, 0.05, 0.02 and 0.01 Hz. Tests were performed in strain control mode (100 µstrain at 10°C and 20°C, and 200 µstrain at 30°C).

A sigmoidal function similar to that used to determine the dynamic modulus was used to construct the flexural dynamic modulus master curve at a reference temperature of 20°C. The shift factor equation used for generating the master curves is shown in Equation 13.4

$$log(a_T(T)) = C \times (T - T_r)$$ (13.4)

where: C is a shift factor constant
T_r is the reference temperature (°C)
T is the testing temperature (°C)

Rutting Performance and Moisture Sensitivity: Hamburg Wheel Track

The Hamburg wheel tracking test (AASHTO T 324) provides an indication of rutting and moisture susceptibility of asphalt mixture pavement samples due to weakness in the aggregate structure, inadequate binder stiffness, or moisture damage. This test method measures the rut depth and number of passes to failure. Tests were conducted with a water temperature of 50°C (122°F).

Rutting Performance: Repeated Load Triaxial

The flow number test (AASHTO T 378) provides an indication of the resistance of an asphalt mix to permanent deformation (rutting). The accumulation of permanent deformation is assumed to occur in primary, secondary, and tertiary phases. Permanent strain typically accumulates rapidly in the primary phase, followed by a lower constant rate through the secondary phase, and then accumulates rapidly again in the tertiary phase. The flow number is defined as the number of cycles at which the tertiary phase starts. Higher flow number values imply that a mix has better rutting (permanent deformation) resistance. In this study, unconfined specimens were subjected to a repeated compressive deviator stress of 600 kPa (87 psi) and a 30 kPa (4.4 psi) contact stress. The resulting cumulative permanent deformation versus the number of loading cycles was recorded with flow number calculations performed automatically by the AMPT software. The numbers of cycles to 1%, 3%, and 5% permanent axial strain were also analyzed to obtain a better understanding of the likely rutting behavior of each of the mixes. According to the test method, the selected testing temperature should be based on the adjusted high PG temperature of the binder identified for the pavement location. Since testing for specific project locations was not included as part of the workplan, all tests were performed at 52°C to obtain a good understanding of how damage accumulated during the test. Running the test at higher temperatures (e.g., ≥64°C) could have resulted in accelerated evolution of permanent deformation, which would not provide a comprehensive indication of how damage accumulated with load repetition. Running the test at lower temperatures would extend the testing time but would probably not provide any additional useful information.

Cracking Performance: Four-Point Beam

The beam fatigue test (AASHTO T 321) provides an indication of the resistance of an asphalt mix to fatigue cracking at a constant deformation (strain). Beam specimens are subjected to four-point bending by applying sinusoidal loading at three different strain levels (high, intermediate,

and low) at a frequency of 10 Hz and temperature of 20°C (68°F). The fatigue life for each strain level was selected by multiplying the maximum stiffness value for that strain level by the number of cycles at which that stiffness value occurred. Laboratory test results will generally correspond with field fatigue or reflection cracking performance for overlays thinner than about 75 mm (0.25 ft.) but may not correspond with expected field performance for thicker layers of asphalt. For thicker layers, the interaction of the pavement structure, traffic loading, temperature, and mix stiffness with the controlled-strain beam fatigue results needs to be simulated using mechanistic analysis in order to rank mixes for expected field performance.

In this UCPRC study, the testing approach currently specified in AASHTO T 321 was modified to optimize the quantity and quality of the data collected. Replicate specimens were first tested at high- and medium-strain levels to develop an initial regression relationship between fatigue life and strain (Equation 13.5). Strain levels were selected, based on experience, to achieve fatigue lives between 10,000 and 100,000 load cycles and between 300,000 and 500,000 load cycles for high and medium strains, respectively. Additional specimens were then tested at lower-strain levels selected based on the results of the initial linear regression relationship to achieve a fatigue life of about 1 million load repetitions. The final regression relationship was then refined to accommodate the measured stiffness at the lower strain level.

$$LnN = A + B \times \varepsilon \tag{13.5}$$

where: N is fatigue life (number of cycles)
ε is the strain level (microstrain [µstrain])
A and B are model parameters

Cracking Performance: Semicircular Bend

The semicircular bend (SCB, AASHTO T 393) test can be used to determine the fracture resistance parameters of asphalt mixtures at intermediate temperature and to rank the cracking resistance of asphalt mixtures containing different binders, modifiers, aggregate gradations, and recycled asphalt pavement. The UCPRC is currently investigating the SCB, IDEAL-CT (ASTM D8225) and other simple cracking tests that relate to beam fatigue test results and can be used for mix design, quality control, and quality assurance purposes. The SCB fracture energy (G_f) and flexibility index (FI) test parameters were selected to compare the performance of mixes. Fracture energy is the area under the load-displacement curve and shows the overall resistance of the mix to crack-

related damage. The flexibility index is calculated from the fracture energy and post-peak slope of the load-displacement curve that represents the average crack growth rate. Increasing fracture energy and flexibility index implies increasing cracking resistance that can be used to identify brittle mixes.

13.3 Specimen Air-Void Contents

Average air-void contents (based on saturated surface-dry bulk specific gravity) for the specimens compacted in a Superpave gyratory compactor (cylindrical AMPT, HWTT, and SCB specimens) and with a rolling-wheel compactor (beam specimens) are shown in Figure 13.1. Whiskers on the data show the lowest and highest air-void contents of the replicate specimens. All specimens were within the target limits (7.0±0.5%), indicating that consistent compaction was achieved.
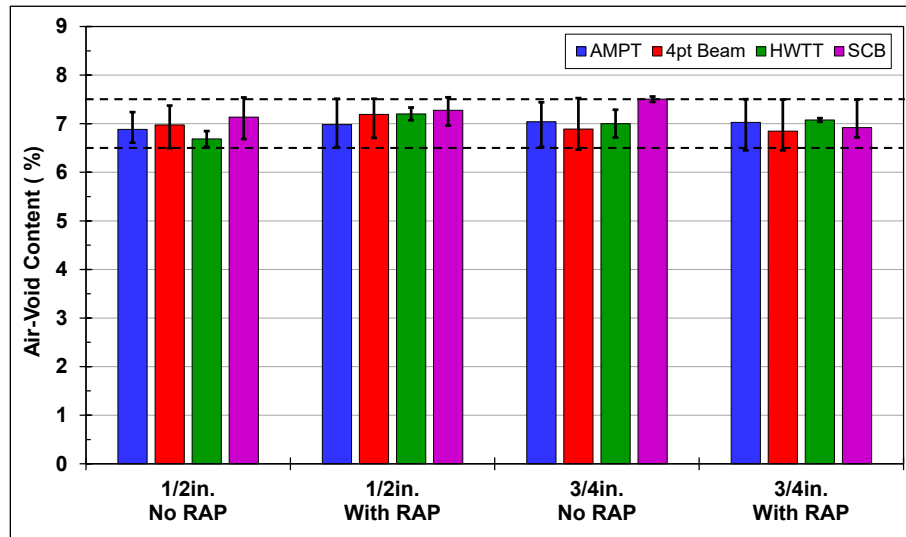

Figure 13.1: Specimen air-void contents.

13.4 Mix Stiffness: Axial Dynamic Modulus

Axial dynamic modulus test results are plotted as master curves for each mix in Figure 13.2. The stiffness results for the 1/2 in. mix with RAP and both 3/4 in. mixes were essentially the same and were consistent with those measured on typical RHMA-G mixes. The control mix (1/2 in. with no RAP) had slightly higher stiffnesses at the medium to higher frequencies, which was attributed to the notably longer time that this mix was stored in the silo on the day of construction. All mixes had similar stiffnesses at the lower frequencies. The higher stiffness on the 1/2 in. mix with no

RAP mix did not equate to improved rutting performance in the HVS test, indicating that section performance was likely influenced more by the underlying layers than the mix properties.
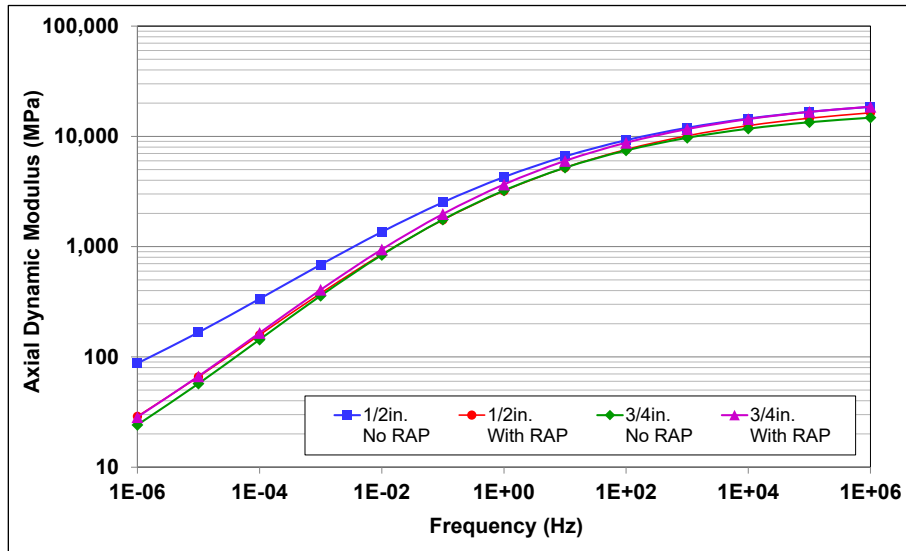
Figure 13.2: Axial dynamic modulus master curves.

13.5   Mix Stiffness: Flexural Dynamic Modulus

Flexural dynamic modulus test results are plotted as master curves for each mix in Figure 13.3.

Figure 13.3: Flexural dynamic modulus master curves.

The results for the 1/2 in. mix with no RAP, 1/2 in. mix with RAP, and the two 3/4 in. mixes were similar to those recorded for the axial dynamic modulus tests. The 3/4 in. mix with no RAP had slightly lower stiffnesses than the other mixes at intermediate and low frequencies.

13.6   Rutting Performance and Moisture Sensitivity: Hamburg Wheel Track

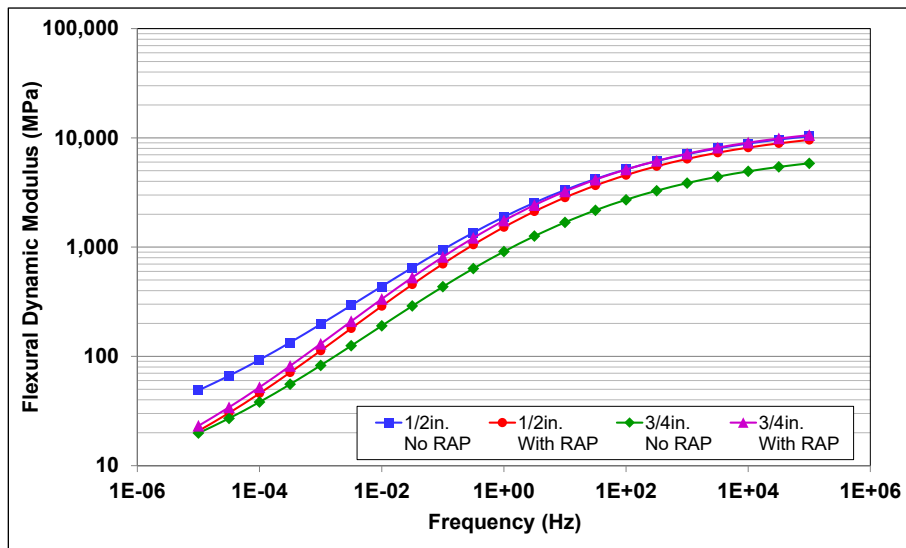Hamburg wheel track results are plotted in Figure 13.4. Although the Caltrans specifications at the time of testing listed a failure criterion of 12.5 mm (0.5 in.) at 20,000 load repetitions, the test was continued to 35,000 load repetitions to determine whether an inflection point could be reached (it was not reached on any mix). The results indicate that rutting performance for all four mixes was essentially the same and that none of the mixes were susceptible to moisture damage. Nominal maximum aggregate size and the use of RAP as aggregate replacement did not appear to influence the results.
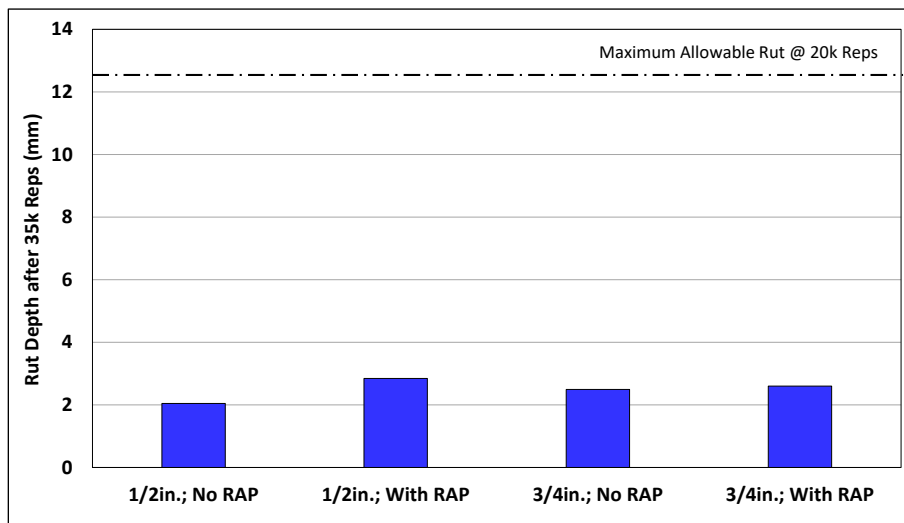
Figure 13.4: Hamburg wheel track results.

13.7   Rutting Performance: Unconfined Repeated Load Triaxial

Figure 13.5 shows the flow number values for the four mixes. The 1/2 in. mix with no RAP had a significantly higher flow number compared to the other three mixes, consistent with the stiffness results. The results for the other three mixes were similar, with a slightly higher number recorded on the 3/4 in. mix with no RAP.

Figure 13.6 shows the number of cycles to 3% and 5% permanent axial strain. Trends observed for the number of cycles to 3% and 5% permanent axial strain were consistent with those observed for the flow number results.
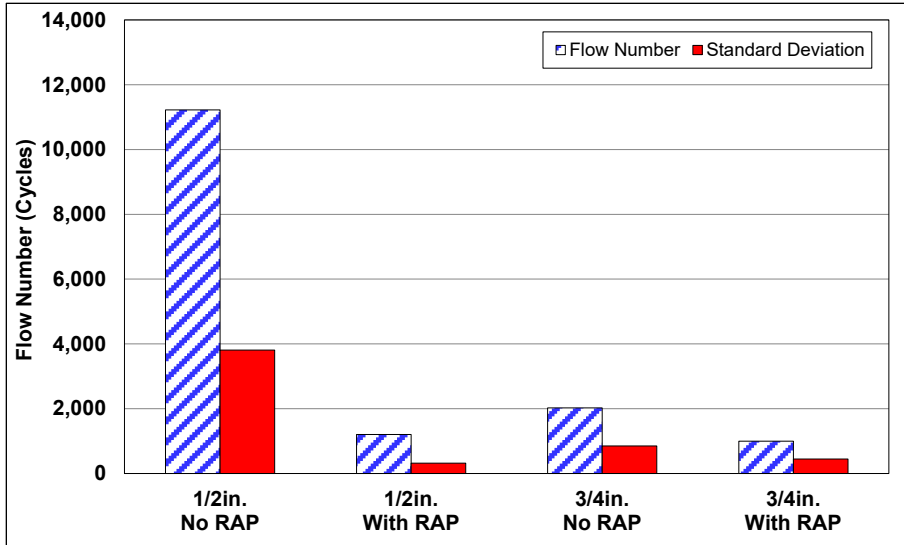
Figure 13.5: Average flow number (Unconfined at 50°C).
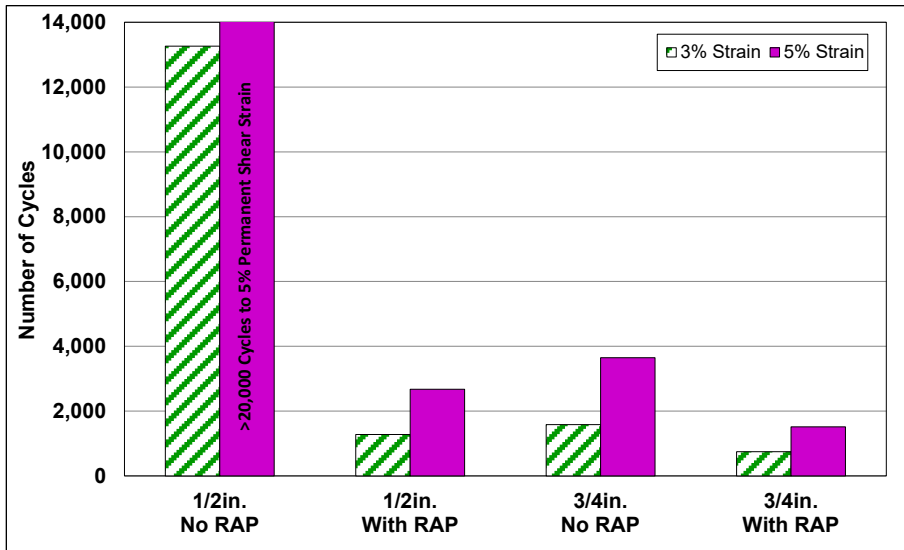
Figure 13.6: Number of cycles to 3% and 5% permanent axial strain.

13.8   Cracking Performance: Four-Point Bending Beam Fatigue

Plots of the fatigue models for each mix are shown in Figure 13.7. The models were considered to be generally appropriate despite the relatively low R-squared values of the model fitting and relatively high variability of the test results at each strain level. The results were consistent with the flexural dynamic modulus results. Calculated fatigue lives at 200, 400, and 600 µstrain of the four mixes are compared in Figure 13.8. Note that no mixes were tested at 200 µstrain and that fatigue life at this strain level was extrapolated.
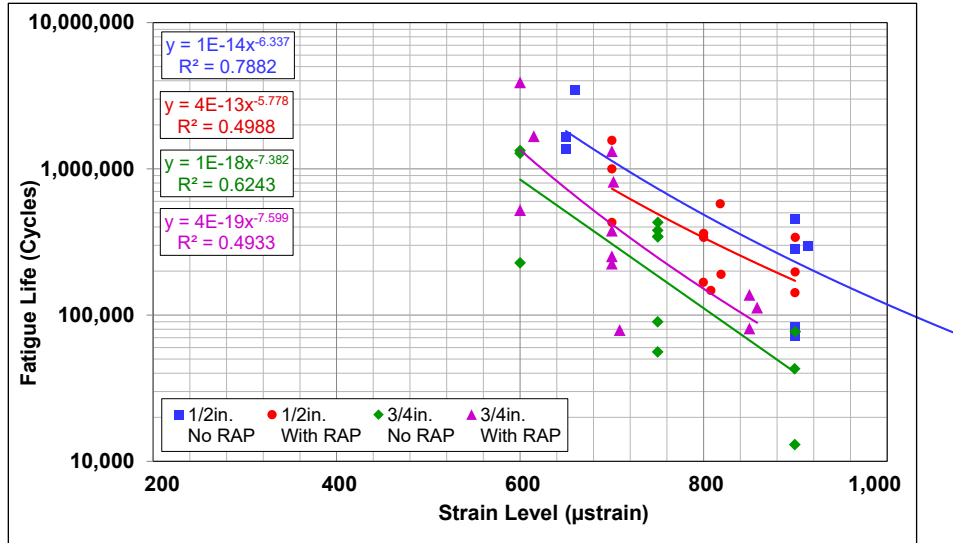
Figure 13.7: Fatigue regression models.
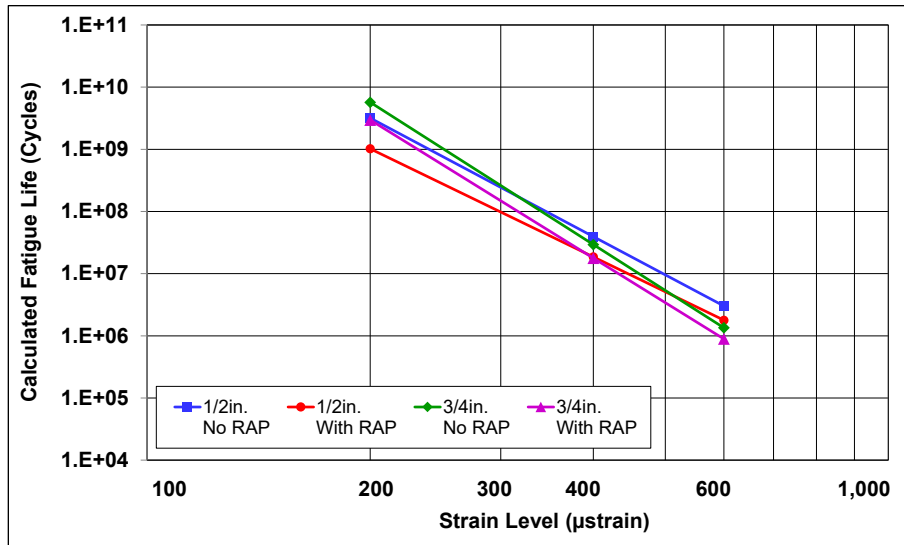
Figure 13.8: Calculated fatigue life at 200, 400, and 600 μstrain.

A review of the data led to the following observations:

- Fatigue life decreased with increasing strain level, as expected.
- Calculated fatigue lives were similar for all mixes at all strains, indicating that NMAS and RAP aggregate replacement did not appear to have any significant influence on fatigue cracking performance.

13.9   Cracking Performance: Semicircular Bend

Average fracture energies and flexibility indices for the four mixes are shown in Figure 13.9 and Figure 13.10. Peak strength is included on the flexibility index plot.
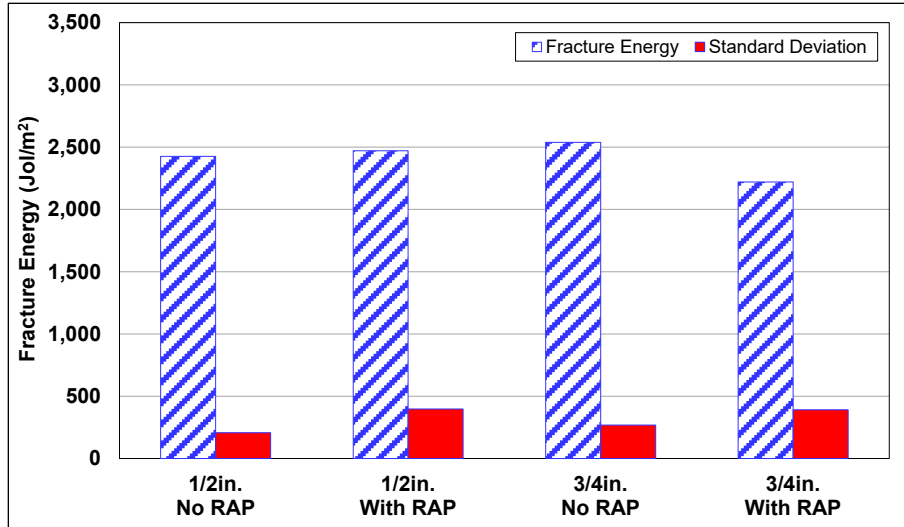
Figure 13.9: Semicircular bend fracture energy.
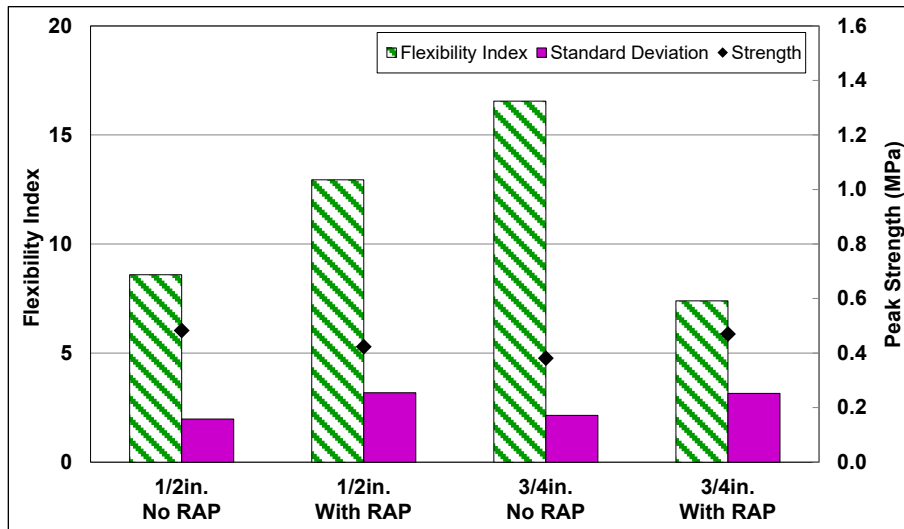
Figure 13.10: Semicircular bend flexibility index.

A review of the data led to the following observations:

- Fracture energies were consistent across three of the four mixes, with the 3/4 in. mix with RAP having a slightly lower fracture energy. Variability between replicate specimens within each mix was also consistent.

- Flexibility indices were different across the four mixes, with no apparent trends. The 1/2 in. mix with no RAP had a lower flexibility index than the 1/2 in. mix with RAP, which was attributed to the significantly longer time that the former mix was kept in the silo before placement. This could have resulted in more aging and consequent stiffening of the mix.

- The 3/4 in. mix with no RAP had the highest flexibility index of all four mixes with the index considerably higher than that recorded for the 3/4 in. mix with RAP. The mix with no RAP also had the lowest flexural modulus. The 3/4 in. mix with RAP had the lowest flexibility

index of the four mixes, which was attributed in part to the longer silo storage time that this mix was subjected to (samples were taken when mix for the second lift was loaded), which probably resulted in more aging/stiffening.

- Peak strengths were similar across the four mixes, with strength rankings opposite to the flexibility indices (i.e., the two mixes with the lowest flexibility indices had slightly higher strengths than the two mixes with higher flexibility indices).

13.10 Change in Axial Dynamic Modulus Over Time

Stiffness change over time in the RHMA-G layers on the test track was monitored by taking 150 mm diameter cores from each test cell at periodic intervals, taking a 38 mm diameter horizontal core from each RHMA-G layer, and then measuring the dynamic modulus on that core following the procedure described in Section 13.2.2 (note that testing on small diameter specimens was necessary because the RHMA-G layer thicknesses were thinner than that required for testing a standard 100 mm diameter specimen). The results from tests conducted 6, 24, and 36 months after construction are plotted in Figure 13.11.
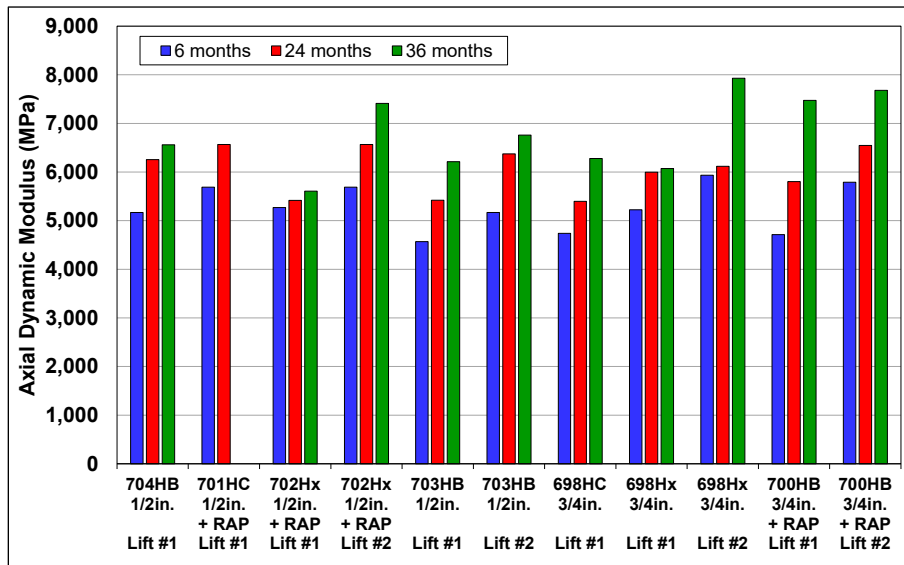
Figure 13.11: Axial dynamic modulus over time at 10 Hz from test track cores.
(Note that Section 702Hx and Section 698Hx were not tested with the HVS.)

The results clearly show the increase in stiffness in the RHMA-G layers over time on all of the test sections. On the sections with two lifts, higher stiffnesses were recorded on the second (top) lift of RHMA-G than in the first (bottom) lift, as expected. These results support the observations about the effect of aging on HVS test results discussed in Chapters 7 through 12.

13.11 Summary

The laboratory test results indicate that nominal maximum aggregate size and RAP aggregate replacement appeared to have a limited effect on rutting and cracking resistance, with time that the mix spent in the silo appearing to have the biggest influence on laboratory test results, and additionally aging over time on HVS test results. Note that although cracking performance test results are discussed in the chapter, no cracking was observed on any of the HVS test sections after testing.

Blank page

14. CONCLUSIONS

This research report summarizes a literature review update, the construction of a test track to assess various aspects of gap-graded rubberized asphalt concrete (RHMA-G) mixes with and without the use of reclaimed asphalt pavement (RAP) as aggregate replacement, a first-level analysis of the results from five of the planned seven Phase 1 Heavy Vehicle Simulator (HVS) tests, which focused on rutting resistance, and a first-level analysis of the laboratory test results on specimens prepared from the four different mixes sampled during production.

Apart from the research previously undertaken by the UCPRC for CalRecycle, only limited published research on the use of RAP in new RHMA mixes was located. The few documents available focused on laboratory testing of dense-graded mixes produced with terminal-blended binders containing completely digested rubber particles smaller than 0.4 mm (passing the #40 sieve). No documented research involving accelerated pavement testing of RHMA-G mixes containing RAP was located.

Four different RHMA-G mixes were placed on seven cells on the test track at the UCPRC. Mixes differed by nominal maximum aggregate size (NMAS; 1/2 and 3/4 in.) and the addition of 10% RAP by weight of the aggregate as a coarse aggregate replacement. Single and double lifts of each mix were placed. Apart from the addition of RAP, the mix designs all met current Caltrans specifications. Although Caltrans currently does not permit more than one lift of RHMA-G on projects, the placement of each lift of each mix on the test track met current Caltrans construction specifications for RHMA-G layers.

The five HVS tests discussed in this report covered the control section (0.2 ft. [60 mm], 1/2 in. NMAS with no RAP), a section with two lifts (0.4 ft. [120 mm]) of the 1/2 in. mix with no RAP, a section with one lift of 1/2 in. mix with RAP, a section with one lift of 3/4 in. mix with no RAP, and a section with two lifts (0.5 ft. [150 mm]) of 3/4 in. mix with RAP. The untested sections included a section with two lifts of 1/2 in. mix with RAP, and a section with two lifts of 3/4 in. mix with no RAP. Results from these five HVS tests and associated laboratory testing indicated the following:

- Performance of all four mixes was satisfactory in terms of the level of trafficking required to reach a terminal average maximum rut of 0.5 in. (12.5 mm).

- Differences in nominal maximum aggregate size and/or the addition of RAP as a coarse aggregate replacement did not appear to have any significant influence on the test results. The time that the mix was stored in the silo prior to placement and the interval between test track construction and the start of HVS testing on a specific section (i.e., aging of the RHMA-G layer) both appeared to have a larger influence.
- Deflection measurements and backcalculated stiffnesses of the RHMA-G layer on each section before and after HVS testing indicate that HVS trafficking generally caused some damage on the sections, as expected. An exception to this observation was noted on the first test, which was attributed in part to stiffening of the mix through diffusion of small amounts of RAP binder, which possibly countered the effect of damage by trafficking, and potentially in part to the method followed to distinguish stiffness contributions of the RHMA-G and CCPR layers. Note that the first lift of RHMA-G placed on this section had very little silo time, while the mix placed in the second lift had spent approximately eight hours in the silo.
- A hydraulic oil spill on one of the sections had a notable negative effect on rutting performance.
- Variation in rutting performance between sections and in the rut depth along the length of individual sections may be attributed to shear failures in the aggregate base layer. Although the layer met all Caltrans specifications for Class 2 Aggregate Base, the uncrushed, rounded particles had poor interlock leading to a layer that appeared to be susceptible to shearing, as observed during construction of the layer and later placement of the CCPR layer. This will be assessed during the forensic investigation.
- No cracks or other distresses were observed on any of the sections after trafficking.

This report covers a first-level analysis of HVS and laboratory test results. A separate report *(2)* will document the second-level analysis of the results in terms of mechanistic simulations to understand long-term performance in typical pavement structures under different traffic volumes and climatic conditions in California. Recommendations will be made in the second-level analysis report, if justified, for changes to limits for nominal maximum aggregate size in relation to RHMA-G lift thickness, RHMA-G lift thickness, whether more than one RHMA-G lift can be considered in pavement designs, the use of reclaimed asphalt pavement as aggregate replacement in RHMA-G mixes, and whether crushed aggregate faces for aggregate base and subbase materials should be a specification requirement.

REFERENCES

1. Alavi, Z., Hung, S., Jones, D. and Harvey, J. 2017. *Preliminary Investigation into the Use of Reclaimed Asphalt Pavement in Gap-Graded Asphalt Rubber Mixes, and Use of Reclaimed Asphalt Rubber Pavement in Conventional Asphalt Concrete Mixes* (Research Report UCPRC-RR-2016-03). Davis and Berkeley, CA: University of California Pavement Research Center.

2. Wu, R., Jones, D., Louw, S., Hammack, J. and Tom, H. 2022. *Second-Level Analysis of Heavy Vehicle Simulator and Laboratory Test Results on Four RHMA-G Mixes to Investigate Nominal Maximum Aggregate Size, Layer Thickness, and Performance with Aggregate Replacement from Reclaimed Asphalt Pavement* (Research Report UCPRC-RR-2022-06). Davis and Berkeley, CA: University of California Pavement Research Center.

3. Xiao, F. 2006. *Development of Fatigue Predictive Models of Rubberized Asphalt Concrete (RAC) Containing Reclaimed Asphalt Pavement (RAP) Mixtures*. PhD dissertation, Clemson University.

4. Xiao, F., Amirkhanian, S.N. and Juang, C.H. 2007. "Rutting Resistance of Rubberized Asphalt Concrete Pavements Containing Reclaimed Asphalt Pavement Mixtures." *Journal of Materials in Civil Engineering* 19, no. 6: 475-483.

5. Xiao, F. and Amirkhanian, S.N. 2009. "Artificial Neural Network Approach to Estimating Stiffness Behavior of Rubberized Asphalt Concrete Containing Reclaimed Asphalt Pavement." *ASCE Journal of Transportation Engineering* 135, no. 8: 580-589.

6. Xiao, F. and Amirkhanian, S.N. 2009. "Laboratory Investigation of Moisture Damage in Rubberized Asphalt Mixtures Containing Reclaimed Asphalt Pavement." *International Journal of Pavement Engineering* 10 no. 5: 319-328.

7. Xiao, F. and Amirkhanian, S.N. 2010. "Laboratory Investigation of Utilizing High Percentage of RAP in Rubberized Asphalt Mixture." *Materials and Structures* 43, no. 1-2: 223-233.

8. Xiao, F., Amirkhanian, S.N., Putman, B.J. and Juang, H. 2012. "Feasibility of Superpave Gyratory Compaction of Rubberized Asphalt Concrete Mixtures Containing Reclaimed Asphalt Pavement." *Construction and Building Materials* 27, no. 1: 432-438.

9. Luo, Z., Xiao, F., Hu, S. and Yang, Y. 2013. "Probabilistic Analysis of Fatigue Life of Rubberized Asphalt Concrete Mixtures Containing Reclaimed Asphalt Pavement." *Construction and Building Materials* 41: pp. 401-410.

10. Vahidi, S., Mogawer, W.S. and Booshehrian, A. 2014. "Effects of GTR and Treated GTR on Asphalt Binder and High-RAP Mixtures." *Journal of Materials in Civil Engineering* 26, no. 4: 721-727.

11. Ambaiowei, D.C. and Tighe, S.L. 2015. "Rubberized Asphalt Mixtures with RAP: A Case for Use in Ontario." *TRB 94th Annual Meeting Compendium of Papers*. Washington, DC: Transportation Research Board.

12. Jones, D., Harvey, J. and Wu, R. 2022. *Site Investigation Guide for Mechanistic-Empirical Design of California Pavements* (Guideline: UCPRC-GL-2020-02). Davis and Berkeley, CA: University of California Pavement Research Center.

13. Jones, D. 2005. *Quality Management System for Site Establishment, Daily Operations, Instrumentation, Data Collection, and Data Storage for APT Experiments* (Contract Report CR-2004/67-v2). Pretoria, South Africa: CSIR Transportek.